

*Immobilization and Kinetics of Wolf-
Lamb type catalysts through electrospun
membranes and printed structures*

DISSERTATION

zur Erlangung des akademischen Grades eines
Doktors der Naturwissenschaften (Dr. rer. nat.)
an der Fakultät für Biologie, Chemie und Geowissenschaften
der Universität Bayreuth

vorgelegt von

Martin Oliver Pretscher

aus *Bad Neustadt a. d. Saale*

Bayreuth, 2020

Die vorliegende Arbeit wurde in der Zeit von (04/2017) bis (09/2020) in Bayreuth am Lehrstuhl *Makromolekulare Chemie II* unter Betreuung von Frau Professorin Dr. *Seema Agarwal* angefertigt.

Vollständiger Abdruck der von der Fakultät für Biologie, Chemie und Geowissenschaften der Universität Bayreuth genehmigten Dissertation zur Erlangung des akademischen Grades eines Doktors der Naturwissenschaften (Dr. rer. nat.).

Dissertation eingereicht am: 29.09.2020

Zulassung durch die Promotionskommission: 08.10.2020

Wissenschaftliches Kolloquium: 11.03.2021

Amtierender Dekan: Prof. R. Matthias Breuning

Prüfungsausschuss:

Prof. Dr. Seema Agarwal	(Gutachterin)
Prof. Dr. Birgit Weber	(Gutachterin)
Prof. Dr. Peter Strohriegl	(Vorsitz)
Prof. Dr. Georg Papastavrou	

Table of content

Table of content	I
List of Publication	II
1. Zusammenfassung	1
2. Abstract	4
3. Introduction	6
3.1. Wolf-Lamb type catalysis	8
3.1.1. Inorganic Wolf-Lamb type catalysts	9
3.1.2. Polymeric Wolf- Lamb type catalysts.....	12
3.2. Kinetics of multi-step one-pot reactions	16
3.3. Methods for polymer processing	18
3.3.1. Electrospinning	18
3.3.2. Printing of polymers.....	22
3.4. Crosslinkable material for electrospinning and printing	25
4. References	27
5. Synopsis	38
5.1. Wolf-Lamb type catalysis in one-pot using electrospun polymeric catalyst membranes .	40
5.1.1. Individual Contribution of Joint Publications	42
5.2. Precise 2D-Patterned Incompatible Catalysts for Reactions in One-Pot	43
5.2.1. Individual Contribution of Joint Publications	45
5.3. Comparison of post-process functionalized catalytic electrospun membranes and 2D printed structures in Wolf-Lamb type catalysis	46
5.3.1. Individual Contribution of Joint Publications	49
6. Reprint of publications	50
6.1. Wolf-Lamb-type Catalysis in One Pot Using Electrospun Polymeric Catalyst Membranes 50	
6.2. Precise 2D-patterned Incompatible Catalysts for Reactions in One-Pot	70
7. Outlook	139
8. Acknowledgment	140
(Eidesstattliche) Versicherungen und Erklärungen	142

List of Publication

[1] Pretscher, Martin O.; Gekle, Stephan; Agarwal, Seema Wolf–Lamb-type Catalysis in One Pot Using Electrospun Polymeric Catalyst Membranes

in Macromolecular Rapid Communications vol. 40 (2019) issue 14. pp. 1900148

[2] Pretscher, Martin O.; Chen, Tingting; Sitaru, Gabriel; Gekle, Stephan; Ji, Jian; Agarwal, Seema

Precise 2D-Patterned Incompatible Catalysts for Reactions in One-Pot
in Chemistry – a European journal vol. 25 (2019) issue 59. pp. 13640-13646

[3] Pretscher, Martin O.; Sitaru, Gabriel; Dietel, Markus; Schmalz, Holger; Gekle, Stephan; Agarwal, Seema

Post-process functionalized catalytic electrospun and 2D printed structures for Wolf-Lamb type catalysis

in ACS Applied Polymer Material Vol 3 (2021) issue 3 pp. 1349–1357

[4] Pretscher, Martin*; Pineda-Contreras, Beatriz A.*; Kaiser, Patrick; Reich, Steffen; Schöbel, Judith; Kuttner, Christian; Freitag, Ruth; Fery, Andreas; Schmalz, Holger; Agarwal, Seema
pH-Responsive Biohybrid Carrier Material for Phenol Decontamination in Wastewater
in Biomacromolecules vol. 19 (2018) issue 8. pp. 3224-3232

[5] Käfer, Florian; Pretscher, Martin; Agarwal, Seema

Tuning the Phase Transition from UCST-Type to LCST-Type by Composition Variation of Polymethacrylamide Polymers

in Macromolecular Rapid Communications vol. 39 (2018) issue 24, pp. 1800640

*Beatriz A. Pineda-Contreras and Martin Pretscher contributed equally to the work.

The following thesis is based on publication [1]-[3].

1. Zusammenfassung

Wolf-Lamm Katalysatoren sind miteinander inkompatible Katalysatoren, die sich bei aufeinander treffen deaktivieren würden. Um diese in mehrstufigen ein-Topf Reaktionen zu nutzen, ist es somit notwendig die Katalysatoren zu immobilisieren und voreinander zu schützen. Durch diese Immobilisation können dann mehrstufige Reaktionen ohne Aufreinigung von Intermediaten katalysiert werden, die anders nicht zugänglich wären. Die aktuell existierenden Systeme enthalten meist Triblockcopolymer, Kern-Schale Mizellen, Sternpolymere oder anorganische Partikel, welche die Anwendung solcher Systeme stark einschränkt, entweder aufgrund von mehrstufigen Syntheseprozessen oder die auf zwei-stufige Katalyse Systeme beschränkt sind.

Ziel dieser Arbeit ist es neue wiederverwendbare Trägersysteme für solche Wolf-Lamm Katalysatoren zu entwerfen. Diese sollen einfach herzustellen und innerhalb von „ein-Topf“ Reaktionen modular verwendbar sein. Innerhalb der ersten Stufen werden Modellsysteme untersucht, welche auf dem sauren Copolymer Polystyrol-*co*-Styrolsulfonsäure-*co*-Methacrylbenzophenon und dem basischen Copolymer Polystyrol-*co*-4-Vinylpyridine-*co*-Methacrylbenzophenon basieren. Diese polymeren Katalysatoren wurden innerhalb einer „ein-Topf“, zwei-Stufen Reaktion verwendet. Diese war die sauer katalysierte Deacetalisierung von Dimethoxybenzyl zu Benzaldehyd gefolgt von der basisch katalysierten Carbonbildenden Reaktion mit Ethylcyanoformat zu Cyano(phenyl)methylethylcarbonat. Die Kinetik der zwei-stufigen Reaktion wurde hierbei über anfügen der zugrundeliegenden Differentialgleichungen untersucht. Die Polymeren Katalysatoren wurden hierbei zu selbstständigen Materialien über Elektrosponnen zu porösen Membranen oder über 2D Druck auf neutrale Netzstrukturen prozessiert. Die polymeren Säure- und Basenkatalysatoren wurden hierbei über freie radikalische Polymerisation mit der für die Prozessierbarkeit notwendigen molekularen Masse mit den Comonomeren Styrol, Styrolsulfonsäure (für das saure Polymer) bzw. 4-Vinylpyridin (für das basische Polymer) und Methacrylbenzophenon (als Vernetzer) synthetisiert.

Für die elektrosponnenen Membranen wurde festgestellt, dass das saure Copolymer als das polymere Salz (Poly(styrol-*co*-Natriumstyrolsulfonat-*co*-methacrylbenzophenon)) verarbeitet werden musste, da sonst die Aktivität des Katalysators aufgrund der Salzbildung während des Prozesses reduziert wurde. Die katalytischen Membranen wurden mit UV-Licht photovernetzt und die saure Membran durch Zugabe von Salzsäure in Methanol protoniert. Das System funktionierte für die zwei-Stufen Reaktion und es wurde innerhalb von 360 Minuten eine

Ausbeute von 95% für die erste Stufe und 80% für die zweite Stufe erreicht. Die kinetischen Studien zeigten, dass ein Parameter Δt implementiert werden musste, da der zweite Schritt einen deutlich verzögerten Start hatte, da dieser erst begann, nachdem genügend Benzaldehyd zur Verfügung stand.

Da Elektrosponnen ein komplexer Prozess ist, der von 15 verschiedenen internen und externen Parametern beeinflusst wird, wurde eine einfachere Methode mit 2D-Druck getestet. Ein Vorteil dieser Methode bestand darin, dass der saure Katalysator direkt gedruckt werden kann und nach der Verarbeitung nicht protoniert werden musste. Die Ergebnisse waren gegenüber dem Elektrosponnverfahren vergleichbar. Innerhalb eines kürzeren Zeitrahmens von 240 Minuten wurde eine Ausbeute von 95% für den ersten Schritt und etwa 65% für den zweiten Schritt erreicht. Der geringere Umsatz innerhalb des zweiten Schritts kann auf die niedrige Basizität von 4-Vinylpyridin zurückzuführen sein sowie mögliche Beschränkungen durch das voluminösere gedruckte Material. Die angepasste Kinetik zeigte, dass der Parameter Δt ebenfalls notwendig ist und der zweite Reaktionsschritt der geschwindigkeitsbestimmende Schritt ist.

Diese Untersuchungen zeigten, dass beide Systeme vielversprechend waren. Daher waren eingehendere Untersuchungen erforderlich, um festzustellen, ob Elektrosponnen oder 2D-Druck das nützlichere System ist. Um die Anwendungsmöglichkeiten weiter zu erweitern, wurde das Basische Copolymer in Richtung Poly(styrol-co-4-vinylbenzylamin-co-acrylamid-benzophenon) geändert. Dieses spezifische Polymer ist durch die radikalische Polymerisation nicht direkt verfügbar, was es zu einem idealen Kandidaten für die weitere Erforschung der Möglichkeiten macht das Copolymer nach der Verarbeitung chemisch zu modifizieren, um in Zukunft weitere modulare Systeme zu entwickeln. 4-Vinylbenzylphtalimid ist ein möglicher Kandidat, da es durch eine Reaktion mit Hydrazin leicht zum primären Amin modifiziert werden kann. Es konnte gezeigt werden, dass die Behandlung mit Hydrazin die Stabilität der Strukturen weder für das gedruckte noch für das elektrosponnene System beeinflusst. Als Reaktion wurde die Deacetalisierung von Dimethoxybenzyl zu Benzaldehyd gefolgt von einer basisch katalysierten Knoevenagel-Reaktion mit Ethylcyanacetat zu Ethyl-2-cyano-3-phenylacrylat in Toluol und DMF verwendet. Die katalytischen Studien zeigten, dass die 2D gedruckten Strukturen zu schnelleren Reaktionen führen. Die kinetischen Studien zeigten eine Abnahme des Parameters Δt innerhalb dieser Systeme, und die Reaktionsgeschwindigkeit war für die Reaktion im ersten Schritt zehnmal höher und für die Reaktion im zweiten Schritt fünfmal höher von gedruckten Systemen zu elektrosponnenen Systemen. Obwohl es zunächst

überraschend ist, da elektrogesponnene Materialien eine größere Oberfläche aufweisen, ist es durch die Quellung der Materialien erklärbar, die zu einem besseren Massentransport durch das System führt und die Erreichbarkeit der funktionellen Gruppen innerhalb der gedruckten Strukturen verbessert.

2. Abstract

Wolf-Lamb type catalysts are mutually incompatible catalysts. Hence, to use such catalysts within a multi-step one-pot reaction, immobilization through site-isolation of the catalysts is necessary to protect them from each other. Through such immobilization, reaction sequences can be catalysed which otherwise would not be available without an intermediate purification step. The existing Wolf-Lamb type carrier systems contain tri-block copolymeric core-shell micelles, star polymers or inorganic particles which utilise multi-step procedures or procedures valid only for two-step catalysts.

In this thesis, it is the aim to study new recyclable carrier systems of these Wolf-Lamb type catalysts, which are easy to prepare and can be used in one-pot reactions in a modular way. Within the first step, model systems were investigated based on the acidic copolymer poly(styrene-*co*-styrene sulfonic acid-*co*-methacryl benzophenone) and the basic copolymer poly(styrene-*co*-4-vinylpyridine-*co*-methacryl benzophenone) for the use in the one-pot two-step, deacetylation of dimethoxybenzyl to benzaldehyde followed by a carbon building reaction with ethylcyanoformate to cyano(phenyl)methyl ethyl carbonate. The polymeric catalysts were processed to self-standing materials by either electrospinning to porous membranes or 2D printing on a neutral mesh substrate. The polymer acid and base catalyst were prepared in high molecular masses, which is required for processing, by free-radical polymerization of styrene, styrene sulfonic acid (for acidic catalyst) or 4-vinylpyridine (for basic copolymer) and methacryl benzophenone (crosslinking agent). The resulting two-step kinetics were investigated by fitting of the underlying differential equations.

For the electrospun membranes, it was determined that the acidic copolymer needed to be processed as the polymeric salt (poly(styrene-*co*-sodium styrene sulfonate-*co*-methacryl benzophenone)) as otherwise the activity of the catalyst was reduced due to salt formation during the process. The catalytic membranes were photo-crosslinked with UV-light and the acidic membrane protonated by addition of hydrochloric acid in methanol. The system worked for the two-step reaction and a yield of 95% for the first step and 80% within 360 minutes was achieved. The kinetic studies showed that a parameter Δt needed to be implemented as the second step had a significant retarded start as it only started after enough benzaldehyde was available.

As electrospinning is a complex process, which is influenced by 15 different internal and external parameters, a simpler method was tested with 2D printing. An advantage of this method

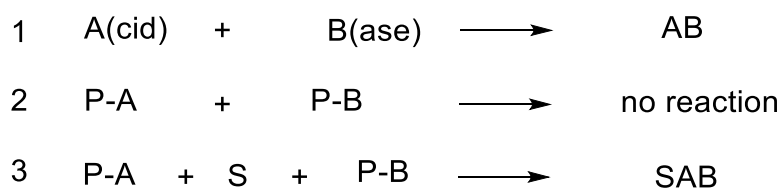
was, that it is possible to directly print the acidic catalyst and it was not necessary to protonate it after processing. The results were comparable towards the electrospinning process. A yield of 95% for the first step and around 65% for the second step, but within a shorter time frame of only 240 minutes. The lower conversion within the second step can be due to the low basicity of 4-vinylpyridine and possible due to the bulkier structure. The fitted kinetics showed that the parameter Δt is also necessary and the second reaction step is the speed determining step.

Through these investigations, it was shown that both systems were promising. Therefore, more in-depth studies were necessary to establish whether electrospinning or 2D printing is the more useful system. To further broaden possible applications, the basic polymer was changed towards poly(styrene-*co*-4-vinylbenzylamine-*co*-*N*-(4-benzoylphenyl)acrylamide). This specific polymer is not directly available through free radical polymerization, which makes it an ideal candidate to further research the possibilities of *post-processing* treatment to develop further modular systems in the future. *N*-(4-vinylbenzyl)phtalimide is a possible candidate, as it can be easily modified to the primary amine by a reaction with hydrazine. It was shown that the treatment with hydrazine influenced the stability of the structures neither for the printed nor for the electrospun system. As a reaction the deacetylation reaction of dimethoxybenzyl to benzaldehyde followed by a basic catalysed Knoevenagel reaction with ethyl cyanoacetate to ethyl-2-cyano-3-phenylacrylate in toluene was used. The catalytic studies showed that the 2D printed structures lead to faster reactions. The kinetical studies showed a decrease of the parameter Δt within these systems and the reaction rate was 10 times higher for the first step and 5 times higher for the second step reaction. While it is surprising at first, as electrospun materials show a higher surface area, it is explainable through the swelling of the substances leading to better mass transport throughout the system and the reachability of the functional groups is improved within printed structures.

3. Introduction

In the 1960s and 70s, polymers were used as carriers for catalysts in organic synthesis due to advantages such as easier purification and possible reusability. The concepts researched were mainly using styrene-based copolymers which were intensively crosslinked using *p*-divinylbenzene. The styrene containing backbone was further functionalized to catalyze the corresponding reactions.^{1,2} The investigation did not stop at that time, however, and has been continued in different forms until the present days, greatly broadening possibilities by functionalizing part of the repeat units or immobilization of catalysts within systems such as complexes or nanoparticles.³⁻⁶

In 1977, *Cohen et al.* used these described systems for heterogeneous catalysis to start the work in multi-step one-pot Wolf-Lamb type reactions. Through the experiences with the immobilization of organic catalysts on polymers to achieve heterogeneous catalytic activities, it was a logical next step to immobilize incompatible catalysts on polymeric substrates, which is described by his concept shown in Scheme 1.^{7,8}



Scheme 1: Concept of *Cohen et al.* for the multi-step one-pot reaction. (1) If A (Acid) and B (Base) were not immobilized on the polymer deactivation would be observable, (2) bound on a polymeric (P) structure they would not interact with each other. (3) By addition of a Substrate (S) both steps can take place and the one-pot multi-step reaction occurs.⁸

Normally, catalyst A and catalyst B would react with each other (e.g. Acid and Base) and hence deactivate each other. Through the immobilization, this reaction is prevented and the reaction with reagent S can be observed. Through this, it was possible to open the field for further studies of such multi-step one-pot reactions within different concepts.^{8,9}

In the following, we want to use the concept of immobilization of catalyst by the use of 2D printing and electrospinning as common processing techniques.^{10,11} The general concept is focused on applicability, which means that the polymerization techniques should be easily up-scalable, such as with free radical polymerization.^{12,13} To enable stability in an organic solvent, a crosslinking unit was included as they are an easy way to implement post-processing crosslinking by exposure to UV light.^{14,15} These structures could be further treated or

chemically modified to obtain necessary functionalities, either by protonation or chemical modification such as deprotection reactions. In this case, the chemical functionalities must be chosen correspondingly. The obtained functional materials can be applied easily in catalytic studies and the kinetics can be observed to enhance the understanding of such model systems.

3.1. Wolf-Lamb type catalysis

Wolf-Lamb type catalysis, as described within the introduction, are catalysts which are mutually incompatible with each other. To use them in multi-step one-pot reactions, it is necessary to immobilize these incompatible catalysts within a matrix, which helps to protect them from each other to prevent deactivation. Depending on the systems, the concept can be divided in inorganic porous material such as metal-organic frameworks (MOF)¹⁶ and zeolites¹⁷, nanoparticles as carrier material¹⁸ or polymeric materials in which a variety of concepts exist, starting from microcapsules^{19,20} and star polymers²¹ to hyper-crosslinked networks²² showing different advantages and disadvantages. In more recent studies, the development of such systems can be described in different ways. Mainly, but not exclusively^{20,23}, acid and base reactions are investigated as easy approachable conceptual reactions.^{22,24}

The systems used for organocatalysis^{23,25} or redox systems are generally complex self-assembled or multi-layered particles²⁰. With such systems, it is possible to combine reactions such as a reduction followed by a Diels-Alder as done by *Ueda et al.* (Figure 1).²³ This combination shows the possibilities of such site-immobilization in catalysis. Nevertheless, it also clearly shows the downside as the structures are difficult to obtain and reuse.

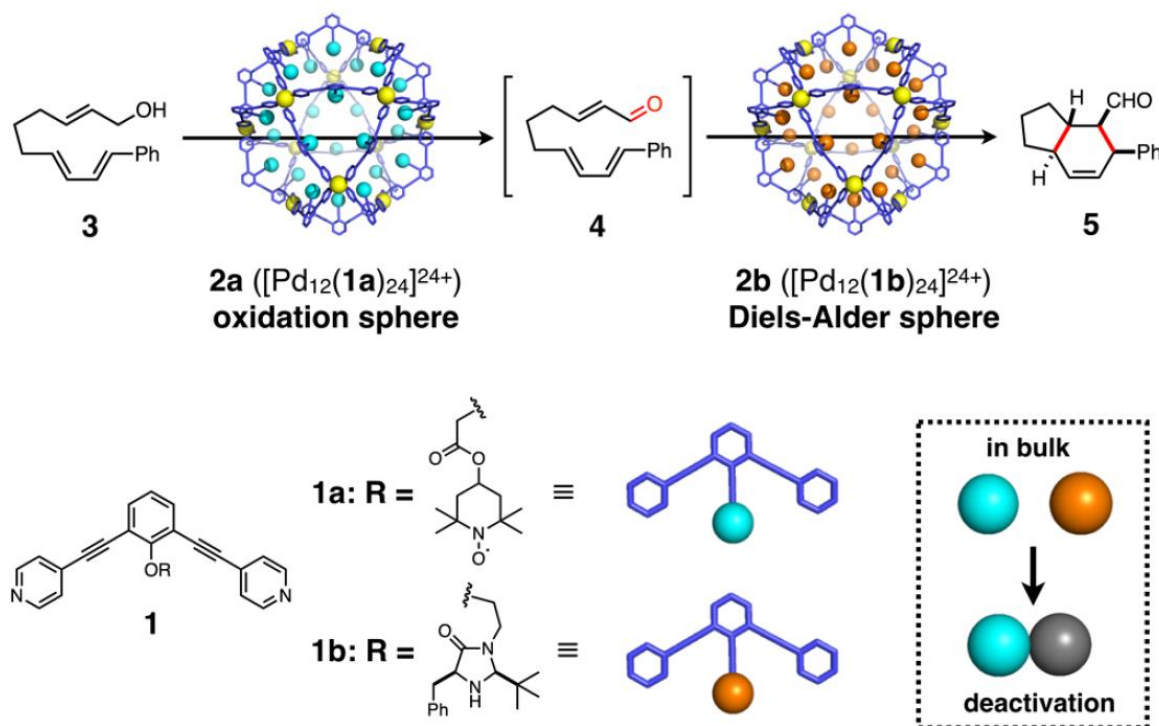
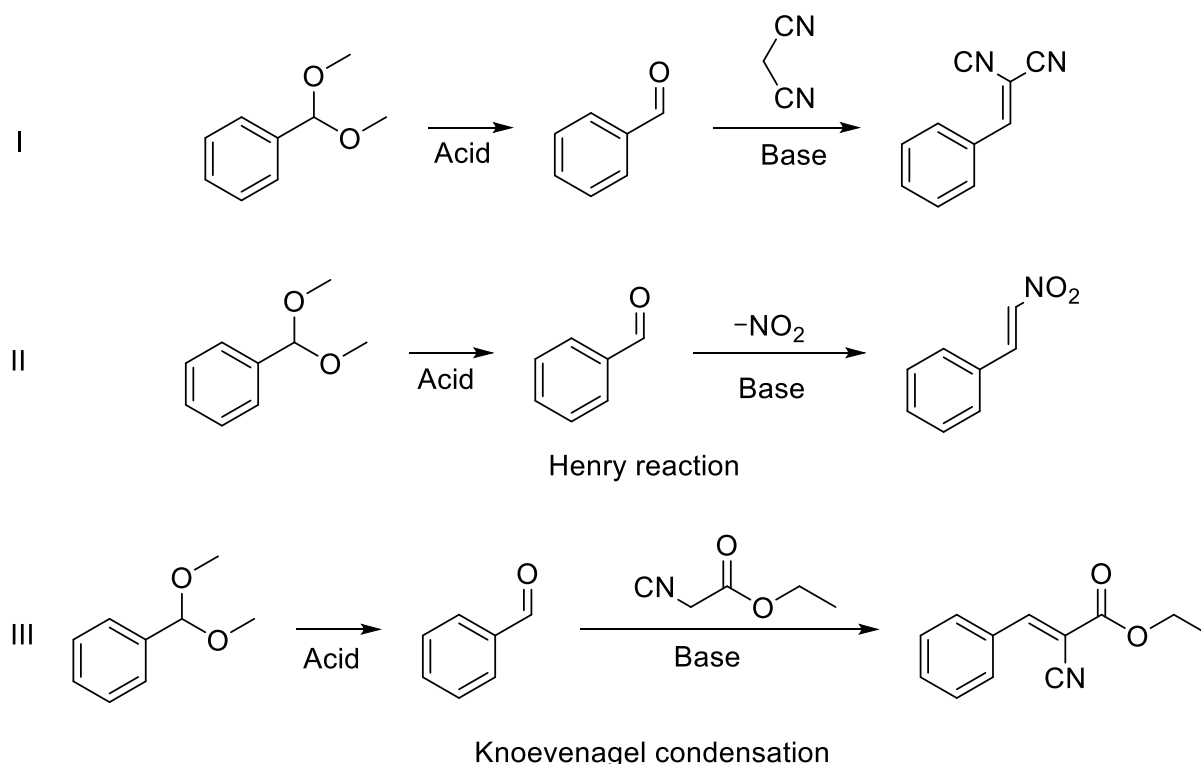


Figure 1: Tandem reaction of the reduction followed by Diels-Alder with the corresponding site-isolation strategy in self-assembled spheres. Reprinted with permission of the publisher.²³

This clearly shows the necessity of further studies. To work around the problem of expensive organo-catalyst which are difficult to synthesize, acid-base reactions are an easy and up-scalable system for such model reaction. The studied reactions with the use of such acid-base reactions mainly contain a deacetylation followed by a C-C bonding reaction such as a Henry reaction (Scheme 2 (I/II)) or a Knoevenagel condensation (Scheme 2 (III)).²⁶⁻²⁸



*Scheme 2: Most commonly studied acid-base reactions within two-step one-pot reactions. Generally, the first reaction contains a deacetylation of dimethoxybenzyl followed by a C C forming Knoevenagel or alternatively Henry reaction.*²⁶⁻²⁸

3.1.1. Inorganic Wolf-Lamb type catalysts

Highly porous materials such as MOFs²⁹⁻³¹ and Zeolites³²⁻³⁴ are widely used as inorganic carrier systems for catalysis as they show a high intrinsic surface area promoting catalytic activity. Consequently, it is not surprising that these advantages are also studied and converted towards incompatible catalyst containing one-pot multi-step reactions. Both catalysts have similar advantages as they have the aforementioned high porosity and a general composition which can be directly used as the immobilization site for the catalyst. In case of zeolites, the group of *Shi* showed that the silica surface can be chemically modified to obtain a surface with amine groups as Lewis bases and protonated aluminium silica oxide groups as Bronsted acids.¹⁷ These silica materials can further interact with each other, leading to a hierarchically structured

material. Through the combination of zeolites and polymers, it is also possible to obtain the desired functionalities. Here, *Kalbasi et al.* showed a system containing a hierarchical zeolite as the acidic component combined with poly(vinylimidazole) as a basic catalyst leading to promising and interesting results with the combination of the deacetylation, followed by a Henry reaction as well as Aldol condensation (*Figure 2*).³⁵ However, not only are hierarchically structured zeolites investigated, but also zeolitic materials with modifications leading to sulfonic acid and amine groups within the structure to obtain highly mesostructured acid-base dual catalyst showing high catalytic activity and selectivity for the Knoevenagel reaction product as well as overall interesting and promising results.³⁶

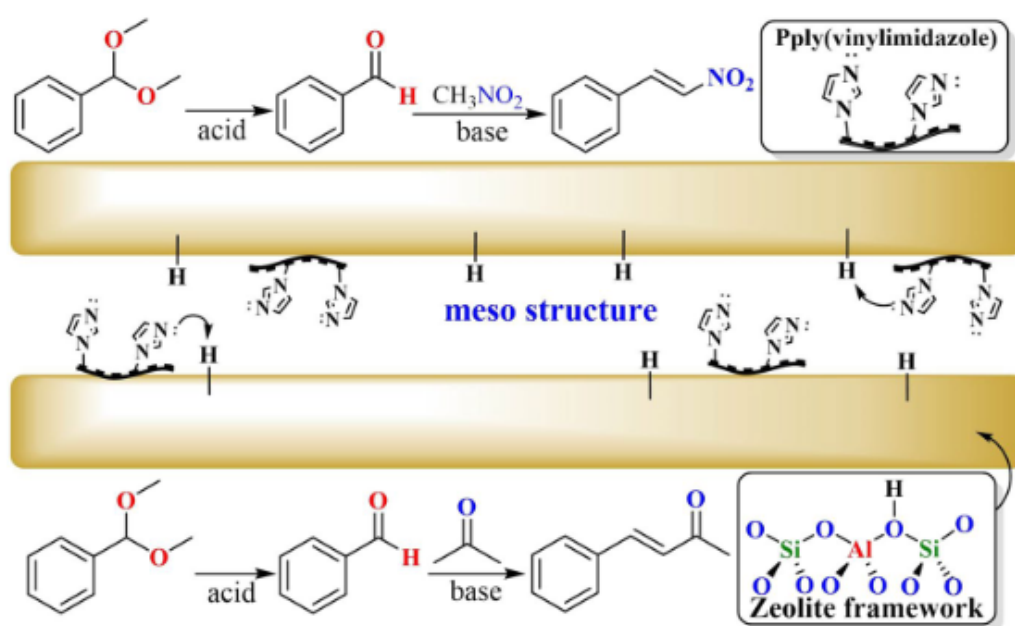


Figure 2: Layered zeolite used as a catalyst for acid-base two-step reactions by *Kalbasi et al.* Reprinted with permission of the publisher.³⁵

Similar to zeolites, MOFs are also used as catalytic carrier materials due to their high intrinsic porosity. MOFs are built from metal cluster as secondary building units combined with bridge ligands as linkers leading towards a 3-dimensional porous crystalline network.³⁷ In the case of multi-step one-pot reactions, the secondary building units as well as the linkers offer opportunities for chemical modification and immobilization of catalytic sites such as acids and bases.^{16,25,38,39} A commonly studied MOF for catalytical studies is MIL-101.^{40,41} This specific MOF is built with terephthalic acid groups as the linkers, which were modified with nitro groups to enable later reduction towards a primary amino group. The sulfonic acid group is coordinated at the Chromium ion. Used for the SBUs, it is leading towards a bifunctional material.⁴² As for zeolites, the same concept of the combination of porous material with *in situ* polymerization

within the porous structure exist as shown by *Zhao et al.* In this case, they incorporated separately within MIL-101 poly(styrene sulfonic acid) and poly(4-vinylbenzylmethylaminopyridine), obtaining basic and acidic modified MOFs showing the protection of the catalytic sites from each other.⁴³ Other MOFs used for multi-step one-pot catalysis are Lanthanoid based as by *Zhang et al.*³⁸ where they used Carboxylic acid groups on the SBUs and Amine groups on the linkers. Another newly synthesized material contains cadmium-based metal centres which, in itself, has Lewis acidity and base groups through azine and pyridine groups immobilized on the specific linkers.⁴⁴

While porous materials are interesting, further inorganic layer structures are another possible immobilization way with high surface area. Comparable to the aforementioned layered zeolites, (organo)aluminosilicate layers are another structure on which functional groups such as sulfonic acid and amine groups can be immobilized and further investigated (Figure 3).^{45,46} These structures, however, are not limited to only (organo)aluminosilicates but also to other layered carrier system structures such as chrome supported magnesium-aluminium hydroxide.⁴⁷ Other similar concepts contain layered clays⁴⁸ and mesoporous materials such as carbonitrides.^{49,50}

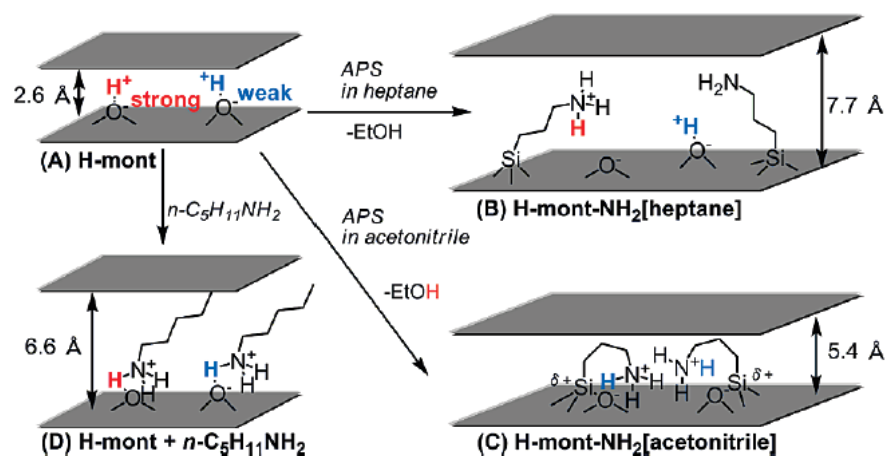


Figure 3: Concept of layered systems for acid-base one-pot reaction, the surface can be used as the acidic catalyst and basic catalysts are immobilized within. Reprinted with permission of the publisher.⁴⁶

Nanoparticles have similar advantages as the previously described mesoporous materials. They have a very high surface area, which can be further functionalized to obtain the desired catalytic sites. Nevertheless, stability of such nanoparticles are of the utmost importance as nanoparticles either without polymeric or charge stabilizer tend to agglomerate.⁵¹ One type of the

nanoparticles used are mesoporous silica nanoparticles.⁵² These nanoparticles contain within pores of 20 -25 Å, either amine or phenyl sulfonic acid groups.¹⁸ Through these placements of catalytic sites, the catalytic groups are separated and can be used actively. A higher complexity is achieved through immobilization within core-shell nanoparticles as done by *Li et al.*,⁵³ where they synthesized the core first and, after an oxidation step, they coated it with the amino groups containing silica.⁵⁴ One of the problems with such systems is the recyclability and reusability of such particles. While they should theoretically stay active, the recyclability of such nanoparticles can be difficult. To solve this specific problem, the group of *Hyeon* introduced Magnetite within these mesoporous particles and the particles showed good reusability while being easily recovered with a magnet (*Figure 4*).⁵⁵ A similar concept was used by *Zhang et al.* where they grafted sulfonic acid and amino groups directly on the surface of the Magnetite nanoparticles.⁵⁶

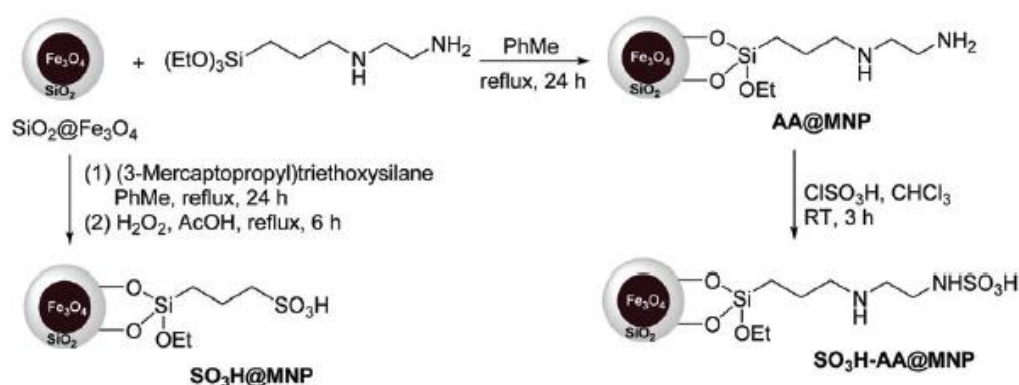


Figure 4: Preparation of nanoparticles as carriers for acid-base catalysis with a core of magnetite. Reprinted with permission of the publisher.⁵⁶

3.1.2. Polymeric Wolf- Lamb type catalysts

Just as the inorganic catalysts can be divided in different categories, polymeric multi-step one-pot catalysts can also be divided in nanoreactors¹⁹, gels⁵⁷ and some special forms which are mixed. In case of nanoreactors, complex polymeric architectures are used to immobilize the catalyst within the structure to obtain a homogeneous catalyst system which prevents deactivation through the special structure. One such example are the star polymers as investigated by the group of *Fréchet*.^{24,58} In this case, they used the core of the star polymers for the confinement of catalytic acid and base sites (*Figure 5*).

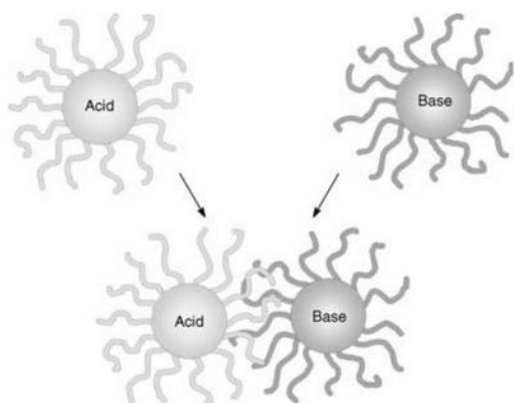


Figure 5: Immobilization of the incompatible catalysts within different star-polymers to prevent deactivation through steric repulsion. Reprinted with permission of the publisher.⁵⁸

Through steric hinderance, deactivation is prevented and the studies for the two-step one-pot reaction showed promising results. Micellar structures or crosslinked micelles are similar. The core of the micellar structure generally contains the base, while the outside part contains acid groups, leading to similar results (*Figure 6*).²¹ Alternatively, the micellar head contains both carboxylic acid and primary amine groups .⁵⁹

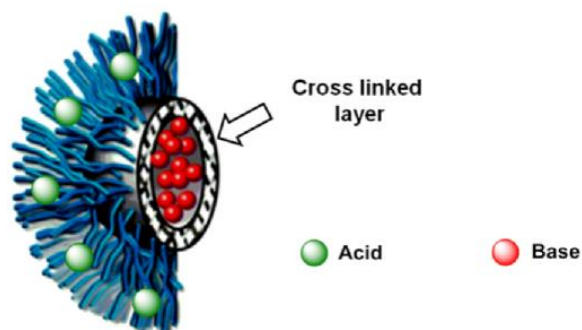


Figure 6: Crosslinked micellar structure containing bases within the head and acids on the tails of the structure used in one-pot acid-base reaction. Reprinted with permission of the publisher.²¹

A special form of such mesostructured nanoreactors are crosslinked bottlebrushes.⁶⁰ These special micellar structures either contain *p*-toluene sulfonic sulfonic acid or *N,N*-dimethyl-4-pyridineamine which are prepared by adding a RAFT agent to poly(glycidyl methacrylate) which works as a core for the brush material. The polymeric brushes are then prepared by sequential polymerization of the acid or basic groups together with a crosslinking unit, followed by *N*-isopropylacrylamide to enhance steric hinderance and stability.⁶⁰

While these nanoreactors and micellar structures are as interesting as polymeric catalysts, they do have specific disadvantages as they have limited reusability and synthetic procedures for star polymers are difficult. One of the existing concepts to prevent these problems is the use of gels and porous polymeric structures. One commonly used approach is the synthesis of styrene-based structures, which is extensively crosslinked through, e.g., divinyl benzyl units. Depending on the concept, there are two approaches as regards the functional material. The functionality can either be introduced in one material or two. If two materials are chosen, one polymer contains groups such as styrene sulfonic acid copolymerized with divinylbenzene as the acidic copolymer and *N*-vinylimidiazolate within the basic structure.⁶¹ In case of a single material, the functionality is achieved through the usage of styrene sulfonic acid as a comonomer and the later introduction of nitro-groups which are reduced towards amines within a second step.²² Such polymers can be achieved easily through free radical polymerization. The use of a reversed emulsion polymerization can lead to interesting results as shown by the group of *Degirmenci*. They developed a system to obtain highly porous structures with a phase volume ratio of 99% (Figure 7). The system itself contains styrene, divinylbenzene and 4-vinylbenzylchloride and can be modified by ATRP with *t*-butyl acrylate which can be hydrolysed towards acrylic acid for the acidic catalyst. The basic catalyst was prepared by grafting glycidyl methacrylate which can be further modified with diethylamine to obtain the basic catalyst.^{62,63}

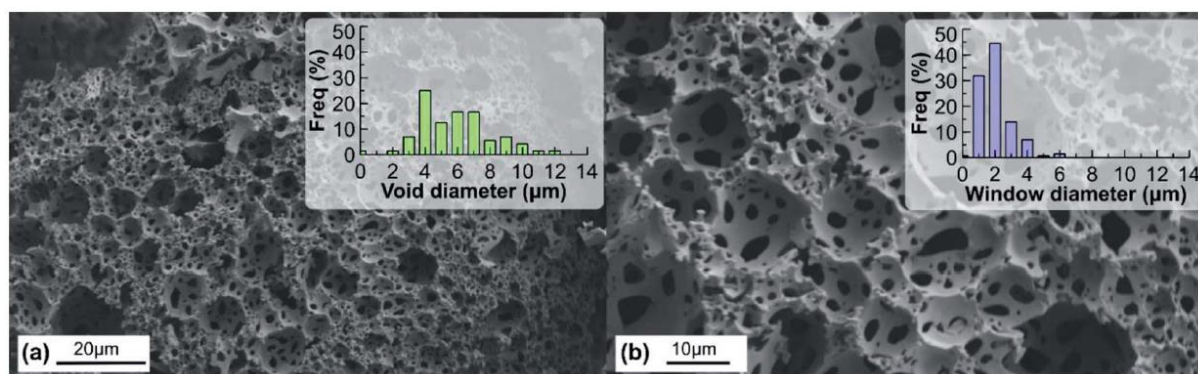


Figure 7: SEM images of the high internal phase emulsion templated polymer (PolyHIPE) material synthesized by the group of *Degirmenci*. High porosity with a phase/Volume ratio of 99% was achieved. Reprinted with permission of the publisher.⁶²

Another approach towards such hyper-crosslinked polymers is the use of benzene and either acidic or basic functionalized benzene, which are polymerized with the addition of formaldehyde dimethyl acetal. In this case, it is possible to directly synthesize the corresponding acidic and basic copolymers without further treatment, having advantages in

terms of time and cost efficiency. The overall catalysts work reasonably well within 5h for full conversion.⁶⁴

Further special morphologies studied are hollow tubes and tube-networks, which might have advantages as a result of the mesostructures. Microporous organic nanotube networks are one of the promising mesostructured materials. The hollow tubes were synthesized by a template method through multiple steps, containing bottlebrush copolymers with functional brushes with either styrene sulfonic acid as acid groups or ethylamine as basic groups within the middle block.⁶⁵ Further studies also showed a way to introduce both groups within one microporous organic nanotube network by reduction of introduced amino-groups.⁶⁶ Another system of hollow tubes contains a system which is polymerized 4-tritylanilin with dimethoxymethane, which can later be carbonized through pyrolyzing and easily modified by grafting sulfonic acid groups.⁶⁷

3.2. Kinetics of multi-step one-pot reactions

One of the problems with the current studies is the lack of kinetic studies. While a vast variety of concepts exist, the reaction times seem to be chosen randomly for the most part or through experience. To further stretch out the use of such reaction, it is important that the underlying kinetics are observed and understood to optimize reaction times and compare systems with each other to find the optimal support for such catalysts.

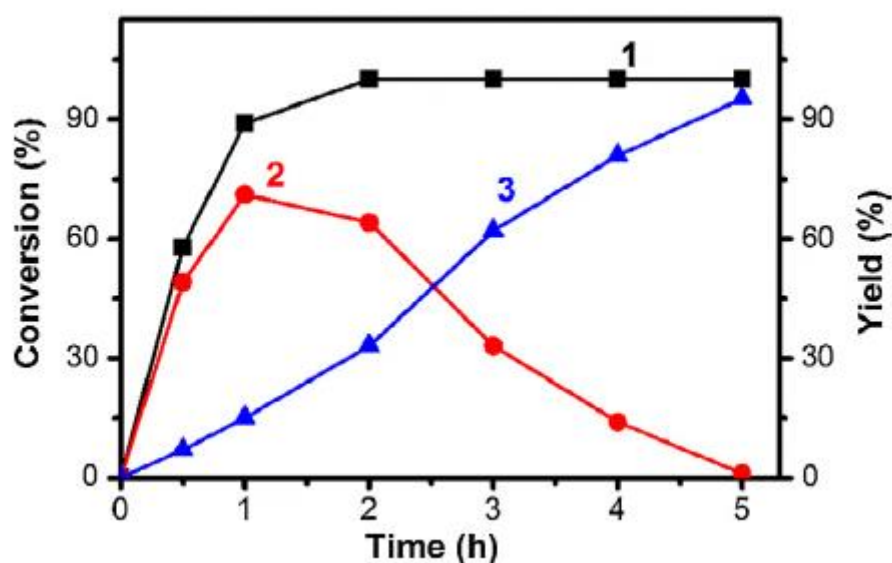


Figure 8: Kinetic studies performed by Wang et al. for an acid-base two-step one-pot reaction. Reprinted with the permission of the publisher.⁶⁴

Wang *et al.* was one of the few people showing the reaction kinetics of such a reaction (Figure 8).⁶⁴ Nevertheless, no further calculations of the studies are performed, thus limiting the overall help of the kinetics. With the help of kinetic parameters, it would be possible to compare the two-steps with information concerning the speed-determining step. Without this, the only information obtained is the timeframe of the reaction. While clearly necessary, further studies are important to compare different systems with each other and to improve the overall understanding.³⁹

The kinetic of a reaction can be described with the help of the general reaction equation depending on the reaction order. Reaction with a first order kinetic is a reaction only showing a unimolecular reaction (Equation 1) and hence the reaction kinetic is only dependent on the concentration of the initial material.⁶⁸

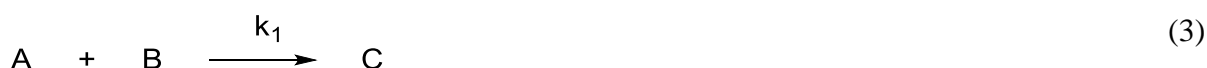


A general reaction described by this is the radioactive decay. The reaction equation can be converted towards a calculation describing the change of concentration c_A (Equation 2) depending on the time t and the kinetical parameter k_1 .

$$\frac{-dc_A}{dt} = k_1 \cdot c_A \quad (2)$$

While this is only limited to very few reactions, it is also true for reaction with a pseudo first order kinetic. This means that the second reaction partner is available in a theoretical unlimited amount, for example, if the second reaction partner is the solvent.⁶⁹

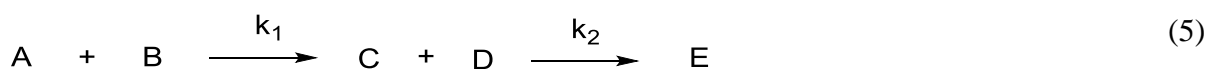
For the second order reactions, the reaction equation describes the involvement of two substrates within the reaction (Equation (3)).



For second order kinetics, the reaction rate is not only dependent on the concentration of substance A, but also on substance B. Hence, it can be calculated by the following differential equation (Equation 4).

$$\frac{-dc_A}{dt} = k_1 \cdot c_A \cdot c_B \quad (4)$$

With the help of this reaction, the kinetics of a reaction can be described. There are possibilities to further solve these differential equations. While this is enough for the general types of reaction, it is slightly different for reaction of the type observed within multi-step one-pot reactions. Within these reaction types, the dependence on the simultaneous working reactions is necessary to elaborate on this topic.⁶⁸ While the reaction equation is comparable to the other aforementioned reactions, the second reaction step is highly dependent on the conversion from the first step leading through the reaction equation (Equation (5) towards Equation (6)).



$$\frac{-dc_C}{dt} = k_1 \cdot c_A \cdot c_B - k_2 \cdot c_C \cdot c_D \quad (6)$$

3.3. Methods for polymer processing

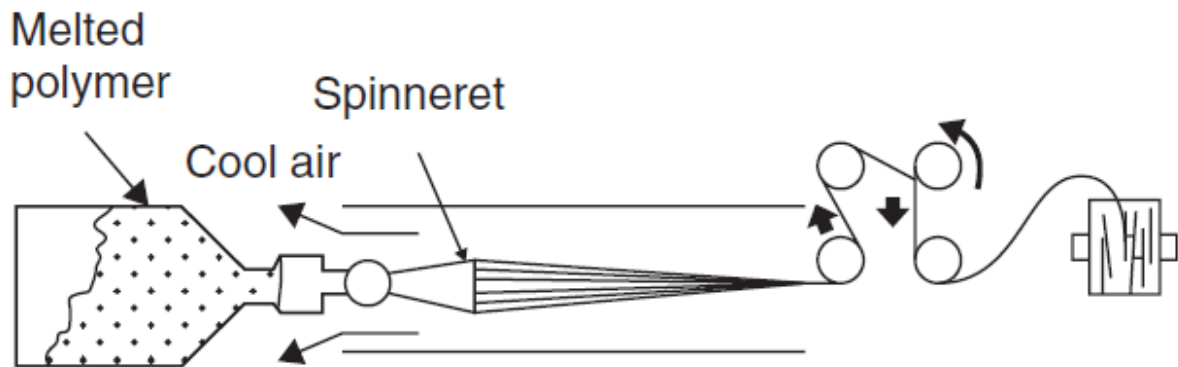
A vast variety of techniques exist to process polymers such as extrusion, melt-blowing and many more. The production of fibers and patterned materials are relevant in this thesis. Within the production of fibers, electrospinning is a technique widely used for fiber formation, especially in research as it is easy to apply and reproduce. It is possible to obtain nanofibers to further study the properties of the material. For the patterning of polymers, a printing technique is desirable. The printing of the polymers leads to a good production speed and reproducibility.

3.3.1. Electrospinning

To obtain polymeric fibers, there are different possibilities, depending on the desired diameter of the fibers and the specific polymeric material used. Some of these techniques are melt spinning^{70,71}, wet spinning^{72,73}, dry spinning^{74,75} or gel spinning^{76,77}. These interesting techniques, on which will be elaborated in the following, usually have diameters above 5 μm . Another method for polymeric fiber production is electrospinning, which can be easily applied in a lab space; fiber diameters from around 100 nm up to around 5 μm are reachable, thus making it an interesting technique to produce fibers within this diameter range. Due to the interesting and good mechanical properties of such fibers, the technique is reaching into industrial application, especially with new technologies such as nozzle-free electrospinning.^{78,79} With such small diameter, the surface chemistry increases and is an important factor for their unique properties. Furthermore, special preparations even enable sub-nanometer diameters as shown by *Jiang et al.*⁸⁰

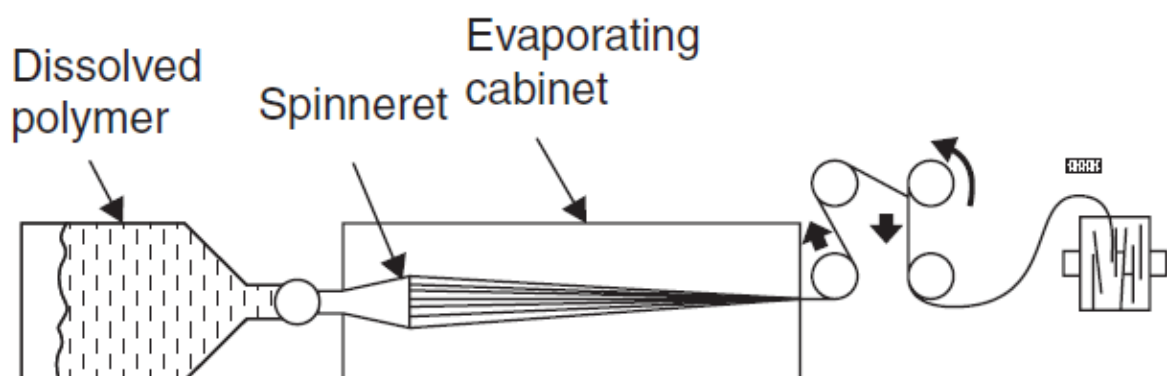
Generally speaking, in order to induce a spinning process, the polymer needs to be converted into a viscoelastic state to be processed into fibers without breakage of the polymers. For this, different techniques exist such as melting or dissolving the polymer, which will be briefly shown in the following steps.^{10,81}

Melt spinning: A melt spinning process (Scheme 3) can be used for polymers which can be extruded. In this case, the polymer is placed in an extruder, plasticized and extruded through a spinneret, which leads to multiple fibrillose structures. During the drawing process with multiple rolls, an orientation is obtained through the high speed of these. Within the first 50 cm, no orientation is observed, followed by an oriented meso phase until 140 cm, which leads to the building of molecular oriented fibers.^{70,82}



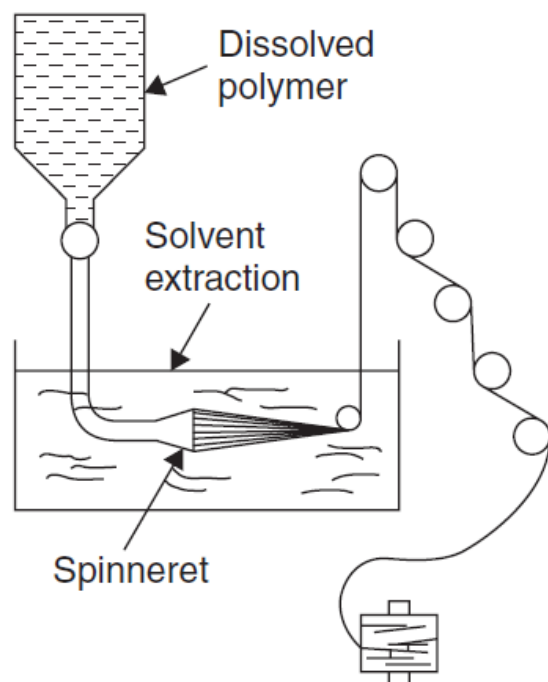
Scheme 3: Example of a melt spinning process; the polymer pellets are plasticized and pressed through a spinneret. The polymer is then stretched through multiple rolls and heated to anneal and collect them. Reprinted with permission of the publisher.⁷⁴

Dry spinning: The viscoelastic state of the polymer cannot only be achieved through the melt but also through a solution with appropriate solvents. This is especially desirable in case no melt of the polymer is obtainable. During the spinning process, the solution is pumped through a spinneret and the polymeric solution is dried by hot air (Scheme 4). The requirement is that the evaporation pressure is high enough to enable quick drying. This heating then leads to the evaporation of the solvent and the fiber formation, which can be stretched and aligned with heat and a roll system.⁷⁴



Scheme 4: System for the dry spinning of a polymeric solution. The polymeric solution is then dried within a drying chamber and collected. Reprinted with permission of the publisher.⁷⁴

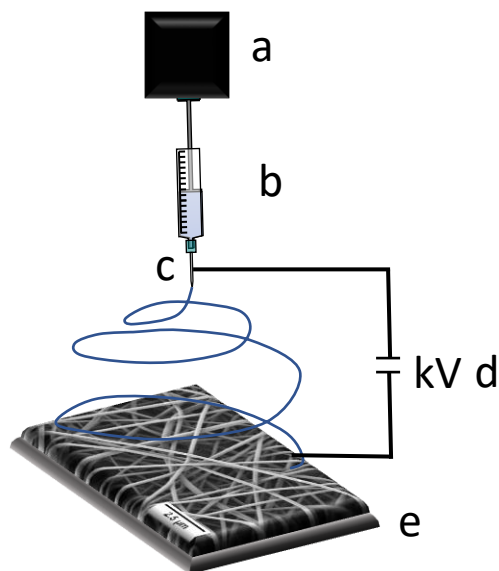
Wet spinning: If the evaporation pressure is too high, dry spinning might not be possible. Therefore, the polymeric fibers can be processed by the wet spinning in which a coagulation bath of a chemical solution is used, which is not able to dissolve the polymer but the solvent. During the coagulation process, the polymer solidifies and is later dried outside of the bath to obtain polymeric fibers (Scheme 5).¹³



Scheme 5: Wet spinning system. The fibres are obtained through the coagulation bath. Reprinted with permission of the publisher.⁷⁴

In the process of electrospinning, a polymer solution is placed in a syringe attached to a syringe pump which manages a constant flow rate through the needle. In such case, a high voltage is applied between the needle and the collector on which the fibers are collected (Scheme 6). Depending on the desired application, different collectors are possible such as a rotating round disc collector, which leads to a more homogeneous distribution of fibers as a membrane, a stationary plate collector which leads to randomly stationed fibers or a rotating wheel collector, which can be used to obtain homogeneously aligned fibers with a high orientation factor, which can be used, for example, in responsive polymers for switchable tubes.^{83,84} Not only is the collector changeable depending on the desired application, but the nozzle itself can also be changed. While the normal single nozzle is great to obtain homogeneous fibers from solution,⁸¹ side-by-side nozzles can be used to spin different polymers on multicomponent fibers⁸⁵ as well as to obtain unique morphologies such as nano springs⁸⁶ or pearl-chain structures.⁸⁷ Other nozzles are the coaxial or triaxial nozzles^{88,89}, which can be used to obtain core-shell structures⁸⁸,

hollow tubes⁸⁹ with or without incorporation of other materials such as nanoparticles⁹⁰, or to load polymeric fibers with different materials such as drugs or bacteria^{91,92} inside. In addition, fibers can be loaded with different structures such as nanostructures either within⁹³ or on the surface⁹⁴ for a multitude of applications. To obtain multicomponent membranes, multiple nozzles can be used at the same time.⁹⁵



Scheme 6: Setup for a conventional electrospinning experiment. a: Syringe pump, b: Syringe with polymer solution, c: Nozzle as electrode, d: DC current source with high voltage, e: collector as counter electrode.

The process itself is influenced by external parameters such as temperature, humidity and air pressure as well as the applied high voltage and distance of electrode influencing the electronic field. Internal parameters which influence the process are the viscosity and conductivity as well as the surface tension of the polymeric solution. The polymer, with its molecular structure, the molecular weight distribution and its specific solubility, is also influencing the result. This explains that the process, while sounding generally easy to apply, can be influenced in many ways and difficult in some cases.^{11,81}

The general process is as follows: At the tip of the syringe, a polymeric solution droplet is found. From this, a jet is formed which stretches the polymeric solution towards the counter electrode. The jet is only stable for a very short distance until it becomes instable and moves laterally and forms a cone. This lateral movement is influenced by different physical instabilities such as the Rayleigh instability which depends on the applied electrical field, asymmetrical instability and

the bending instability. These instabilities result in the stretching and bending of the jet, and thus playing an important role in the building of the nanofibers.^{11,81,96}

The Rayleigh instability⁹⁷ is the result of to the opposing forces of the surface tension, which tries to decrease the jet diameter and the repulsion of the electrostatic charges on top of the surface of the jet. Depending on the fluid, at some point, one of these forces will be dominant. In case of polymers, with high molecular weight and high viscosity solutions, the diameter will decrease continuously until a solid fiber is obtained.⁹⁶ The axisymmetric instability is generally driven by the change of surface charge density during the general spinning process at the jet, resulting in tangential forces, and can lead to the formation of beads.^{11,81} The bending instabilities are dependent on the applied electrical field and are modified by the conductivity of the electrospinning solution, for example through the addition of additives. During the process, the jet is bended in a lateral way, leading to a loop which increases with further distance. This loop formation further thinning the diameter of the resulting fiber.^{11,81}

3.3.2. Printing of polymers

The printing of polymers, also known as additive manufacturing, is a technique which mainly started in the early 2000s and is becoming continuously more important as it leads to structures which would otherwise not be available through standard processing techniques such as injection molding. It furthermore has great possibilities for fast prototyping without the necessity of new tools. Therefore, it is an ideal candidate for both industrial as well as research applications, as the scale of the 3D printer can be realized in a lab scale, explaining the success of this technique.⁹⁸⁻¹⁰⁰

Generally, there are four different ways to print structures, namely material jetting^{101,102}, vat polymerization^{103,104}, powder bed fusion^{105,106} and material extrusion^{107,108} (*Figure 9*). The optimal technique depends on aspects such as the specific polymer, the desired application and form as well as the possible curing techniques. Hence, the optimal printing way can be chosen and adjusted individually.

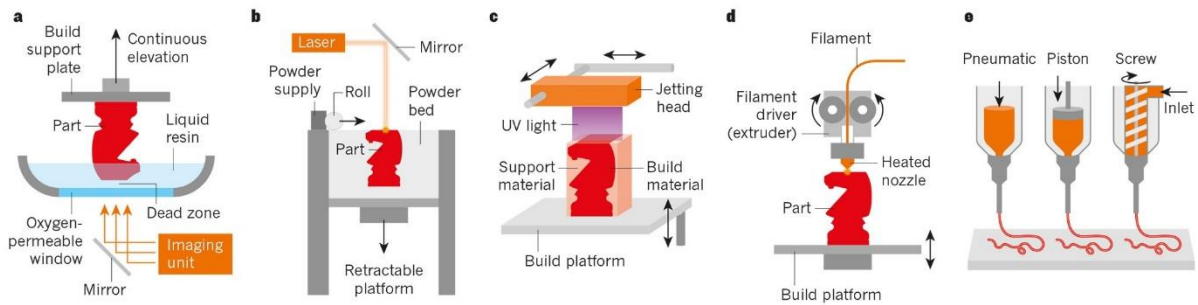


Figure 9: Different methods for 3D printing of polymers. Reprinted with the permission of the publisher. (a) Vat polymerization (b) ink-jet printing and (c) powder bed fusion (d) and (e) material extrusion. Reprinted with permission of the publisher.¹⁰⁹

Material Extrusion: The printing material is extruded by mechanical force through a nozzle to form a continuous filament, but viscoelastic solutions are also possible. The filament is placed on top of a platform with either the nozzle or the platform being able to be moved in x-y-z direction to form the desired structure within multiple layers. If necessary, the system can be modified by addition of a curing system to stabilize the structure. Different possible extrusion techniques exist while the most common one presumably is the use of a filament which is transported through rollers towards the heated liquefier. A pneumatic system also exists for viscoelastic liquids. In such case, it is melted, and the melt can be pressed through the nozzle to lead to the substrate. The optimal temperature depends on the polymer and, generally speaking, a higher temperature reduces the viscosity of the melt and is therefore better for the final product. It also increases the overall performance of the material. However, if the temperature chosen is too high, it can result in thermal degradation and the mechanical stability can drop significantly.^{101,110–112}

Material jetting: Material jetting can be called ink-jet printing. Droplets are formed which are deposited on a substrate in the desired form. Two different ways for Material jetting exist with Continuous Inkjet printing and Drop-on-Demand printing. For both systems, the substrate is placed on a platform, which is moveable x-y-z direction, and a curing system is available such as UV light or heat. Continuous Inkjet printing is, as the name suggests, a constant flow of droplets. These droplets are charged, and an electrical field is applied to deflect droplets which are not needed. For Drop-on-demand, droplets are only deposited on the substrate through a force such as air pressure when they are needed.¹¹⁰ While the deposition speed of the Drop-on-Demand method is slowed, it has a higher resolution than the Continuous Inkjet printing. The

printing of 3D structures is more challenging as in other printing techniques as the material is still liquid during its deposition.^{110,113,114}

Vat polymerization: Vat polymerization is a technique used to print through light activated polymerization techniques. The process is introduced by the emission of light towards the polymerizable liquid photopolymer to form the desired structure in a layer-by-layer way. The targeted introduction of light can be achieved through different methods, e.g. through specific mirrors or liquid-crystal masks, which can improve the printing speed greatly. The material basically has two necessities. The first necessity is that it must be photocurable with a system sensitive to specific wavelength, leading to linking through radical, cationic or both reactions. The second necessity is a low viscosity of the system as no distributor is used.^{104,110,115}

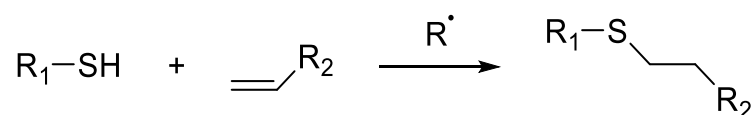
Powder bed fusion: Powder bed fusion is a three-step process: First, the powder is distributed homogeneously. Second, through a laser and heat, the polymer is melted as specified positions to obtain the desired structure. The last step is the down movement of the platform to restart the process. To obtain a high printing speed, the temperature within the printer is kept slightly lower than the softening point of the material to enhance the sintering speed with the laser as the material must not be heated from low temperatures. To prevent problems with quality through, e.g. shrinkage, the size of the polymeric powder is between 10-100 μm , leading to structures above 100 μm .^{110,116,117}

3.4. Crosslinkable material for electrospinning and printing

Crosslinking within materials is either used to obtain special mechanical properties or stability within water or organic solvents. It can be achieved either through physical linkers or covalent bonding. Both mechanisms are used in such materials and a variety of possible units exist to obtain the crosslinking properties. The mechanism which can be used as well as the crosslinking depend on the structure of the polymer, but it can only be crosslinked after processing, as otherwise the material would not show the necessary shear viscosity in solution which is a key property for successful printing and electrospinning.¹¹⁸

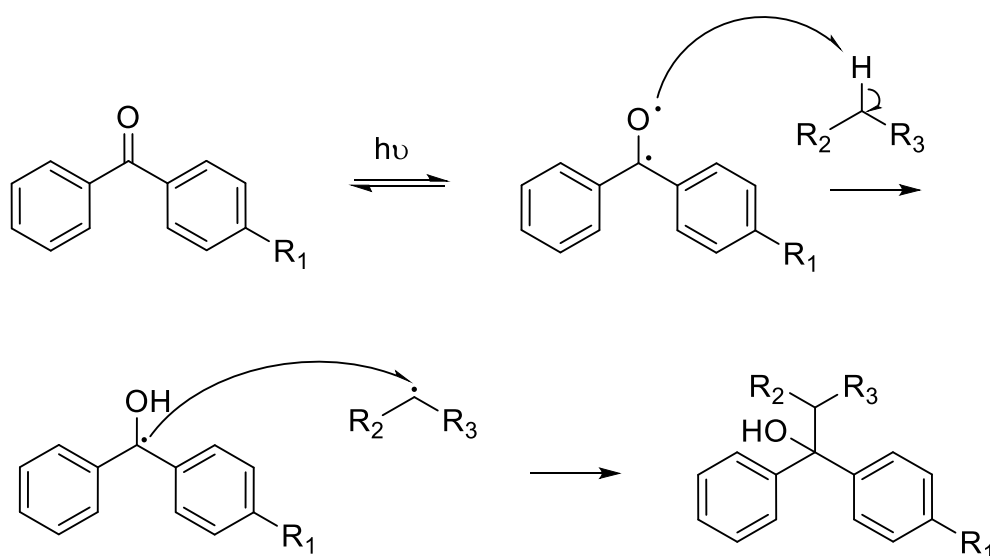
Crosslinking through physical means can help to stabilize structures and increase the mechanical properties for both electrospun membranes and printed structures.¹¹⁹ If a polyelectrolyte is used as the material, physical crosslinking is possible through the use of ions as crosslinking units.¹²⁰ Further heat treatment can be applied to melt together the structures and increase the mechanical stability through the connected junction points.¹²¹ Another way to apply a fusion within the structures, especially for electrospinning, is the use of junction fusion. In such case, the distance of the electrospinning process is adjusted in a way that a slight amount of solvent stays at the fibers and thus leads to the fusion of the fibers.¹²²

In contrast to physical cross-linking, the strength of covalent bonded materials is increased, but the brittleness can increase as well. Click-chemistry is a possible way to introduce covalent bonding within polymeric structures. It is interesting to see that it is highly selective in this case and, due to their thermodynamically favorability, mild conditions are possible. One possible reaction is the introduction of thiol-ene click chemistry. The thiol group can be activated through a radical reaction, which then reacts with alkene groups, followed by the abstraction of thiol-hydrogens for the continuous reaction. The fact that the reaction is not inhibited by oxygen (Scheme 7)^{123,124} is advantageous for the use of this crosslinking method within fibers or printed structures.



Scheme 7: Thiol-Ene click chemical reaction. The radical reacts with the thiol-group by hydrogen abstraction which can then react with the alkene group and start a new reaction by hydrogen abstraction.

Another widely used method for covalent crosslinking is the use of methyl acryloyl anhydride as a crosslinking agent. This unit can react with functional groups of the polymeric material, e.g. amine or hydroxy-groups, leading to a photo-polymerizable functional group within the polymeric backbone. Especially for printing techniques, the crosslinking can be achieved directly during the process, enabling solutions with low viscosity, however, similar effects can be achieved in electrospinning.¹²⁵⁻¹²⁷ For copolymers, it is possible to incorporate crosslinking units directly within the polymer by functionalization with, e.g., benzophenone as a UV-crosslinking unit. Under UV radiation, a diradical is built which can abstract hydrogen of any place within the polymer, leading to good covalent crosslinking (Scheme 8).¹²⁸



Scheme 8: Mechanism of the crosslinking procedure of benzophenone. Under UV radiation, a diradical is built from the carbonyl-group and can abstract hydrogen from hydrocarbons of the polymeric backbone. The resulting single radical can then be used for covalent crosslinking with other radicals. Reprinted with permission of the publisher.¹²⁹

4. References

- (1) Leznoff, C. C. The use of insoluble polymer supports in organic chemical synthesis. *Chem. Soc. Rev.* **1974**, *3*, 65.
- (2) Overberger, C. G.; Sannes, K. N. Polymers as Reagents in Organic Synthesis. *Angew. Chem. Int. Ed. Engl.* **1974**, *13*, 99–104.
- (3) Lu, J.; Toy, P. H. Organic polymer supports for synthesis and for reagent and catalyst immobilization. *Chemical reviews* **2009**, *109*, 815–838.
- (4) Jia, X.; Liang, Z.; Chen, J.; Lv, J.; Zhang, K.; Gao, M.; Zong, L.; Xie, C. Porous Organic Polymer Supported Rhodium as a Reusable Heterogeneous Catalyst for Hydroformylation of Olefins. *Organic letters* **2019**, *21*, 2147–2150.
- (5) Mahmoudi, H.; Valentini, F.; Ferlin, F.; Bivona, L. A.; Anastasiou, I.; Fusaro, L.; Aprile, C.; Marrocchi, A.; Vaccaro, L. A tailored polymeric cationic tag–anionic Pd(II) complex as a catalyst for the low-leaching Heck–Mizoroki coupling in flow and in biomass-derived GVL. *Green Chem.* **2019**, *21*, 355–360.
- (6) Yuan, M.; Yang, R.; Wei, S.; Hu, X.; Xu, D.; Yang, J.; Dong, Z. Ultra-fine Pd nanoparticles confined in a porous organic polymer: A leaching-and-aggregation-resistant catalyst for the efficient reduction of nitroarenes by NaBH₄. *Journal of colloid and interface science* **2019**, *538*, 720–730.
- (7) Cohen, B. J.; Kraus, M. A.; Patchornik, A. Organic synthesis involving multipolymer reactions. Polymeric trityllithium. *J. Am. Chem. Soc.* **1977**, *99*, 4165–4167.
- (8) Cohen, B. J.; Kraus, M. A.; Patchornik, A. "Wolf and Lamb" reactions equilibrium and kinetic effects in multipolymer systems. *J. Am. Chem. Soc.* **1981**, *103*, 7620–7629.
- (9) Voit, B. Sequential one-pot reactions using the concept of "site isolation". *Angewandte Chemie (International ed. in English)* **2006**, *45*, 4238–4240.
- (10) Seema Agarwal; Matthias Burgard; Andreas Greiner; Joachim Wendorff. Electrospinning: A Practical Guide to Nanofibers. In *Electrospinning: A Practical Guide to Nanofibers*; Greiner, A., Wendorff, J., Burgard, M., Eds.; De Gruyter, 2016.
- (11) Greiner, A.; Wendorff, J. H. Electrospinning: a fascinating method for the preparation of ultrathin fibers. *Angewandte Chemie (International ed. in English)* **2007**, *46*, 5670–5703.
- (12) *Hydrogels Based on Natural Polymers*; Elsevier, 2020.
- (13) Tieke, B. *Makromolekulare Chemie: Eine Einführung*, 3. Aufl.; Wiley-VCH: Weinheim, 2014.

- (14) Dormán, G.; Prestwich, G. D. Benzophenone photophores in biochemistry. *Biochemistry* **1994**, *33*, 5661–5673.
- (15) Pretscher, M. O.; Chen, T.; Sitaru, G.; Gekle, S.; Ji, J.; Agarwal, S. Precise 2D-Patterned Incompatible Catalysts for Reactions in One-Pot. *Chemistry (Weinheim an der Bergstrasse, Germany)* **2019**, *25*, 13640–13646.
- (16) Toyao, T.; Fujiwaki, M.; Horiuchi, Y.; Matsuoka, M. Application of an amino-functionalised metal–organic framework: an approach to a one-pot acid–base reaction. *RSC Adv.* **2013**, *3*, 21582.
- (17) Ge, T.; Hua, Z.; Zhu, Y.; Song, Y.; Tao, G.; Zhou, X.; Chen, L.; Ren, W.; Yao, H.; Shi, J. Amine-modified hierarchically structured zeolites as acid–base bi-functional catalysts for one-pot deacetalization–Knoevenagel cascade reaction. *RSC Adv* **2014**, *4*, 64871–64876.
- (18) Huang, Y.; Trewyn, B. G.; Chen, H.-T.; Lin, V. S.-Y. One-pot reaction cascades catalyzed by base- and acid-functionalized mesoporous silica nanoparticles. *New J. Chem.* **2008**, *32*, 1311.
- (19) Jia, Z.; Wang, K.; Tan, B.; Gu, Y. Hollow Hyper-Cross-Linked Nanospheres with Acid and Base Sites as Efficient and Water-Stable Catalysts for One-Pot Tandem Reactions. *ACS Catal.* **2017**, *7*, 3693–3702.
- (20) Kuepfert, M.; Cohen, A. E.; Cullen, O.; Weck, M. Shell Cross-Linked Micelles as Nanoreactors for Enantioselective Three-Step Tandem Catalysis. *Chemistry (Weinheim an der Bergstrasse, Germany)* **2018**, *24*, 18648–18652.
- (21) Lee, L.-C.; Lu, J.; Weck, M.; Jones, C. W. Acid–Base Bifunctional Shell Cross-Linked Micelle Nanoreactor for One-Pot Tandem Reaction. *ACS Catal.* **2016**, *6*, 784–787.
- (22) Sun, Z.; Yang, X.; Huang, X.; Zhang, M.; Bian, G.; Qi, Y.; Yang, X.; Zhang, W. Mesoporous polymeric catalysts with both sulfonic acid and basic amine groups for the one-pot deacetalization–Knoevenagel reaction. *New J. Chem.* **2019**, *43*, 16676–16684.
- (23) Ueda, Y.; Ito, H.; Fujita, D.; Fujita, M. Permeable Self-Assembled Molecular Containers for Catalyst Isolation Enabling Two-Step Cascade Reactions. *J. Am. Chem. Soc.* **2017**, *139*, 6090–6093.
- (24) Chi, Y.; Scroggins, S. T.; Fréchet, J. M. J. One-pot multi-component asymmetric cascade reactions catalyzed by soluble star polymers with highly branched non-interpenetrating catalytic cores. *J. Am. Chem. Soc.* **2008**, *130*, 6322–6323.
- (25) Chen, D.-F.; Han, Z.-Y.; Zhou, X.-L.; Gong, L.-Z. Asymmetric organocatalysis combined with metal catalysis: concept, proof of concept, and beyond. *Accounts of chemical research* **2014**, *47*, 2365–2377.

- (26) Poe, S. L.; Kobaslija, M.; McQuade, D. T. Mechanism and application of a microcapsule enabled multicatalyst reaction. *J. Am. Chem. Soc.* **2007**, *129*, 9216–9221.
- (27) Zhang, F.; Jiang, H.; Li, X.; Wu, X.; Li, H. Amine-Functionalized GO as an Active and Reusable Acid–Base Bifunctional Catalyst for One-Pot Cascade Reactions. *ACS Catal.* **2014**, *4*, 394–401.
- (28) Lee, Y.-R.; Chung, Y.-M.; Ahn, W.-S. A new site-isolated acid–base bifunctional metal–organic framework for one-pot tandem reaction. *RSC Adv.* **2014**, *4*, 23064.
- (29) Hermannsdörfer, J.; Friedrich, M.; Kempe, R. Colloidal size effect and metal-particle migration in M@MOF/PCP catalysis. *Chemistry (Weinheim an der Bergstrasse, Germany)* **2013**, *19*, 13652–13657.
- (30) Jiao, L.; Wang, Y.; Jiang, H.-L.; Xu, Q. Metal-Organic Frameworks as Platforms for Catalytic Applications. *Advanced materials (Deerfield Beach, Fla.)* **2018**, *30*, e1703663.
- (31) Kim, S.; Lee, J.; Jeoung, S.; Moon, H. R.; Kim, M. Dual-fixations of europium cations and TEMPO species on metal-organic frameworks for the aerobic oxidation of alcohols. *Dalton transactions (Cambridge, England : 2003)* [Online early access]. DOI: 10.1039/d0dt01324b.
- (32) Čejka, J.; Morris, R. E.; Serrano, D. P. Catalysis on Zeolites – Catalysis Science & Technology. *Catal. Sci. Technol.* **2016**, *6*, 2465–2466.
- (33) Desai, N. C.; Chudasama, J. A.; Patel, B. Y.; Jadeja, K. A.; Karkar, T. J.; Mehta, J. P.; Godhani, D. R. Catalysis by the entangled complexes in matrix structure of zeolite-Y over α -pinene. *Microporous and Mesoporous Materials* **2017**, *242*, 245–255.
- (34) Salavati-fard, T.; Caratzoulas, S.; Lobo, R. F.; Doren, D. J. Catalysis of the Diels–Alder Reaction of Furan and Methyl Acrylate in Lewis Acidic Zeolites. *ACS Catal.* **2017**, *7*, 2240–2246.
- (35) Javad Kalbasi, R.; Mansouri, S.; Mazaheri, O. In situ polymerization of poly(vinylimidazole) into the pores of hierarchical MFI zeolite as an acid–base bifunctional catalyst for one-pot C–C bond cascade reactions. *Res Chem Intermed* **2018**, *44*, 3279–3291.
- (36) Lee, Y.-R.; Do, X. H.; Hwang, S. S.; Baek, K.-Y. Dual-functionalized ZIF-8 as an efficient acid-base bifunctional catalyst for the one-pot tandem reaction. *Catalysis Today* [Online early access]. DOI: 10.1016/j.cattod.2019.06.076.
- (37) Bauer, S.; Stock, N. MOFs – Metallorganische Gerüststrukturen. Funktionale poröse Materialien. *Chem. Unserer Zeit* **2008**, *42*, 12–19.

- (38) Zhang, Y.; Wang, Y.; Liu, L.; Wei, N.; Gao, M.-L.; Zhao, D.; Han, Z.-B. Robust Bifunctional Lanthanide Cluster Based Metal-Organic Frameworks (MOFs) for Tandem Deacetalization-Knoevenagel Reaction. *Inorganic chemistry* **2018**, *57*, 2193–2198.
- (39) Li, H.; Pan, Q.; Ma, Y.; Guan, X.; Xue, M.; Fang, Q.; Yan, Y.; Valtchev, V.; Qiu, S. Three-Dimensional Covalent Organic Frameworks with Dual Linkages for Bifunctional Cascade Catalysis. *J. Am. Chem. Soc.* **2016**, *138*, 14783–14788.
- (40) Hermannsdörfer, J.; Kempe, R. Selective palladium-loaded MIL-101 catalysts. *Chemistry (Weinheim an der Bergstrasse, Germany)* **2011**, *17*, 8071–8077.
- (41) Hermannsdörfer, J.; Friedrich, M.; Miyajima, N.; Albuquerque, R. Q.; Kümmel, S.; Kempe, R. Ni/Pd@MIL-101: synergistic catalysis with cavity-conform Ni/Pd nanoparticles. *Angew. Chem. Int. Ed. Engl.* **2012**, *51*, 11473–11477.
- (42) Mu, M.; Yan, X.; Li, Y.; Chen, L. Post-modified acid-base bifunctional MIL-101(Cr) for one-pot deacetalization-Knoevenagel reaction. *J Nanopart Res* **2017**, *19*.
- (43) Zhao, J.-H.; Yang, Y.; Che, J.-X.; Zuo, J.; Li, X.-H.; Hu, Y.-Z.; Dong, X.-W.; Gao, L.; Liu, X.-Y. Compartmentalization of Incompatible Polymers within Metal-Organic Frameworks towards Homogenization of Heterogeneous Hybrid Catalysts for Tandem Reactions. *Chemistry (Weinheim an der Bergstrasse, Germany)* **2018**, *24*, 9903–9909.
- (44) Mistry, S.; Sarkar, A.; Natarajan, S. New Bifunctional Metal–Organic Frameworks and Their Utilization in One-Pot Tandem Catalytic Reactions. *Crystal Growth & Design* **2019**, *19*, 747–755.
- (45) Gaona, A.; Díaz, U.; Corma, A. Functional Acid and Base Hybrid Catalysts Organized by Associated (Organo)aluminosilicate Layers for C–C Bond Forming Reactions and Tandem Processes. *Chem. Mater.* **2017**, *29*, 1599–1612.
- (46) Motokura, K.; Tada, M.; Iwasawa, Y. Layered materials with coexisting acidic and basic sites for catalytic one-pot reaction sequences. *J. Am. Chem. Soc.* **2009**, *131*, 7944–7945.
- (47) Varghese, S. A.; Rangappa, S. M.; Siengchin, S.; Parameswaranpillai, J. Natural polymers and the hydrogels prepared from them. *Hydrogels Based on Natural Polymers*; Elsevier, 2020; pp 17–47.
- (48) Motokura, K.; Fujita, N.; Mori, K.; Mizugaki, T.; Ebitani, K.; Kaneda, K. An acidic layered clay is combined with a basic layered clay for one-pot sequential reactions. *J. Am. Chem. Soc.* **2005**, *127*, 9674–9675.
- (49) Shang, F.; Sun, J.; Liu, H.; Wang, C.; Guan, J.; Kan, Q. One-pot cascade reactions catalyzed by acid–base mesoporous MCM-41 materials. *Materials Research Bulletin* **2012**, *47*, 801–806.

- (50) Zhong, L.; Anand, C.; Lakhi, K. S.; Lawrence, G.; Vinu, A. Bifunctional Mesoporous Carbon Nitride: Highly Efficient Enzyme-like Catalyst for One-pot Deacetalization-Knoevenagel Reaction. *Scientific reports* **2015**, *5*, 12901.
- (51) Lim, E. W. C.; Feng, R. Agglomeration of magnetic nanoparticles. *The Journal of chemical physics* **2012**, *136*, 124109.
- (52) Peng, W.-H.; Lee, Y.-Y.; Wu, C.; Wu, K. C.-W. Acid–base bi-functionalized, large-pored mesoporous silica nanoparticles for cooperative catalysis of one-pot cellulose-to-HMF conversion. *J. Mater. Chem.* **2012**, *22*, 23181.
- (53) Li, P.; Cao, C.-Y.; Chen, Z.; Liu, H.; Yu, Y.; Song, W.-G. Core-shell structured mesoporous silica as acid-base bifunctional catalyst with designated diffusion path for cascade reaction sequences. *Chemical communications (Cambridge, England)* **2012**, *48*, 10541–10543.
- (54) Yang, Y.; Liu, X.; Li, X.; Zhao, J.; Bai, S.; Liu, J.; Yang, Q. A yolk-shell nanoreactor with a basic core and an acidic shell for cascade reactions. *Angew. Chem. Int. Ed. Engl.* **2012**, *51*, 9164–9168.
- (55) Jun, S. W.; Shokouhimehr, M.; Lee, D. J.; Jang, Y.; Park, J.; Hyeon, T. One-pot synthesis of magnetically recyclable mesoporous silica supported acid-base catalysts for tandem reactions. *Chemical communications (Cambridge, England)* **2013**, *49*, 7821–7823.
- (56) Wang, Z.; Yuan, X.; Cheng, Q. 'a.; Zhang, T.; Luo, J. An efficient and recyclable acid–base bifunctional core–shell nano-catalyst for the one-pot deacetalization–Knoevenagel tandem reaction. *New J. Chem.* **2018**, *42*, 11610–11615.
- (57) Akagawa, K.; Sakamoto, S.; Kudo, K. Resin-supported acid- and base-catalyzed one-pot sequential reaction including an enantioselective step. *Tetrahedron Letters* **2007**, *48*, 985–987.
- (58) Helms, B.; Guillaudeu, S. J.; Xie, Y.; McMurdo, M.; Hawker, C. J.; Fréchet, J. M. J. One-pot reaction cascades using star polymers with core-confined catalysts. *Angewandte Chemie (International ed. in English)* **2005**, *44*, 6384–6387.
- (59) Zhao, Q.; Wang, H.; Zheng, H.; Sun, Z.; Shi, W.; Wang, S.; Wang, X.; Jiang, Z. Acid–base bifunctional HPA nanocatalysts promoting heterogeneous transesterification and esterification reactions. *Catal. Sci. Technol.* **2013**, *3*, 2204.
- (60) Xiong, L.; Zhang, H.; Zhong, A.; He, Z.; Huang, K. Acid- and base-functionalized core-confined bottlebrush copolymer catalysts for one-pot cascade reactions. *Chemical communications (Cambridge, England)* **2014**, *50*, 14778–14781.

- (61) Wang, X.; Zhang, L.; Guo, Z.; Shi, Y.; Zhou, Y.; Wang, J. Synergistic catalysis of one-pot cascade reactions by acidic and basic binary porous polymers. *Applied Surface Science* **2019**, *478*, 221–229.
- (62) Yavuz, E.; Cherkasov, N.; Degirmenci, V. Acid and base catalysed reactions in one pot with site-isolated polyHIPE catalysts. *RSC Adv.* **2019**, *9*, 8175–8183.
- (63) Zhang, Y.; Pan, J.; Chen, Y.; Shi, W.; Yan, Y.; Yu, L. HIPEs template: Towards the synthesis of polymeric catalysts with adjustable porous structure, acid–base strength and wettability for biomass energy conversion. *Chemical Engineering Journal* **2016**, *283*, 956–970.
- (64) Wang, K.; Jia, Z.; Yang, X.; Wang, L.; Gu, Y.; Tan, B. Acid and base coexisted heterogeneous catalysts supported on hypercrosslinked polymers for one-pot cascade reactions. *Journal of Catalysis* **2017**, *348*, 168–176.
- (65) Zhang, H.; Xiong, L.; He, Z.; Zhong, A.; Wang, T.; Xu, Y.; Huang, K. Microporous organic nanotube network supported acid and base catalyst system for one-pot cascade reactions. *New J. Chem.* **2016**, *40*, 7282–7285.
- (66) Wang, T.; Xu, Y.; He, Z.; Zhang, H.; Xiong, L.; Zhou, M.; Yu, W.; Shi, B.; Huang, K. Acid-Base Bifunctional Microporous Organic Nanotube Networks for Cascade Reactions. *Macromol. Chem. Phys.* **2017**, *218*, 1600431.
- (67) Modak, A.; Bhaumik, A. High-throughput Acid-Base Tandem Organocatalysis over Hollow Tube-Shaped Porous Polymers and Carbons. *ChemistrySelect* **2016**, *1*, 1192–1200.
- (68) Lechner, M. D. *Einführung in die Kinetik*; Springer Berlin Heidelberg: Berlin, Heidelberg, 2018.
- (69) Atkins, P. W.; Paula, J. de. *Physikalische Chemie*, 4., vollst. überarb. Aufl., 2. Nachdr; Wiley-VCH: Weinheim, 2012.
- (70) GEORGE, H. H. Modeling the Melt Spinning Process. In *Polymers for Fibers and Elastomers*; Arthur, J. C., Diefendorf, R. J., Yen, T. F., Needles, H. L., Schaeffgen, J. R., Jaffe, M., Logothetis, A. L., Eds.; ACS Symposium Series; American Chemical Society: Washington, D.C., 1984; pp 355–369.
- (71) Qin, Y. A brief description of textile fibers. *Medical Textile Materials*; Elsevier, 2016; pp 23–42.
- (72) Ozipek, B.; Karakas, H. Wet spinning of synthetic polymer fibers. *Advances in Filament Yarn Spinning of Textiles and Polymers*; Elsevier, 2014; pp 174–186.
- (73) Foroughi, J.; Mirabedini, A.; Warren, H. Hydrogels Fibers. In *Hydrogels*; Haider, S., Haider, A., Eds.; InTech, 2018.

- (74) Imura, Y.; Hogan, R.M.C.; Jaffe, M. Dry spinning of synthetic polymer fibers. *Advances in Filament Yarn Spinning of Textiles and Polymers*; Elsevier, 2014; pp 187–202.
- (75) McHugh, A. J. Modelling of fibre spinning and film blowing. *Plastics, Rubber and Composites* **2008**, *37*, 105–112.
- (76) Yasuda, H.; Ban, K.; Ohta, Y. Gel spinning processes. *Advanced Fiber Spinning Technology*; Elsevier, 1994; pp 172–186.
- (77) Kuo, C. J.; Lan, W. L. Gel spinning of synthetic polymer fibres. *Advances in Filament Yarn Spinning of Textiles and Polymers*; Elsevier, 2014; pp 100–112.
- (78) Petrik, S.; Maly, M. Production Nozzle-Less Electrospinning Nanofiber Technology. *MRS Proc.* **2009**, *1240*.
- (79) Persano, L.; Camposeo, A.; Tekmen, C.; Pisignano, D. Industrial Upscaling of Electrospinning and Applications of Polymer Nanofibers: A Review. *Macromol. Mater. Eng.* **2013**, *298*, 504–520.
- (80) Jian, S.; Zhu, J.; Jiang, S.; Chen, S.; Fang, H.; Song, Y.; Duan, G.; Zhang, Y.; Hou, H. Nanofibers with diameter below one nanometer from electrospinning. *RSC Adv.* **2018**, *8*, 4794–4802.
- (81) Greiner, A.; Wendorff, J.; Burgard, M., Eds. *Electrospinning: A Practical Guide to Nanofibers*; De Gruyter, 2016.
- (82) Murase, Y.; Nagai, A. Melt spinning. *Advanced Fiber Spinning Technology*; Elsevier, 1994; pp 25–64.
- (83) Liu, L.; Ghaemi, A.; Gekle, S.; Agarwal, S. One-Component Dual Actuation: Poly(NIPAM) Can Actuate to Stable 3D Forms with Reversible Size Change. *Advanced materials (Deerfield Beach, Fla.)* **2016**, *28*, 9792–9796.
- (84) Liu, L.; Jiang, S.; Sun, Y.; Agarwal, S. Giving Direction to Motion and Surface with Ultra-Fast Speed Using Oriented Hydrogel Fibers. *Adv. Funct. Mater.* **2016**, *26*, 1021–1027.
- (85) Yang, J.; Wang, K.; Yu, D.-G.; Yang, Y.; Bligh, S. W. A.; Williams, G. R. Electrospun Janus nanofibers loaded with a drug and inorganic nanoparticles as an effective antibacterial wound dressing. *Materials science & engineering. C, Materials for biological applications* **2020**, *111*, 110805.
- (86) Jiang, S.; Jin, Q.; Agarwal, S. Template Assisted Change in Morphology from Particles to Nanofibers by Side-by-Side Electrospinning of Block Copolymers. *Macromol. Mater. Eng.* **2014**, *299*, 1298–1305.

- (87) Gernhardt, M.; Peng, L.; Burgard, M.; Jiang, S.; Förster, B.; Schmalz, H.; Agarwal, S. Tailoring the Morphology of Responsive Bioinspired Bicomponent Fibers. *Macromol. Mater. Eng.* **2018**, *303*, 1700248.
- (88) Jiang, S.; Duan, G.; Zussman, E.; Greiner, A.; Agarwal, S. Highly flexible and tough concentric triaxial polystyrene fibers. *ACS applied materials & interfaces* **2014**, *6*, 5918–5923.
- (89) Zanjani, J. S. M.; Saner Okan, B.; Menciloglu, Y. Z.; Yildiz, M. Design and fabrication of multi-walled hollow nanofibers by triaxial electrospinning as reinforcing agents in nanocomposites. *Journal of Reinforced Plastics and Composites* **2015**, *34*, 1273–1286.
- (90) Kronawitt, J.; Dulle, M.; Schmalz, H.; Agarwal, S.; Greiner, A. Poly(p -xylylene) Nanotubes Decorated with Nonagglomerated Gold Nanoparticles for the Alcoholysis of Dimethylphenylsilane. *ACS Appl. Nano Mater.* **2020**, *3*, 2766–2773.
- (91) Letnik, I.; Avrahami, R.; Rokem, J. S.; Greiner, A.; Zussman, E.; Greenblatt, C. Living Composites of Electrospun Yeast Cells for Bioremediation and Ethanol Production. *Biomacromolecules* **2015**, *16*, 3322–3328.
- (92) Pretscher, M.; Pineda-Contreras, B. A.; Kaiser, P.; Reich, S.; Schöbel, J.; Kuttner, C.; Freitag, R.; Fery, A.; Schmalz, H.; Agarwal, S. pH-Responsive Biohybrid Carrier Material for Phenol Decontamination in Wastewater. *Biomacromolecules* **2018**, *19*, 3224–3232.
- (93) Pschyklenk, L.; Wagner, T.; Lorenz, A.; Kaul, P. Optical Gas Sensing with Encapsulated Chiral-Nematic Liquid Crystals. *ACS Appl. Polym. Mater.* **2020**, *2*, 1925–1932.
- (94) Hils, C.; Dulle, M.; Sitaru, G.; Gekle, S.; Schöbel, J.; Frank, A.; Drechsler, M.; Greiner, A.; Schmalz, H. Influence of patch size and chemistry on the catalytic activity of patchy hybrid nonwovens. *Nanoscale Adv.* **2020**, *2*, 438–452.
- (95) Yu, Y.; Zhang, F.; Liu, Y.; Zheng, Y.; Xin, B.; Jiang, Z.; Peng, X.; Jin, S. Waterproof and breathable polyacrylonitrile/(polyurethane/fluorinated-silica) composite nanofiber membrane via side-by-side electrospinning. *J. Mater. Res.* **2020**, *35*, 1173–1181.
- (96) Garg, K.; Bowlin, G. L. Electrospinning jets and nanofibrous structures. *Biomicrofluidics* **2011**, *5*, 13403.
- (97) Rayleigh. XX. On the equilibrium of liquid conducting masses charged with electricity. *The London, Edinburgh, and Dublin Philosophical Magazine and Journal of Science* **1882**, *14*, 184–186.
- (98) Ngo, T. D.; Kashani, A.; Imbalzano, G.; Nguyen, K. T.Q.; Hui, D. Additive manufacturing (3D printing): A review of materials, methods, applications and challenges. *Composites Part B: Engineering* **2018**, *143*, 172–196.

- (99) Prasad, L. K.; Smyth, H. 3D Printing technologies for drug delivery: a review. *Drug development and industrial pharmacy* **2016**, *42*, 1019–1031.
- (100) Khoo, Z. X.; Teoh, J. E. M.; Liu, Y.; Chua, C. K.; Yang, S.; An, J.; Leong, K. F.; Yeong, W. Y. 3D printing of smart materials: A review on recent progresses in 4D printing. *Virtual and Physical Prototyping* **2015**, *10*, 103–122.
- (101) N. Turner, B.; Strong, R.; A. Gold, S. A review of melt extrusion additive manufacturing processes: I. Process design and modeling. *Rapid Prototyping Journal* **2014**, *20*, 192–204.
- (102) Dilag, J.; Chen, T.; Li, S.; Bateman, S. A. Design and direct additive manufacturing of three-dimensional surface micro-structures using material jetting technologies. *Additive Manufacturing* **2019**, *27*, 167–174.
- (103) Davoudinejad, A.; Diaz-Perez, L. C.; Quagliotti, D.; Pedersen, D. B.; Albajez-García, J. A.; Yagüe-Fabra, J. A.; Tosello, G. Additive manufacturing with vat polymerization method for precision polymer micro components production. *Procedia CIRP* **2018**, *75*, 98–102.
- (104) Cullen, A. T.; Price, A. D. Fabrication of 3D conjugated polymer structures via vat polymerization additive manufacturing. *Smart Mater. Struct.* **2019**, *28*, 104007.
- (105) Chatham, C. A.; Long, T. E.; Williams, C. B. A review of the process physics and material screening methods for polymer powder bed fusion additive manufacturing. *Progress in Polymer Science* **2019**, *93*, 68–95.
- (106) Chueh, Y.-H.; Wei, C.; Zhang, X.; Li, L. Integrated laser-based powder bed fusion and fused filament fabrication for three-dimensional printing of hybrid metal/polymer objects. *Additive Manufacturing* **2020**, *31*, 100928.
- (107) Raasch, J.; Ivey, M.; Aldrich, D.; Nobes, D. S.; Ayranci, C. Characterization of polyurethane shape memory polymer processed by material extrusion additive manufacturing. *Additive Manufacturing* **2015**, *8*, 132–141.
- (108) Peng, F.; Vogt, B. D.; Cakmak, M. Complex flow and temperature history during melt extrusion in material extrusion additive manufacturing. *Additive Manufacturing* **2018**, *22*, 197–206.
- (109) Truby, R. L.; Lewis, J. A. Printing soft matter in three dimensions. *Nature* **2016**, *540*, 371–378.
- (110) Zhou, L.-Y.; Fu, J.; He, Y. A Review of 3D Printing Technologies for Soft Polymer Materials. *Adv. Funct. Mater.* **2020**, *30*, 2000187.

- (111) He, Y.; Yang, F.; Zhao, H.; Gao, Q.; Xia, B.; Fu, J. Research on the printability of hydrogels in 3D bioprinting. *Scientific reports* **2016**, *6*, 29977.
- (112) Bellini, A.; Güçeri, S. Mechanical characterization of parts fabricated using fused deposition modeling. *Rapid Prototyping Journal* **2003**, *9*, 252–264.
- (113) Fathi, S.; Dickens, P. Droplet characterisation of molten caprolactam for additive manufacturing applications. *Proceedings of the Institution of Mechanical Engineers, Part B: Journal of Engineering Manufacture* **2012**, *226*, 1052–1060.
- (114) Calvert, P. Inkjet Printing for Materials and Devices. *Chem. Mater.* **2001**, *13*, 3299–3305.
- (115) Ng, W. L.; Lee, J. M.; Zhou, M.; Chen, Y.-W.; Lee, K.-X. A.; Yeong, W. Y.; Shen, Y.-F. Vat polymerization-based bioprinting-process, materials, applications and regulatory challenges. *Biofabrication* **2020**, *12*, 22001.
- (116) Chueh, Y.-H.; Zhang, X.; Ke, J. C.-R.; Li, Q.; Wei, C.; Li, L. Additive manufacturing of hybrid metal/polymer objects via multiple-material laser powder bed fusion. *Additive Manufacturing* **2020**, *36*, 101465.
- (117) Fan, K. M.; Cheung, W. L.; Gibson, I. Movement of powder bed material during the selective laser sintering of bisphenol-A polycarbonate. *Rapid Prototyping Journal* **2005**, *11*, 188–198.
- (118) Chimene, D.; Kaunas, R.; Gaharwar, A. K. Hydrogel Bioink Reinforcement for Additive Manufacturing: A Focused Review of Emerging Strategies. *Advanced materials (Deerfield Beach, Fla.)* **2020**, *32*, e1902026.
- (119) Ewaldz, E.; Brettmann, B. Molecular Interactions in Electrospinning: From Polymer Mixtures to Supramolecular Assemblies. *ACS Appl. Polym. Mater.* **2019**, *1*, 298–308.
- (120) Fang, D.; Liu, Y.; Jiang, S.; Nie, J.; Ma, G. Effect of intermolecular interaction on electrospinning of sodium alginate. *Carbohydrate Polymers* **2011**, *85*, 276–279.
- (121) Liang, Y.; Cheng, S.; Zhao, J.; Zhang, C.; Sun, S.; Zhou, N.; Qiu, Y.; Zhang, X. Heat treatment of electrospun Polyvinylidene fluoride fibrous membrane separators for rechargeable lithium-ion batteries. *Journal of Power Sources* **2013**, *240*, 204–211.
- (122) Huang, L.; Manickam, S. S.; McCutcheon, J. R. Increasing strength of electrospun nanofiber membranes for water filtration using solvent vapor. *Journal of Membrane Science* **2013**, *436*, 213–220.
- (123) Aimetti, A. A.; Machen, A. J.; Anseth, K. S. Poly(ethylene glycol) hydrogels formed by thiol-ene photopolymerization for enzyme-responsive protein delivery. *Biomaterials* **2009**, *30*, 6048–6054.

- (124) Brown, T. E.; Anseth, K. S. Spatiotemporal hydrogel biomaterials for regenerative medicine. *Chem. Soc. Rev.* **2017**, *46*, 6532–6552.
- (125) Lee, B. H.; Shirahama, H.; Cho, N.-J.; Tan, L. P. Efficient and controllable synthesis of highly substituted gelatin methacrylamide for mechanically stiff hydrogels. *RSC Adv.* **2015**, *5*, 106094–106097.
- (126) Ouyang, L.; Highley, C. B.; Sun, W.; Burdick, J. A. A Generalizable Strategy for the 3D Bioprinting of Hydrogels from Nonviscous Photo-crosslinkable Inks. *Advanced materials (Deerfield Beach, Fla.)* **2017**, *29*.
- (127) Ismail, H. M.; Zamani, S.; Elrayess, M. A.; Kafienah, W.; Younes, H. M. New Three-Dimensional Poly(decanediol-co-tricarballylate) Elastomeric Fibrous Mesh Fabricated by Photoreactive Electrospinning for Cardiac Tissue Engineering Applications. *Polymers* **2018**, *10*.
- (128) Preston, G. W.; Wilson, A. J. Photo-induced covalent cross-linking for the analysis of biomolecular interactions. *Chem. Soc. Rev.* **2013**, *42*, 3289–3301.
- (129) Pretscher, M. O.; Chen, T.; Sitaru, G.; Gekle, S.; Ji, J.; Agarwal, S. Precise 2D-Patterned Incompatible Catalysts for Reactions in One-Pot. *Chemistry – A European Journal* **2019**, *25*, 13640–13646.

5. Synopsis

In this thesis, a new way for site-isolation with an easy and up-scalable approach of incompatible Wolf-Lamb type catalysis for two-step one-pot reactions was investigated. The focus was on applicability to reach these properties through easy-to-apply methods as well as a modular system to access necessary catalysts in future studies. Hence, free radical polymerization was chosen and an easy-to-apply crosslinking unit was used within the copolymers. The first part of the thesis was the establishment of model systems for Wolf-Lamb type catalysts processed through electrospinning and 2D printing to obtain the procedures and a general understanding of the catalysis by calculation of the kinetical reaction parameters. The second part compares the methods and further broadens the applicability by the studying of a possible post-process treatment to investigate the stability of the obtained materials through the modifications. Overall, this thesis consists of three linked individual papers.

The first two papers use commercial acidic and basic monomers from which the copolymers with poly(styrene-*co*-styrene sulfonic acid-*co*-meth acryl benzophenone) as acidic copolymer and poly(styrene-*co*-4-vinylpyridine-*co*-methacrylbenzophenone) as basic copolymer were synthesized. In the first paper, the polymers were electrospun while poly(styrene-*co*-styrene sulfonic acid-*co*-meth acryl benzophenone) was used as the synthesized poly(styrene-*co*-sodium styrene sulfonate -*co*-meth acryl benzophenone) and later protonated in methanol by immersion and hydrochloric acid was added dropwise. Investigations of the catalysis showed that the second reaction step started only after enough of the intermediate was built (**Publication 1**).

In the second paper, the same copolymers were used to test the system with printed structures. In this case, it was possible to print the poly(styrene-*co*-styrene sulfonic acid-*co*-meth acryl benzophenone) directly to obtain the catalyst. The substrate for printing was a PET mesh and similar results were obtained. The time for the second reaction step was reduced, but the overall conversion decreased (**Publication 2**). The results were in good alignment with the previous publication.

Lastly, the systems were made comparable by keeping the same concentrations and amounts. The basic copolymer was changed to poly(styrene-*co*-4-vinylbenzylamine-*co*- *N*-(4-benzoylphenyl)acrylamide). The developed processing and treatment methods from the first two publications were used again and the overall performance of the catalysts show that the

printed catalyst has a better performance because of diffusion within the polymers
(Publicaation 3).

5.1. Wolf-Lamb type catalysis in one-pot using electrospun polymeric catalyst membranes

This paper was published by Martin O. Pretschner, Stephan Gekle, Seema Agarwal, in *Macromolecular Rapid Communication*, **2019**, 1900148; DOI: <https://doi.org/10.1002/marc.201900148>.

The aim of this paper was the use of catalytic porous fibrous membranes made directly from the corresponding Wolf-Lamb type catalyst by the process of electrospinning for one-pot two-step reactions. This approach offers several unique advantages in cascade reactions, especially with Wolf-Lamb type catalysts, such as 1) the direct use of catalytic membranes for one-pot cascade reactions with Wolf-Lamb type catalysts – even for multistep reactions in the future; 2) the preparation of catalytic membranes in large amounts and sizes, and 3) the preparation of catalytic membranes by direct spinning of polymeric acid and bases synthesized by simple radical polymerization, avoiding the need for any precise chemistry for the immobilization of catalytic functional groups.

The catalytic copolymers were electrospun from DMF, photo-crosslinked and used as separate membranes for the catalytic studies. Poly(styrene-*co*-sodium styrene sulfonate-*co*-methacryl benzophenone) was used as acidic copolymer while poly(styrene-*co*-4-vinylpyridine-*co*-methacrylbenzophenone) was used as a basic copolymer catalyst. The separation between the Wolf-Lamb type catalysts is easily achieved by fixing individual membranes in frames and inserting them in a reaction medium in one-pot.

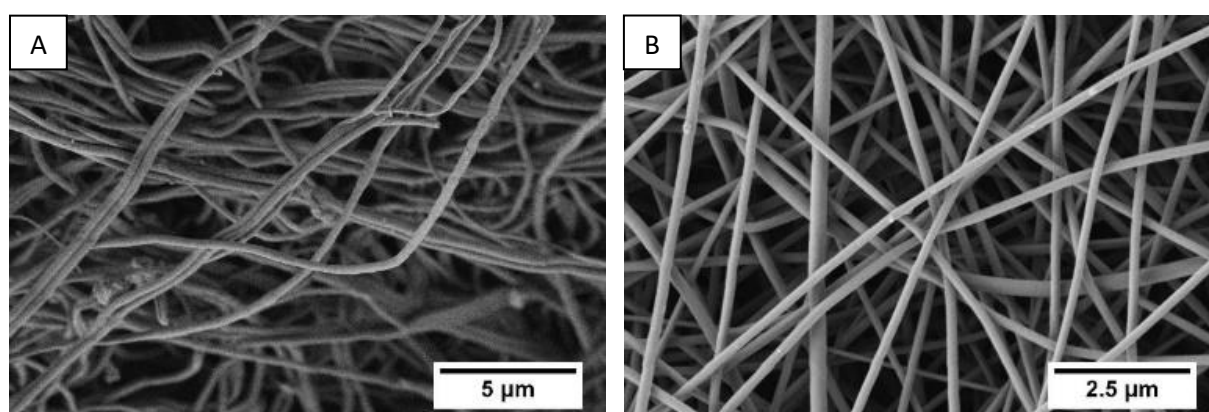
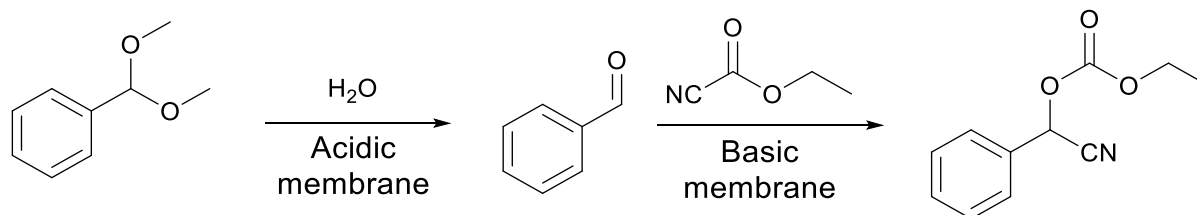


Figure 10: Electrospun membranes A) acidic membrane B) basic membrane.

The acidic electrospun membrane (*Figure 10A*) was further protonated and then, together with the basic membranes (*Figure 10B*), used for the catalytic one-pot reaction with a deacetylation

of dimethoxybenzyl to benzaldehyde, followed by a carbonate building reaction towards cyano(phenyl)methyl ethyl carbonate (Scheme 9).



Scheme 9: Reaction scheme for a two-step, one-pot reaction; first step is the acidic catalysed deacetylation of dimethoxybenzyl to benzaldehyde, which reacts basic catalysed to cyano(phenyl)methyl ethyl carbonate in the second step.

The reaction was monitored by gas chromatography measurements to observe the conversion over time and the resulting data was fitted to the corresponding reaction equations (Figure 11). Only by the addition of a parameter Δt the fit shows a reasonable alignment with the reaction. The first step takes until 180 minutes for a conversion of 80% is achieved after 360 minutes.

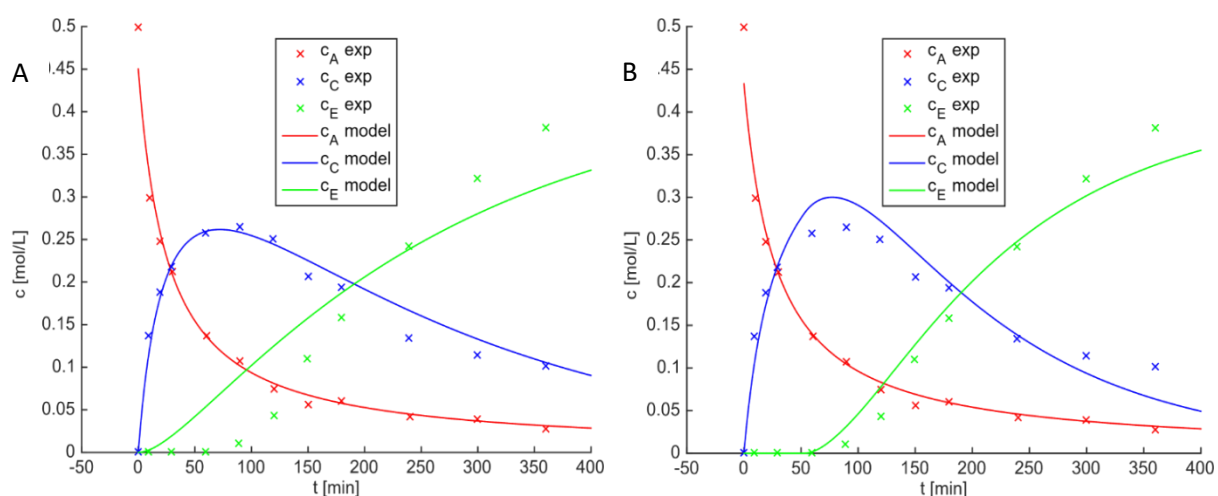


Figure 11: Time-concentration diagram obtained by the monitoring of the reaction. (A) The fit without the parameter Δt (B) with the parameter Δt .

Overall, it was shown that the electrospun membranes are a promising material for site-isolation of Wolf-Lamb type catalysts. A high conversion is achieved, and the kinetic studies showed that only with the implementation of a parameter $\Delta t = 67$ min a reasonable fit of the underlying differential equations is possible. The reaction rate of the first step is $k_1 = 0.081 \text{ mol (L min)}^{-1}$ and for the second-step reaction $k_2 = 0.013 \text{ mol (L min)}^{-1}$. This shows that the second reaction step only starts after a significant amount of benzaldehyde is obtained or the reagent needs to diffuse towards the second catalytic membrane and that the second step is significantly slower.

5.1.1. Individual Contribution of Joint Publications

The synthesis of the copolymers and the characterization and the catalytic studies were done by me. The manuscript was jointly written with the contribution of all authors. Prof. Dr. Gekle performed the fitting of the catalytic data and helped with the discussion. Prof. Dr. Agarwal (corresponding author) was responsible for supervising, helping with the design of the concept as well as with the discussion.

5.2. Precise 2D-Patterned Incompatible Catalysts for Reactions in One-Pot

This paper was published by Martin O. Pretscher, Tingting Chen, Gabriel Sitaru, Stephan Gekle, Jian Ji and Seema Agarwal in *Chemistry A European Journal*, **2019**, *25*, 13640. DOI: <https://doi.org/10.1002/chem.201903486>

2D printing offers the possibility of precise material structuring, size and shape modulations that can be of high utility in heterogeneous catalysis. These unique possibilities were used for the site-isolation of new Wolf-Lamb type catalysts. The aim is to research if these properties can be used within such catalytic materials. Therefore, it was elaborated on the possibility of printed materials as carrier for Wolf-Lamb type catalyst. In this case, the same polymers as in the first paper were used, however, the amount of styrene sulfonic acid within the polymers was reduced to 15 mol%. The procedure for printing made it possible to directly print the acidic catalyst without the protonation step. The acidic poly(styrene-*co*-styrene sulfonic acid-*co*-methacryl benzophenone) was printed from a mixture of THF/DMF (8/2) and the basic copolymer poly(styrene-*co*-4-vinylpyridine-*co*-methacryl benzophenone) from a mixture of THF/DMF (9/1) on PET meshes to stabilize the printed structure. The resulting prints are shown in *Figure 12*.

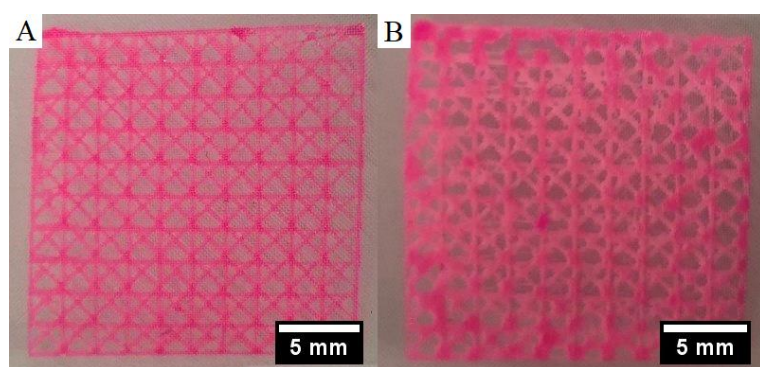


Figure 12: Printed structure of the acidic copolymer poly(styrene-*co*-styrene sulfonic acid-*co*-methacryloylbenzophenone) (A) and the basic copolymer poly(styrene-*co*-4-vinylpyridine-*co*-methacryloylbenzophenone) (B).

With the help of Raman-imaging, it was possible to determine the distribution of the polymer on the PET mesh. In this case, it could be established that most of the polymer is within the meshes and only a very small amount is on top of it. As it is the dissolved form of the polymeric material, it flows towards these cavities and hardens there (Figure 13).

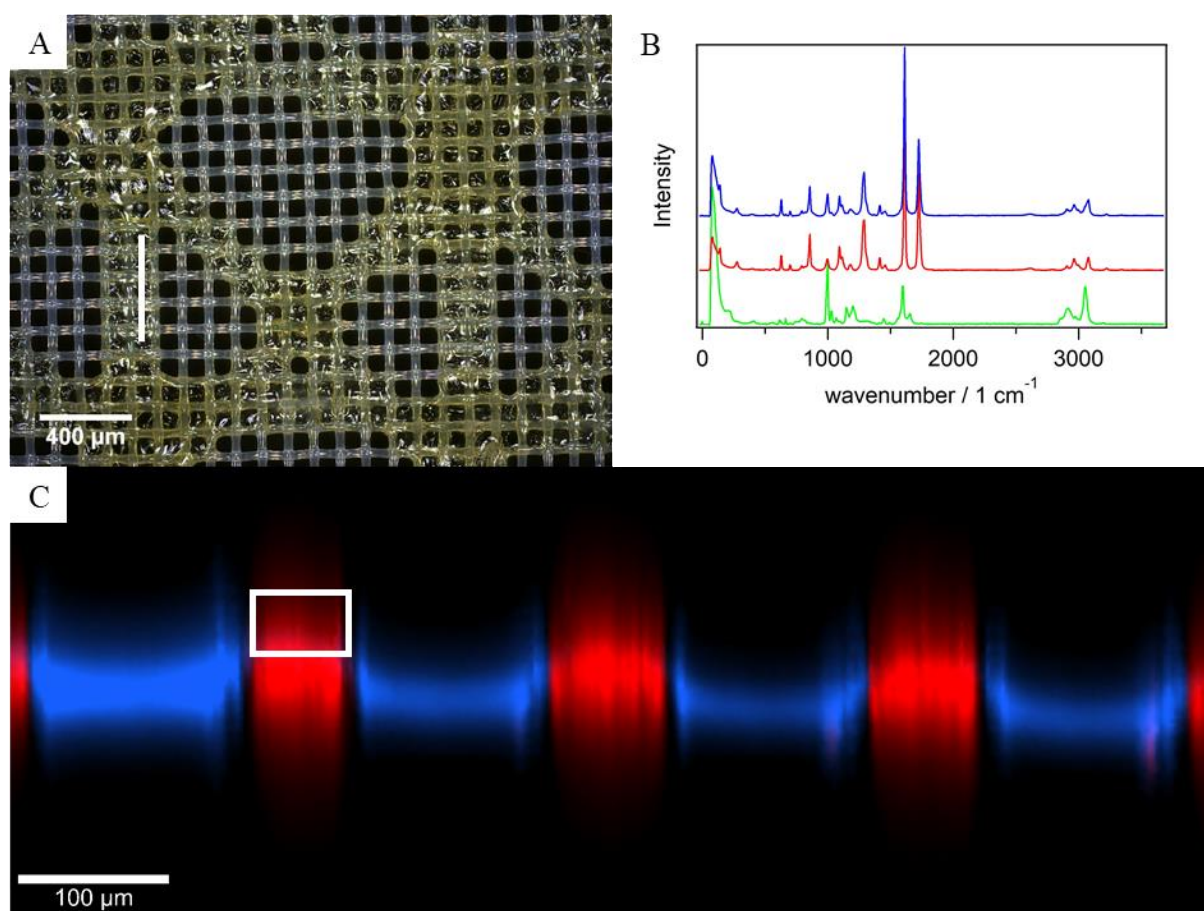


Figure 13: Microscopy image of the 3D-printed basic polymer (A) with a white line indicating the measured position in Raman imaging, the Raman spectrum for PET (blue), basic polymer (green) and for the white box in the image the Raman imaging (red), in which the red part is the PET mesh and the blue part the 3D-printed polymer (C).

The materials could be used in the same reaction as in the first publication and the reaction was monitored through gas chromatography and the results were again fitted to the reaction equation.

The results of the catalytic experiment are comparable with the first results and the necessity of the parameter $\Delta t = 39$ min is shown once again (Figure 14). The yield is 95% within the first step and around 65% for the second step. The determined reaction rate of the first step is $k_1 = 0.51 \text{ mol (L min)}^{-1}$ and $k_2 = 0.01 \text{ mol (L min)}^{-1}$. Further showing the problem with the second reaction step within this system. Nevertheless, the reaction was finished after 240 minutes and hence, faster than the electrospun membrane. Overall, it was shown that printed structures were a suitable site-isolated material for Wolf-Lamb type catalysis, which might need further optimization towards higher yield.

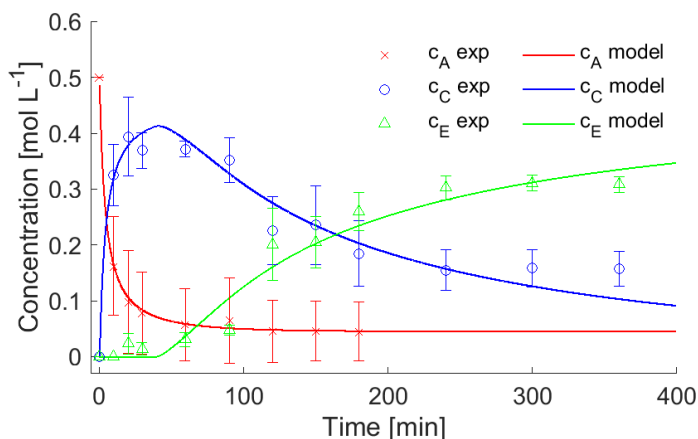


Figure 14: Kinetic fitted parameters of the two-step cascade reaction catalyzed by incompatible acid-base catalysts: red, blue and green are the amounts of (dimethoxy)methyl benzene, benzaldehyde and cyano(phenyl)methyl ethyl carbonate, respectively.

5.2.1. Individual Contribution of Joint Publications

The synthesis and analysis of the copolymers as well as the kinetical studies were done by me. The development of the printing file was done by Dr. Tingting Chen under the supervision of Prof. Jian Ji. The printing was executed by Dr. Tingting Chen and me. Gabriel Sitaru did the fitting of the reaction equation under the supervision of Prof. Dr. Stephan Gekle. The manuscript was written with the contribution of all authors. Prof. Dr. Seema Agarwal (corresponding author) was responsible for supervising, helping with the design of the concept as well as with the discussion.

5.3. Comparison of post-process functionalized catalytic electrospun membranes and 2D printed structures in Wolf-Lamb type catalysis

This paper is ready to be submitted and the participating authors are Martin O. Pretschner, Gabriel Sitaru, Markus Dietel, Holger Schmalz, Stephan Gekle, Seema Agarwal

As the model systems showed promising results, this paper focused on the modular system by investigating post-processing treatment of the material by chemical modification. The aim was to answer the question about reusability of such materials, the direct comparison of the printed and electrospun system as well as the broadening of possible applications. Hence, the basic copolymer was changed towards a primary amine with higher basicity, which makes post-process treatment necessary. In this case, the Gabriel synthesis was used to obtain *N*-(4-vinylbenzyl)phtalimide as a precursor monomer which can react with hydrazine towards the primary amine. The crosslinking unit was based on *N*-(4-benzoylphenyl)acrylamide to prevent reactions of the hydrazine with the ester bond of the previously used crosslinking monomer. The system was tested for electrospinning and printing in toluene as well as for electrospun materials in DMF.

For the copolymerization, free radical polymerization was used to produce the polymeric catalyst. The copolymer with the primary amine (poly(styrene-*co*-4-vinylbenzylamine-*co*- *N*-(4-benzoylphenyl)acrylamide) could not be used directly as the solubility is too low for the processing techniques. A polyamide net was used as the material for printing to obtain stability against bases as well as to obtain good adhesion with the polymeric substrate. The material was analyzed by solid state NMR for electrospun material and Raman spectroscopy for printed structures, by comparing it with prior analyzed deprotected electrospun material and for both systems a successful deprotection was observed (*Figure 15*).

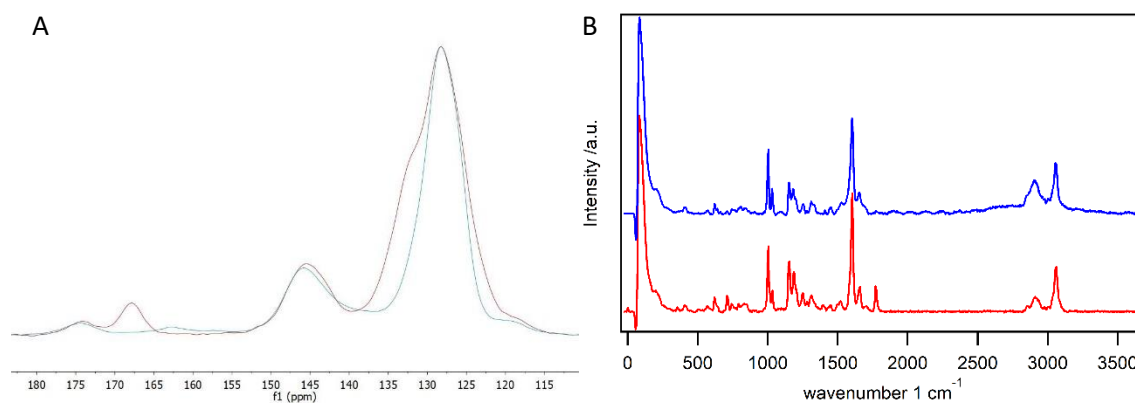
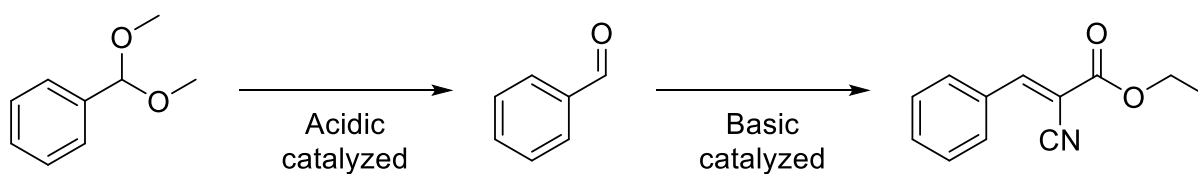


Figure 15: (A) Solid state NMR shows that the signal for the carbonylic and benzylic Carbon disappears, showing the successful reaction in electrospun membranes. (B) shows the primary amine peak between 2500 cm^{-1} and 3000 cm^{-1} and the carboxylic peak at 1800 cm^{-1} .

The material was used for the catalytic studies of the acidic catalyzed deacetylation reaction, followed by a basic catalyzed Knoevenagel condensation (*Scheme 10*).



Scheme 10: Deacetylation of dimethoxybenzyl to benzaldehyde, followed by the Knoevenagel condensation with cyanoethyl acetate towards ethyl-2-cyano-3-phenylacrylate.

The catalytic reaction was monitored through gas chromatography and the different catalytic results were compared. It overall showed that the system made reactions possible which were not available, due to the weak character of 4-vinylpyridine. While the difference between the system in toluene and DMF only differed slightly. Both systems were finished with full conversion around 150 Minutes with the catalytic experiment in DMF being slightly faster. In comparison the printed structure showed full conversion already after 40 minutes. Showing an advantage of such printed structures compared to electrospun material. While theoretically the electrospun material as a fiber material should have advantages, the gel character of such polymeric material lead to advantages for mass transport within the printed material. The results of the fitted differential equations further show that the first step is ten times faster than for the electrospun materials and around five times faster for the second reaction step (*Table 1*).

Overall, while both systems are viable, there are clear advantages for the printed structures. Only a slight influence of solvent towards the reactivity of the material is observed and for

further studies, the systems can be chosen in accordance with the properties of the substrates. The modular character was shown as post-process treatment through chemical modification is possible and the structures stay stable due to the crosslinking.

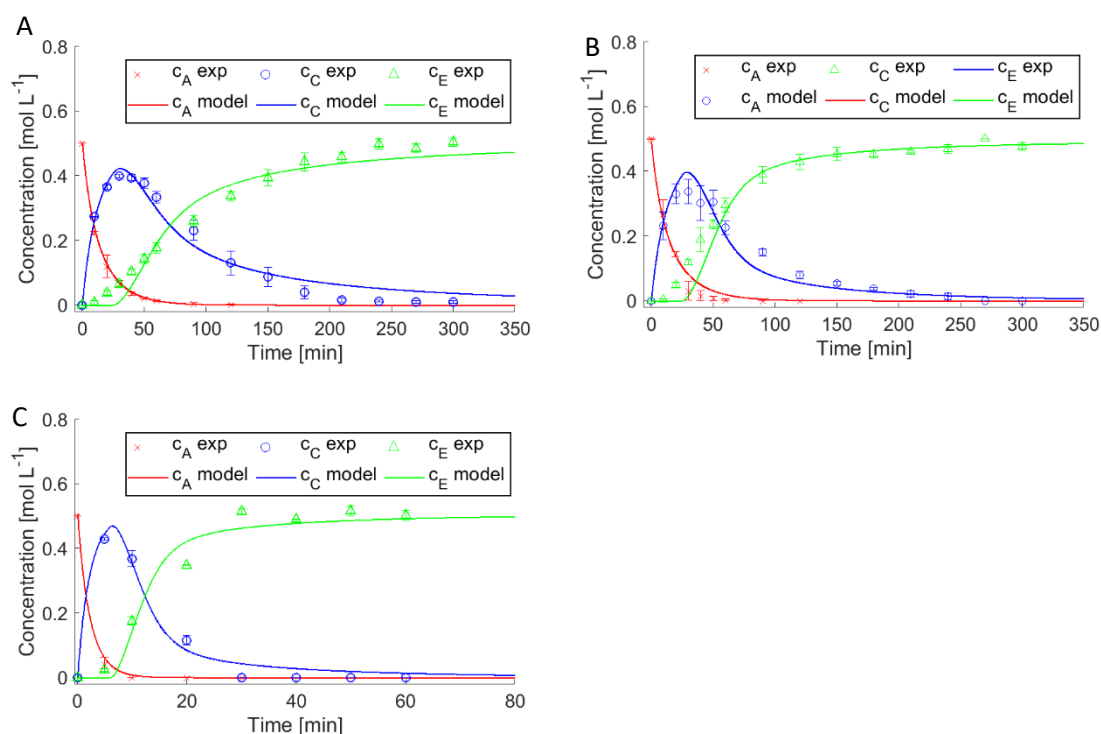


Figure 16 (A) shows the time conversion curve for catalytic membranes in toluene, (B) is the time concentration diagram for catalytic membrane in DMF and (C) is the time-concentration curve of the printed structure in toluene. Red is the amount of dimethoxy benzyl, blue is the amount of benzaldehyde and C is the amount of ethyl-2-cyano-3-phenylacrylate.

Table 1: Fitted parameters for the first cycle of different solvent and structure.

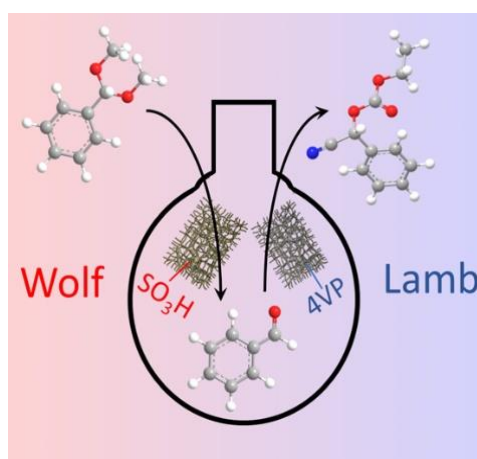
	Electrospun DMF	Electrospun toluene	Printed toluene [mol (L min) ⁻¹]
c_{A0}	0.50 mol L ⁻¹	0.49 mol L ⁻¹	0.50 mol L ⁻¹
c_{B0}	1.27 mol L ⁻¹	1.10 mol L ⁻¹	0.80 mol L ⁻¹
c_{D0} (fixed)	0.6 mol L ⁻¹	0.6 mol L ⁻¹	0.6 mol L ⁻¹
k_1	0.067 (mol L min) ⁻¹	0.073 mol L ⁻¹	0.94 mol (L min) ⁻¹
k_2	0.035 (mol L min) ⁻¹	0.059 mol L ⁻¹	0.250 mol (L min) ⁻¹

5.3.1. Individual Contribution of Joint Publications

The synthesis and analysis of the copolymers as well as the kinetical studies and the processing of the polymeric materials were done by me. Markus Dietel helped with the development of the *N*-(4-vinylbenzyl)phtalimide containing copolymer. The Raman imaging and spectroscopy was done by Dr. Holger Schmalz. Gabriel Sitaru did the fitting of the reaction equation under the supervision of Prof. Dr. Stephan Gekle. The manuscript was written with the contribution of all authors. Prof. Dr. Seema Agarwal (corresponding author) was responsible for supervising, helping with the design of the concept as well as with the discussion.

6. Reprint of publications

6.1. Wolf-Lamb-type Catalysis in One Pot Using Electrospun Polymeric Catalyst Membranes



Abstract

Multistep catalytic transformations using incompatible catalysts (Wolf-Lamb-type) in a one-pot reaction cascade requires site isolation of different catalysts by compartmentalization. In this work, we show the use of different electrospun catalytic membranes in a modular way as individual compartments are shown for one-pot Wolf-Lamb-type reaction cascades. The data are presented for one-pot cascade reaction sequences catalyzed by acidic and basic membranes made by electrospinning of polymeric acid (poly (styrene-co-styrene sulfonic acid-co-4-methacryloyl-oxybenzophen)) and basic (poly(styrene-co-4-vinylpyridine-co-4-methacryloyl-oxybenzophen)) catalysts, respectively. The two-step one-pot system used is the acidic catalyzed deacetylation of dimethoxybenzylacetale to benzaldehyde to result in a high yield of product (over 90%) under base-catalyzed conditions. The reaction kinetics are further monitored and evaluated by using differential equations showing the necessity of a parameter Δt to represent a retarded start for the second reaction step. The concept provides an easy and up-scalable approach for use in Wolf-Lamb-type systems.

Wolf-Lamb-type catalysis is a concept for the parallel use of incompatible catalysts as already investigated by *Cohen et al.* in 1977.¹ Here, the incompatible catalysts are

immobilized and separated from each other while staying in the same reaction chamber.^{2,3} Hence, it is possible to prevent deactivation and obtain multi-step one-pot reactions. One of the major challenges in the field of one-pot Wolf-Lamb-type catalysis is the use of appropriate catalytic carriers that prevent the contact and, hence, the deactivation of catalysts while being easy to make and up-scalable. The known concepts of immobilizing the wolf-lamb-type catalysts utilize both homogenous and heterogenous catalysis. In homogenous catalysis, mainly star polymers as investigated by *Voit*⁴ or microcapsules as shown by *Jones et al.*, were mainly used.²⁻⁵ The problems here are time- and energy-consuming synthetical procedures and the difficult separation of the catalysts.⁶ To prevent such problems, a common approach is the immobilization of the catalyst on a heterogenous substrate, leading to an easy separable system.^{2,7} Different concepts are used, such as metal organic frameworks by *Park et al.*,⁸ which have great possibilities in catalytic reactions based on the cavities inside, which enables immobilization of nanoparticles, or alternatively, the sites themselves can contain acidic or basic functionalities having great advantages for multi-step reactions.^{8,9} Nevertheless, the crystalline structure can be damaged by solvents or reaction conditions, while the pore size might be too small for some reagents leading to a deactivation through limited mass transport.⁹ Further, commonly approached systems are silica¹⁰ and gels.⁶ These architectures require multi-step synthetic procedures that are possible only in small amounts.

Organic fibers and textile immobilized with organocatalysts have also been explored as heterogenous catalysts.¹¹ The textile fibers, such as cotton, polypropylene, nylon, and polyethylene terephthalate, are modified either with the functional groups for catalysis by photo grafting or immobilized with metal nanoparticles.¹²⁻¹⁶

Our approach focused on the use of catalytic porous fibrous membranes made directly from the corresponding polymeric acid and base catalysts by the process of electrospinning in a simple way.¹⁷⁻¹⁹ This approach offers several unique advantages for using electrospun membranes in cascade reactions, especially with Wolf-Lamb-type catalysts. The separation between the Wolf-Lamb-type catalysts is easily achieved by fixing individual membranes in frames and inserting them in a reaction medium in one-pot. The approach offers several other unique advantages, such as 1) the direct use of catalytic membranes for one-pot cascade reactions with Wolf-Lamb-type catalysts even for multistep reactions in the future; 2) the preparation of catalytic membranes in large amounts and sizes, and 3) the preparation of catalytic membranes by direct spinning of

polymeric acid and bases synthesized by simple radical polymerization avoiding the need for any precise chemistry for the immobilization of catalytic functional groups. The electrospun membranes, also generally have an inherent porosity of more than 60 – 70% which could be an additional add-on for better mass transport for catalytic uses.²⁰⁻²³ The stability of the electrospun catalytic membranes in solution will be provided by photo crosslinking.

We show the proof of concept by using an acidic copolymers catalyst of styrene (S), sodium styrene sulfonic acid (SSA), and 4-benzoylphenyl methacrylate (MABP) (p(S-co-SSA-co-MABP)). As a basic catalyst, a copolymer of S, 4-vinylpyridine (4VP) and MABP (p(S-co-4VP-co-MABP)).

The polymers were synthesized through free radical polymerization, and photo crosslinkable MABP was incorporated in polymers to make the electrospun catalytic membranes stable in solvents by photocrosslinking. The MABP is widely used for crosslinking of macromolecular chains in the literature.^{24,25} Determination of the amount of sodium styrene sulfonate in the copolymer with the help of ¹H-NMR was not possible due to the overlay of the protons of the phenyl ring of comonomers, S and SSNa. Therefore, a combination of elemental analysis and ¹H-NMR was used for copolymer composition calculation. The acidic catalyst (p(S-co-SSNa-co-MABP)) has 27 mol% SSNa, 58 mol% S and 15 mol% MABP (Table S1 and Figure S2, Supporting Information). The molecular weight, det

ermined through gel permeation chromatography (GPC) in DMF, is (number average molecular weight) $\overline{M}_n = 170000$ with a dispersity of $\mathcal{D} = 2.0$ (Figure S1, Supporting Information). The p(4VP-co-S-co-MABP) has a copolymer composition (determined through ¹H-NMR in CDCl₃; Figure S4, Supporting Information) of 50 mol% 4VP, 40 mol% styrene and 11 mol% MABP. The molecular weight, determined through GPC in DMF, is $\overline{M}_n = 60000$ with a dispersity $\mathcal{D} = 1.5$ (Figure S3, Supporting Information).

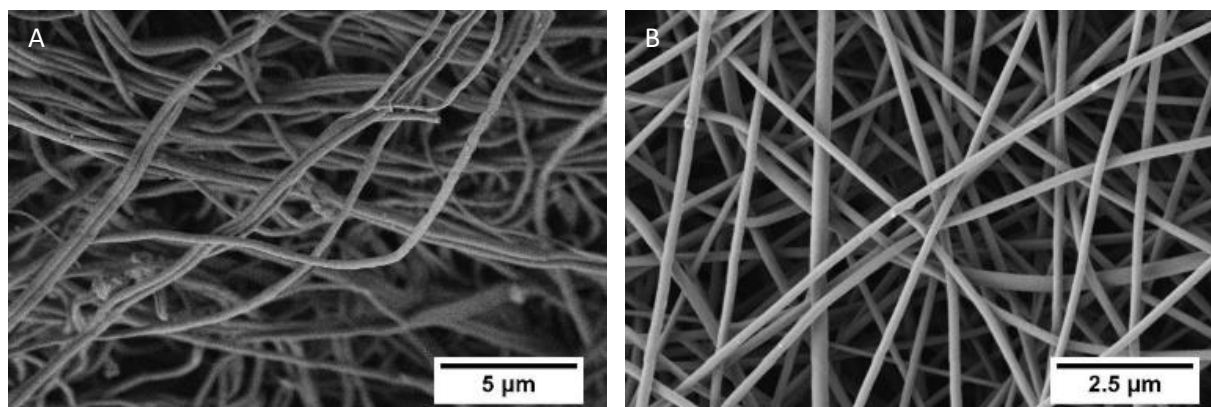
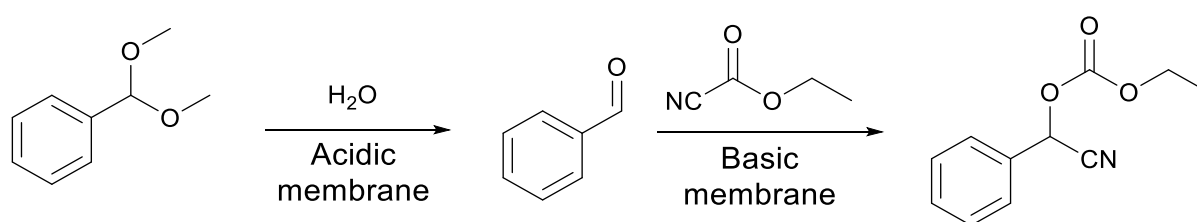


Figure 17: Scanning electron microscope images of A) p(S-co-SSNa-co-MABP) and B) p(S-co-4VP-co-MABP) as electrospun membranes with a homogenous fiber structure.

The polymers obtained were processed by electrospinning to produce a heterogenous catalytic system in the form of a porous membrane. The electrospun p(S-co-4VP-co-MABP) (thickness $150 \pm 10 \mu\text{m}$, density: 160 mg cm^{-3}) was used directly, while the acidic catalyst p(S-co-SSNa-co-MABP) (thickness: $180 \pm 20 \mu\text{m}$, density: 40 mg cm^{-3}) was further protonated by immersion in methanol and dropwise addition of concentrated hydrochloric acid to obtain p(S-co-SSA-co-MABP). The electrospun fibrous membranes were crosslinked by exposure to UV-light (2 h per side with 60 mW cm^{-2}). The obtained crosslinked fibers are displayed in Figure 17, showing a homogenous randomly laid fiber structure (average fiber diameter for p(S-co-SSNa-co-MABP) (Figure 17 A) is $340 \pm 80 \text{ nm}$ and for p(S-co-4VP-co-MABP) (Figure 17 B) is $240 \pm 60 \text{ nm}$). The membranes were stable after immersion in DMF (reaction solvent) due to the photo-crosslinking.



Scheme 11. Reaction scheme for the two-step one-pot reaction used. The first reaction is the acidic catalyzed deacetylation of dimethoxybenzylacetale to benzaldehyde, which reacts with ethyl cyanofomate basic catalyzed to cyano(phenyl)methyl ethyl carbonate.

A two-step one-pot acid-base catalyzed reaction sequence was tested for the catalytic experiment (Scheme 11). The first reaction step is the acidic catalyzed deacetylation of dimethoxybenzylacetale to benzaldehyde, which reacts with ethyl cyanofomate in the presence of the basic catalyst to cyano(phenyl)methyl ethyl carbonate. Dimethoxybenzylacetale (0.5 mol

L⁻¹), water (1 mol L⁻¹) and ethyl cyanofornate (0.6 mol L⁻¹) were used for the reactions. The amount of catalytic site was 5 mol% in case of the p(S-co-SSA-co-MABP) and 25 mol% for p(S-co-4VP-co-MABP). These values correspond to 62 wt% electrospun catalytic membrane of p(S-co-4VP-co-MABP) with respect to the amount of dimethoxybenzylacetale. The depletion of the dimethoxybenzylacetale, the depletion and increase of benzaldehyde and the overall increase of cyano(phenyl)methyl ethyl carbonate were monitored with gas chromatography (*Figure 18*). Undecane was used as an internal standard.

A yield of over 90% is obtained for the first step (deacetylation). The deacetylation reaches a conversion of over 50% within the first 30 minutes and is finished at around 150 minutes, as seen by measuring the amount of dimethoxybenzyl acetate by GC (*Figure 18*, red curve). The individual acid and base catalyzed reactions were also carried out under similar conditions as those used in the cascade reaction (*Figure S7*, Supporting Information). The reaction were slowed down in one-pot compared to the individual reaction steps. Although a slight deactivation of the acid catalyst might occur due to the proton conduction by water in the presence of base membrane within the reaction mixture slowing down the reaction, the reaction was still completed within a reasonable time frame. A maximum amount of benzaldehyde is reached at 60 minutes, after which, it decreased below to around 20% due to the start of the second-step reaction with ethyl cyanofornate, in which an induction time of around 60 min is observed. The induction time is also observed for the base catalyzed reaction carried out individually in a separate experiment, but the time is shorter (about 30 min) compared to the cascade reaction (*Figure S7B*, Supporting Information). The overall yield of cyano(phenyl)methyl ethyl carbonate is about 80%. The induction effect in the ZnO-catalyzed Knoevenagel condensation reaction between benzaldehyde and ethyl cyanoacetate is reported in the literature.²⁶ In the present work, the polymer (p(S-co-4VP-co-MABP)) is a weak base. This might be due to the diffusion-controlled local enrichment of the reactants on the polymeric catalytic membrane leading to the start of the reaction after an induction period. The local enrichment effect of the reactants is used to explain the unexpected increase in catalytic reaction rates in some reactions in the literature.²⁷

By comparison, the *p*-toluene sulfonic acid and 4VP used with no further immobilization showed, that no conversion of cyano(phenyl)methyl ethyl carbonate was achieved after 6h, proving the necessity of the immobilized polymeric materials.

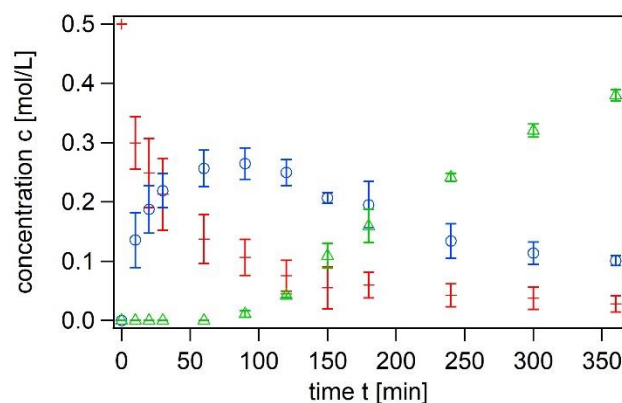
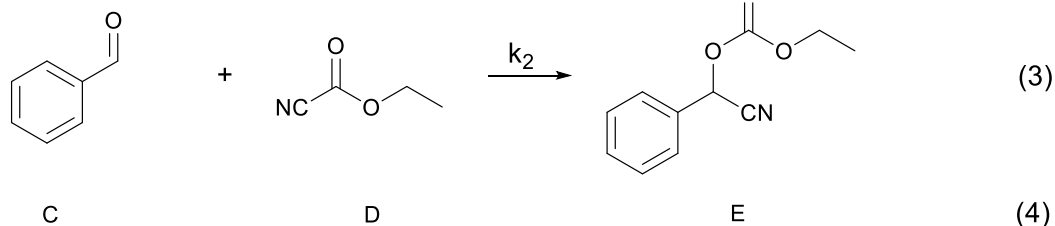
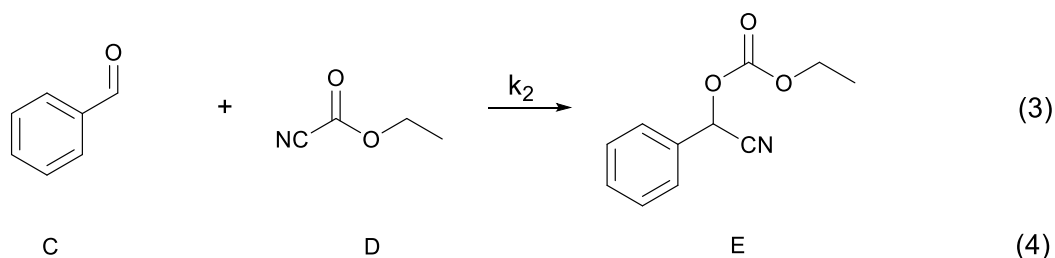
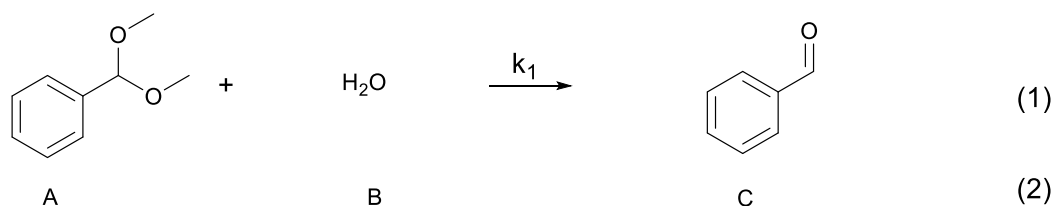


Figure 18. Obtained data of the two-step reaction. “Red plus” are the amount of dimethoxybenzylacetate, “Blue circles” are the amount of the product of the first reaction: benzaldehyde. “Green triangles” show the conversion to the final product, cyano(phenyl)methyl carbonate.

The data obtained were further investigated through different differential fitting functions to obtain a better understanding of the underlying reaction dynamics. Therefore, the reaction equation (*Scheme 11*) was separated in the following reactions and equations to determine these parameters (*Scheme 12*).



Scheme 12: Separated reaction equations for the solution of the differential equations. A is dimethoxybenzylacetale, B is water, C is benzaldehyde, D is ethyl cyanofornate and E is cyano(phenyl)methyl ethyl carbonate. k_1 and k_2 are the reaction kinetical parameters for the first, respectively second reaction step.

With the help of these reaction equations (*Equation 2* and *Equation 4* in *Scheme 2*), it is possible to develop the differential equations for the calculations (*Equation 5* – *Equation 9*).

$$\frac{dc_A}{dt} = -k_1 c_A(t) c_B(t) \quad (5)$$

$$\frac{dc_B}{dt} = -k_1 c_A(t) c_B(t) \quad (6)$$

$$\frac{dc_C}{dt} = k_1 c_A(t) c_B(t) - k_2 c_C(t - \Delta t) c_D(t) \quad (7)$$

$$\frac{dc_D}{dt} = -k_2 c_C(t - \Delta t) c_D(t) \quad (8)$$

$$\frac{dc_E}{dt} = k_2 c_C(t - \Delta t) c_D(t) \quad (9)$$

Fitting these equations to the time conversion curves obtained lead to the results shown in *Figure 3*. Through *Figure 19A* ($\Delta t = 0$), it was possible to determine that the second reaction has a retarded starting time, which is expressed with the parameter Δt in *Equation 7* – *Equation 9*. The fit for the amount of dimethoxy benzyl acetal and benzaldehyde showed a good alignment with the experimental values, but the fitted curve did not show a reasonable alignment for the amount of compound E (cyano(phenyl)methyl ethyl carbonate) (values are shown in the *Table S2*, Supporting Information), furthermore, the obtained value for $c_D^0 = 252 \text{ mol L}^{-1}$ is clearly too high.

It can be seen that the second reaction step started only after the conversion of benzaldehyde reached a sufficient amount and cyano(phenyl)methyl ethyl carbonate was obtained. It seems that, while C is produced quickly by the first reaction, it requires a certain amount of time before it becomes available for the second reaction. A fit can be achieved through the addition of a fitting parameter Δt to describe the delayed start of the second reaction step, which shows the conversion of the product within a reasonable error (*Figure S8* and *Table S3*, Supporting Information). The value of $c_D^0 = 20.4 \text{ mol L}^{-1}$ gets closer to the starting value but is still too high. In the next step, therefore, it was fixed at 0.6 mol L^{-1} to stay at the experimental starting value (*Figure 19B*).

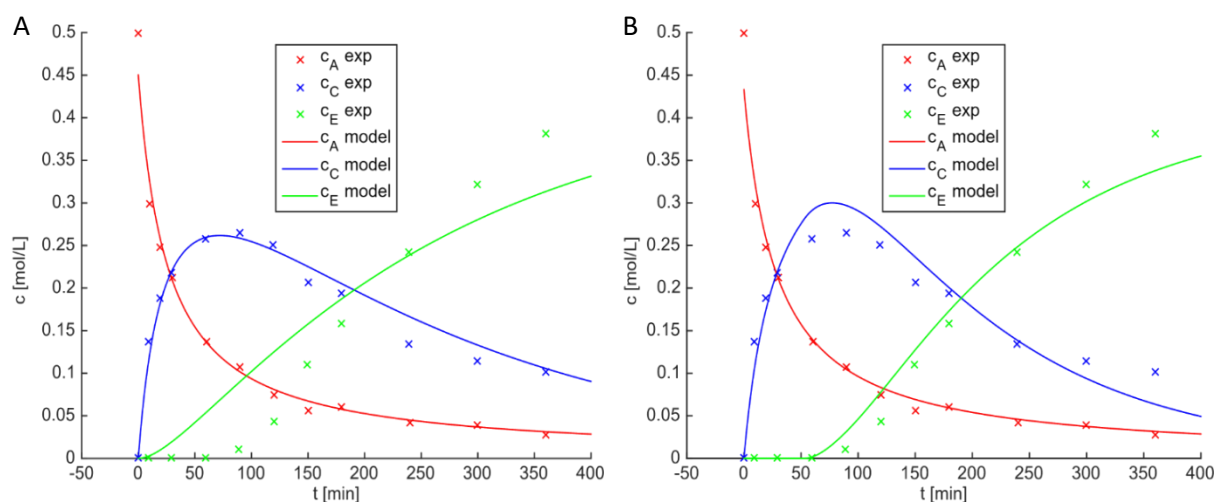


Figure 19: Kinetic study of the catalytic reaction. A shows the obtained values fitted through a second order kinetic. The obtained fit function shows a good validity for the amount of dimethoxybenzyl acetal as well as the benzaldehyde, but the fit for the cyano(phenyl)methyl ethyl carbonate, does not show a good validity. Through the addition of a Δt parameter for a retarded reaction start, a fit is obtained showing good results for all parameters (B).

The alignment of the fitted amount of product ($c_E(t)$) is much better through the addition of the fixed value of c_D^0 , and the intermediate benzaldehyde ($c_C(t)$) fitted is only changed minimally but stays within a reasonable mistake resulting in $c_A^0 = 0.43 \text{ mol L}^{-1}$, $c_B^0 = 0.43 \text{ mol L}^{-1}$, $c_D^0 = 0.6 \text{ mol L}^{-1}$, $k_1 = 0.081 \text{ mol (L min)}^{-1}$, $k_2 = 0.013 \text{ mol (L min)}^{-1}$ and $\Delta t = 67 \text{ min}$. Fixing c_A^0 and c_B^0 leads to worse results.

Two conclusions can be drawn from these parameters. First, the amount of water for the reaction is lower than expected. It seems water is not available in the amount intended and it is possibly adsorbed at the catalytic membranes and, thus, further investigations are needed. Second, the implementation of a retarded start parameter Δt already leads to a reasonable fit. This, furthermore, shows that the delay is not due to special mechanisms, but the second reaction step starts only after sufficient amount of $c_C(t)$ is reached.

In our work, we were able to show the successful production of catalytic membranes by direct electrospinning of acid and base polymers individually. These catalytic membranes were then photo crosslinked with UV light to ensure stability in organic solvents. A successful two-step reaction was established with an acidic catalyzed deacetylation followed by a basic catalyzed reaction with ethyl cyanofornate to cyano(phenyl)methyl ethyl carbonate. The overall yield obtained was approximately 80% and it was shown that polymeric electrospun membranes are a promising material for Wolf-Lamb-type catalysis. Kinetic observation showed that the second reaction step has a retarded start. A more complex modeling effort, including full numerical

simulations of material flows, is currently on-going and will be presented in a future publication. Other polymeric catalysts will be investigated in the future for broadening the application of such systems in a modular way.

Acknowledgements

For financial support we thank the DFG (SFB 840). Rika Schneider is thanked for analytical assistance.

References

- [1] (a) B. J. Cohen, M. A. Kraus, A. Patchronik, *J. Am. Chem. Soc.* **1977**, *99*, 4165;
(b) B. J. Cohen, M. A. Kraus, A. Patchronik, *J. Am. Chem. Soc.* **1981**, *103*, 7620.
- [2] L.-C. Lee, J. Lu, M. Weck, C. W. Jones, *ACS Catal.* **2016**, *6*, 784.
- [3] M. B. J. Atkinson, S. Oyola-Reynoso, R. E. Luna, D. K. Bwabok, M. M. Thuo, *RSC Adv.* **2015**, *5*, 597.
- [4] B. Voit, *Angew. Chem., Int. Ed.* **2006**, *45*, 4238.
- [5] A. L. Miller, N. B. Bowden, *Adv. Mater.* **2008**, *20*, 4195.
- [6] N. Singh, K. Zhang, C. A. Angulo-Pachón, E. Mendes, J. H. van Esch, B. Escuder, *Chem. Sci.* **2016**, *7*, 5568.
- [7] Y. Chi, S. T. Scroggins, J. M. J. Fréchet, *J. Am. Chem. Soc.* **2008**, *130*, 6322.
- [8] K. Akagawa, S. Sakamoto, K. Kudo, *Tetrahedron Lett.* **2007**, *48*, 985.
- [9] J. Park, J.-R. Li, Y.-P. Chen, J. Yu, A. A. Yakovenko, Z. U. Wang, L.-B. Sun P. B. Balbuena, H.-C. Zhou, *Chem. Commun.* **2012**, *48*, 9995.
- [10] A. Dhakshinamoorthy, H. Garcia, *ChemSusChem* **2014**, *7*, 2392-2410.
- [11] J.-W. Lee, T. Mayer-Gall, K. Opwis, C. E. Song, J. S. Gutmann, B. List, *Science* **2013**, *341*, 1225.
- [12] J. Du, M. Tao, W. Zhang, *ACS Sustainable Chem. Eng.* **2016**, *4*, 4296.
- [13] S. Shylesh, A. Wagener, A. Seifert, S. Ernst, W. R. Thiel, *Angew. Chem., Int. Ed.* **2009**, *49*, 184.
- [14] G. Bredig, F. Gerstner, H. Lang, *Biochem. Z.* **1935**, *88*, 282.
- [15] T. Mayer-Gall, J.-W. Lee, K. Opwis, B. List, J. S. Gutmann, *ChemCatChem* **2016**, *8*, 1428.
- [16] W. Feng, T. Huang, L. Gao, X. Yang, W. Deng, R. Zhou, H. Liu, *RSC Adv.* **2018**, *8*, 6288.

- [17] G. Chang, W. Ullah, Y. Hu, L. Lin, X. Wang, C. Z. Li, *Macromol. Rapid Commun.* **2018**, 39, 1800102.
- [18] S. Agarwal, J. H. Wendorff, A. Greiner, *Macromol. Rapid Commun.* **2010**, 31, 1317.
- [19] G. Duan, M. Koehn-Serrano, A. Greiner, *Macromol. Rapid Commun.* **2017**, 38, 1600511.
- [20] M. Stasiak, A. Studer, A. Greiner, J. H. Wendorff, *Chem. - Eur. J.* **2007**, 13, 6150.
- [21] M. Stasiak, C. Röben, N. Rosenberger, F. Schleth, A. Struder, A. Greiner, J. H. Wendorff, *Polymer* **2007**, 48, 5208.
- [22] F. Mitschang, H. Schmalz, S. Agarwal, A. Greiner, *Angew. Chem., Int. Ed.* **2014**, 53, 4972.
- [23] E. Formo, J. Xie, W. L. Liu, Y. Xia, *Acc. Chem. Res.* **2017**, 50, 1976.
- [24] E. Giebel, C. Mattheis, S. Agarwal, A. Greiner, *Adv. Funct. Mater.* **2013**, 23, 3156.
- [25] S. Jiang, G. Duan, U. Kuhn, M. Mörl, V. Altstädt, L. Yarin, A. Greiner, *Angew. Chem., Int. Ed.* **2017**, 56, 3285.
- [26] J. P. H. Li, A. A. Adesina, E. M. Kennedy, M. Stockenhuber, *Phys. Chem. Chem. Phys.* **2017**, 19, 26630.
- [27] H. Seto, K. Imai, Y. Hosino, Y. Miura, *Polym. J.* **2016**, 48, 897.

Supporting Information

Experimental Section

Materials

THF (p.a. grade), DMF (p.a. grade) and DMSO (p.a. grade) were purchased from Alfa Aesar. 4-vinylpyridine (98%, Alfa Aesar) and styrene (98%, Alfa Aesar) was distilled in vacuo prior to use. Sodium styrene sulfonate (90%, Alfa Aesar) was recrystallized from a mixture of ethanol and water. For catalytic experiments ethyl cyanofornate (98% Alfa Aesar), dimethoxybenzyl acetal (99%, Alfa Aesar) and undecane (>99%, Alfa Aesar) were used as received.

Methods

Nuclear magnetic resonance (NMR) spectroscopy: ^1H -NMR experiments were recorded on a Ultrashield-300 spectrometer at room temperature in either CDCl_3 or DMSO-d_6 . Spectra were calibrated according to the residue protons of the deuterated solvent signal. Evaluation of spectra was done with MestReNova (Mestrelab research, version 6.1).

Electrospinning experiments were performed with an electrospinning machine built by the electronic and mechanical workshop of University of Bayreuth. For making p(S-co-SSNa-co-MABP) fibers, a solution of 20 wt% in DMF was prepared and electrospinning was conducted with a conventional one-needle setup at a high voltage of 14 kV. The fibers were collected on a rotational disc collector on baking paper with a flow rate of $150 \mu\text{L h}^{-1}$.

For p(S-co-4VP-co-MABP) membrane, the solution used was 40wt% and a high voltage of 12 kV is used. The flow rate was $300 \mu\text{L h}^{-1}$.

Scanning electron microscopy (SEM): The surface morphology was observed with a Zeiss LEO 1530, operating at an acceleration voltage of 3 kV employing an Everhart-Thornley secondary electron detector. Before imaging, the samples were sputtered with a thin platinum layer of 2 nm (Sputter Coater 208HR, Cressington).

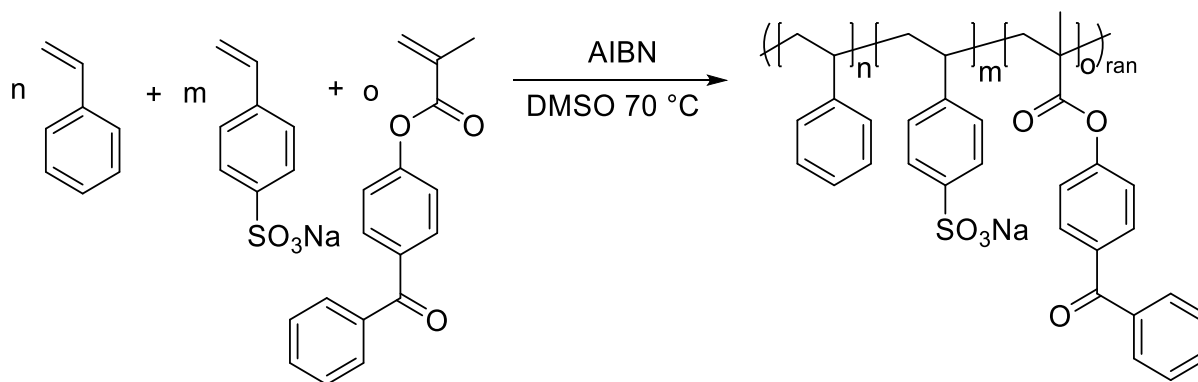
Gel Permeation Chromatography (GPC) measurements were performed in DMF (HPLC grade) with lithium bromide (5 g L^{-1}) as eluent and solvent and an internal standard of toluene on 2 PSS-GRAM gel columns (particle size = $10 \mu\text{m}$) with a porosity of 100 to 3000 \AA with a flow rate of 0.5 mL min^{-1} and a refractive index detector (Agilent Technologies) on a SEC 1260 Infinity (Agilent Technologies). For calibration narrowly distributed polystyrene homopolymer were used (PSS calibration kit).

Gas Chromatography (GC): GC measurements were performed on a GC-FID system (GC-2010 Plus, Shimadzu), using Nitrogen as a carrier gas. $10 \mu\text{L}$ of the reaction mixture was dissolved

in 1 mL acetonitrile. 1 μL was injected with a split ratio of 1:50 and measured from 50 $^{\circ}\text{C}$ (2 min hold) up to 300 $^{\circ}\text{C}$ with a heating rate of 15K min^{-1} .

Mathematical operations for fitting of reaction parameters were done with Matlab Version R2015a.

Synthesis of p(S-co-SSNa-co-MABP)



Scheme S1: Reaction scheme for the free radical polymerization of styrene, sodium styrene sulfonate and 4-methacryloyl-oxybenzophenone to p(S-co-SSNa-co-MABP).

0.1 eq 4-methacryloyl-oxybenzophenone and 0.25 eq recrystallized sodium styrene sulfonate were placed in a round bottle Schlenk flask and dissolved in DMSO ($c = 4 \text{ mol L}^{-1}$). To the solution, 0.65 eq styrene was added and the reaction mixture was degassed with argon, heated to 70 $^{\circ}\text{C}$ and 0.6 wt% AIBN was added. The polymer was then precipitated in Isopropanol and dried at 60 $^{\circ}\text{C}$ in vacuo.

^1H NMR (300 MHz, CDCl_3): δ/ppm : 1.0-1.6 (polymer backbone, $-\text{CH}_2-$; $-\text{CH}_3$); 1.6-2.5 (polymer backbone $-\text{CH}-$); 6.0-6.6 (aromatic, $-\text{C}-\text{CH}=\text{C}-\text{H}$; $-\text{CH}-\text{CH}=\text{CH}-$; $-\text{C}-\text{CH}=\text{CH}-\text{SO}_3$); 6.6-7.2 (aromatic, $-\text{CH}-\text{CH}=\text{CH}-$); 7.4-7.7 (aromatic $-\text{C}-\text{CH}=\text{CH}-$; $-\text{CH}-\text{CH}=\text{C}-$)

DMF-GPC measurements

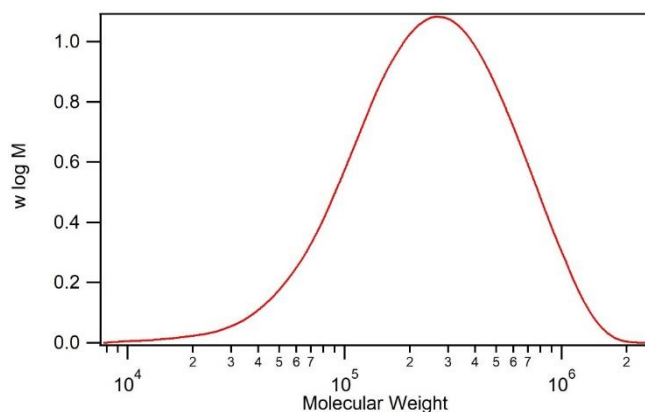


Figure S1: DMF-GPC measurement of p(S-co-SSNa-co-MABP).

Elemental analysis

Table S2: Elemental analysis for the calculation of the amount of sodium styrene sulfonate.

Element	Amount [wt%]
H	5.939
C	70.310
N	0.025
S	4.429
O	16.146

Amount of styrene sulfonic acid calculated through chemical elemental analysis: 27%
Calculation were as follows:

First, all amounts were calculated into mol% (equation 1 and 2).

$$mol_{Element} = \frac{wt_{sample} * wt\%}{100 * M_{Element}} \quad (S1)$$

$$mol\% = \frac{mol_{Element}}{mol_C + mol_S + mol_O} \quad (S2)$$

Second, from these amounts the corresponding amount of carbon of the different monomers were calculated, based on sodium styrene sulfonate.

$$mol\%_{C(SSA)} = mol\%_S \times 8 \quad (S3)$$

$$mol\%_{C(MABP)} = (mol\%_O - mol\%_C \times 3) \times 17 \quad (S4)$$

$$mol\%_{C(S)} = mol\%_C - mol\%_{C(SSA)} - mol\%_{MABP} \quad (S5)$$

The obtained value of $mol\%_{SSA}$ was used as a fixed value and the amount of styrene and methyl acrylbzophenone was calculated with the help of $^1\text{H-NMR}$ (Figure S2).

To calculate the values by use of $^1\text{H-NMR}$ following assumptions were used: \int "1 – 5" is the amount of styrene and styrene sulfonic acid and equals 2.21. \int "6 – 19" equals the integral of MABP. To calculate the amount of MABP and Styrene sulfonic acid following equation was used:

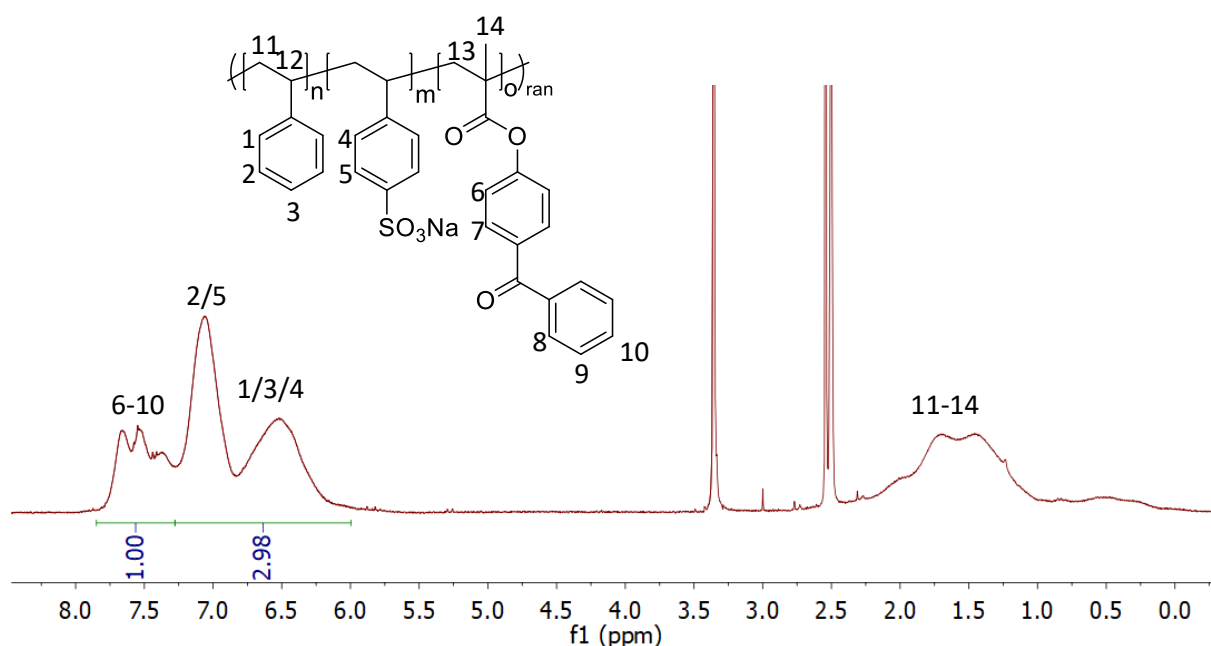


Figure S2: $^1\text{H-NMR}$ of the copolymer $p(\text{S-co-SSNa-co-MABP})$ measured in DMSO-d_6 and referenced to the residue protons of the deuterated solvent.

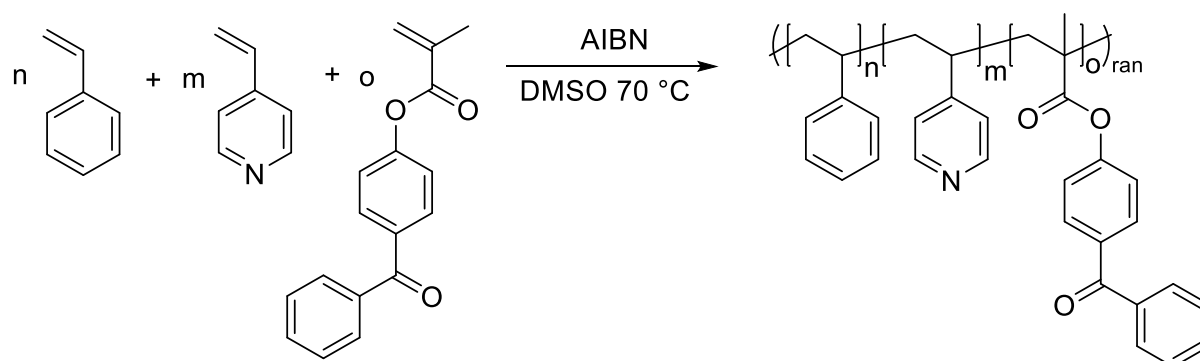
$$mol\%_{SSA} = \frac{\frac{x}{4}}{\frac{1}{9} + \frac{2,11-x}{5} + \frac{x}{4}} \quad (S6)$$

With x the amount of SSA of \int "1 – 5". By using $mol\%_{SSA} = 0,27$, x equals 0,61. With that the equation can be solved for mol% of styrene and MABP leading to the following values:

Styrene = SSA = 27% MABP = 15% Styrene = 58%.

Overall, the amount of MABP is slightly higher than in the feed, leading to the assumption, that it is preferably used in the polymer.

Synthesis of p(S-co-4VP-co-MABP)



Scheme S2: Reaction scheme of the free radical polymerization of styrene, 4-vinylpyridine and 4-methacryloyl-oxybenzophenone to p(S-co-4VP-co-MABP).

0.1 eq 4-methacryloyl-oxybenzophenone was placed in a round bottled Schlenk flask and dissolved in THF ($c_{Monomer} = 3 \text{ mol L}^{-1}$). To the mixture subsequently 0.4 eq styrene and 0.5 eq 4-vinylpyridine were added and the reaction mixture was degassed with Argon for 30 minutes. The reaction mixture was heated to 60 °C, 0.8 wt% AIBN was added and it was stirred for 16 h. The polymer was precipitated in diethyl ether. The crude product was then dried at 40 °C in vacuo.

$^1\text{H NMR}$ (300 MHz, CDCl_3): δ/ppm : 1.0-1.6 (polymer backbone, $-\text{CH}_2-$; $-\text{CH}_3$); 1.6-2.5 (polymer backbone $-\text{CH}-$); 6.0-6.6 (aromatic, $-\text{C}-\text{CH}=\text{C}-\text{H}$; $-\text{CH}-\text{CH}=\text{CH}-$; $-\text{C}-\text{CH}=\text{CH}-\text{N}=\text{C}$); 6.6-7.2 (aromatic, $-\text{CH}-\text{CH}=\text{CH}-$); 7.4-7.7 (aromatic $-\text{C}-\text{CH}=\text{CH}-$; $-\text{CH}-\text{CH}=\text{C}-$); 8.1-8.5 (aromatic, $-\text{CH}-\text{CH}=\text{N}-$)

$^{13}\text{C NMR}$ (75 MHz, CDCl_3): δ/ppm : 20 (polymer backbone, $-\text{CH}_3$), 36-50 (polymer backbone, $-\text{CH}_2-$), 120-144 (aromatic, $-\text{CH}=\text{C}$), 148-155 (aromatic, $\text{N}-\text{CH}=\text{C}$), 174 (ester, $-\text{C}-\text{C}-\text{O}-$), 195 (carbonyl $-\text{C}-\text{C}-\text{C}-$)

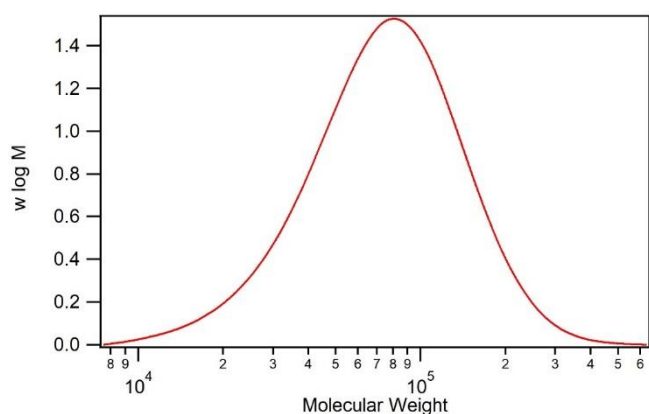


Figure S3: DMF-GPC measurement of p(S-co-4VP-co-MABP).

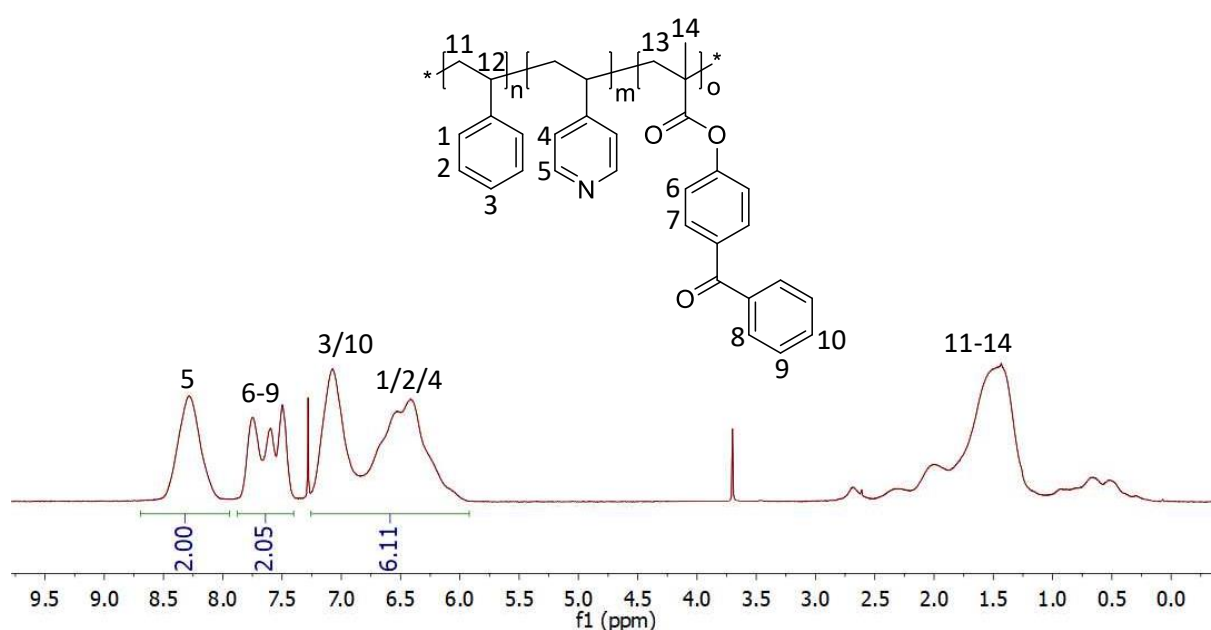


Figure S4: $^1\text{H-NMR}$ spectrum of p(S-co-4VP-co-MABP) measured in CDCl_3 .

Copolymer composition was determined through $^1\text{H-NMR}$ with the following formula:

$$\%4VP = \frac{\frac{f^{5''}}{2}}{\frac{f^{5''}}{2} + \frac{f^{6-9''}}{8} + \frac{f^{3/10/1/2/4''} - \frac{f^{6-9/5''} - f^{5''}}{8} - \frac{f^{5''}}{2}}{5}} \times 100\% \quad (\text{S7})$$

Here $\frac{f^{5''}}{2}$ is the amount of 4VP, $\frac{f^{6-9''}}{8}$ is the amount of 4-methacryloyl-oxybenzophenone,

$\frac{f^{3/10/1/2/4''} - \frac{f^{6-9/5''} - f^{5''}}{8} - \frac{f^{5''}}{2}}{5}$ is the amount of styrene.

Through the calculation following amounts were obtained:

49% 4VP, 11% MABP, 40% S.

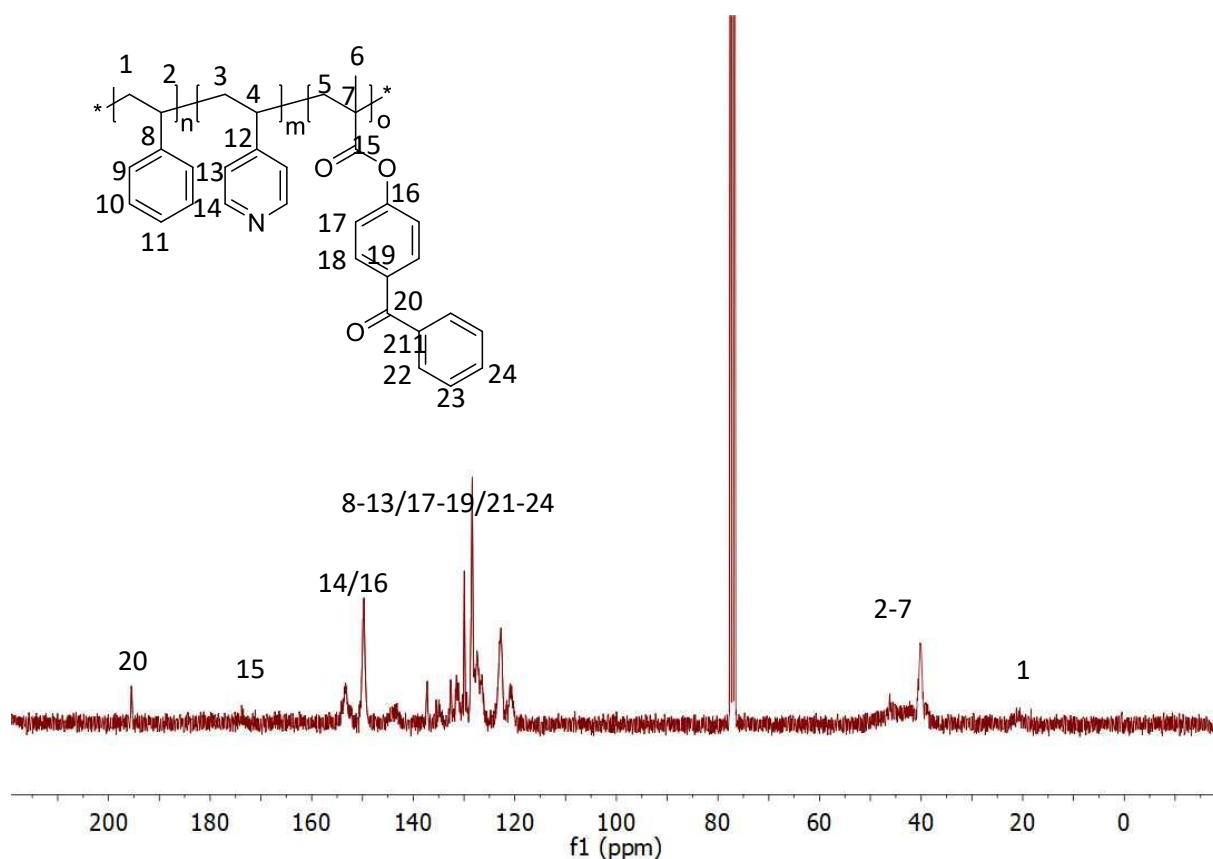


Figure S5: ^{13}C -NMR of $p(\text{S-co-4VP-co-MABP})$ measured in CDCl_3 .

Preparation of membrane for catalytic experiments

The prepared membranes were crosslinked with UV light (Honle UVAHAND 250 GS) at a distance of 15 cm (23 mW cm^{-1} for 2h at each side)

Membranes made of $p(\text{S-co-SSNa-co-MABP})$ were immersed in methanol and concentrated HCl solution was added dropwise. The membrane was washed with methanol and dried at room temperature overnight.

TGA data of dried membranes are shown in Figure S6.

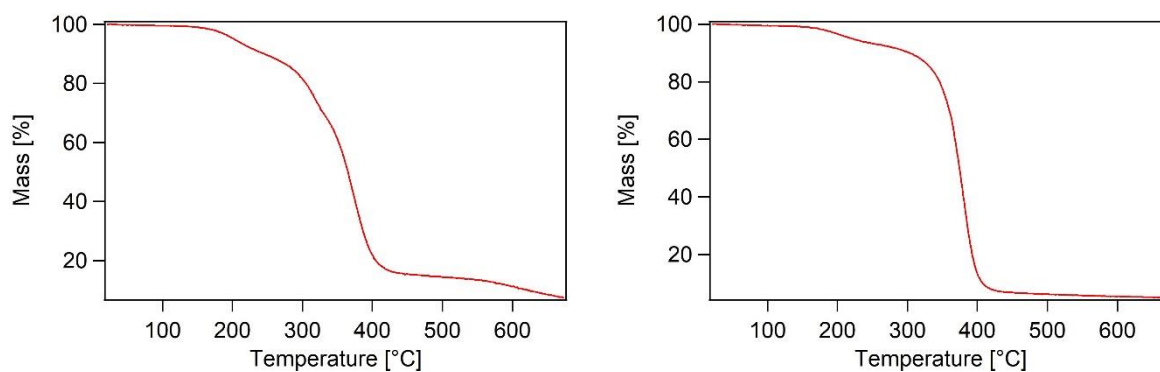
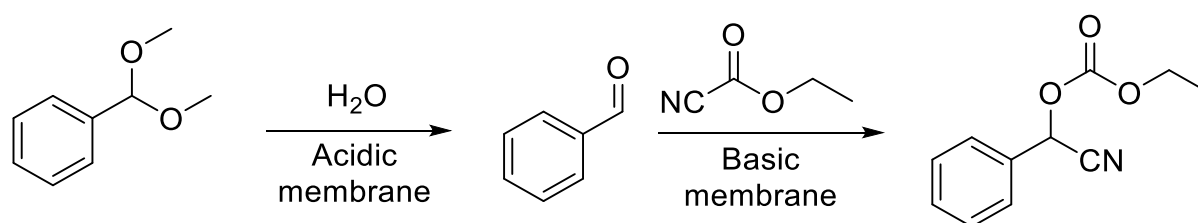


Figure S6: TGA data for p(S-co-SSH-co-MABP) (A) membranes and p(S-co-4VP-co-MABP) (B) after immersion in DMF and followed by drying the membranes *in vacuo*.

Catalytic experiment two step system



Scheme S3: Reaction scheme of the catalytic one-pot two-step reaction.

Catalytic membranes were placed in metal meshes for easy separation from the reaction mixture and prevention of damaging the membranes with the magnetic stirrer bar.

For the catalytic experiments, 1.89 mL (12.5 mmol, 1 eq) dimethoxybenzyl acetal was dissolved in 25 mL DMF ($c = 0.5$ mol/L) and subsequently 1.48 mL (15.0 mmol, 1.2 eq) ethyl cyanoformate and 450 μ L (25.0 mmol, 2 eq) water (Milli-Q) and undecane as an internal standard were added. The reaction mixture was heated to 80 °C and the immobilized membranes (800 mg p(S-co-4VP-co-MABP) and 350 mg p(S-co-SSH-co-MABP)) were immersed in the reaction medium (25 mL DMF). 10 μ L of the reaction mixture was dissolved in 1 mL Acetonitril in GC vials and the catalytic experiment was monitored through a GC, the product was determined through GC coupled with a mass spectrometer.

For a blind test, 376 μL (380 mg, 1 eq) dimethoxybenzyl acetal, 278 μL (297 mg, 1.2 eq) ethyl cyanoformate, 90 μL (90 mg, 2 eq) water and 296 μL Undecane were added in 5 mL DMF.

21.5 mg (125 μmol , 5 mol%) *p*-toluene sulfonic acid and 53.2 μL (52.5 mg, 20 mol%) 4-vinylpyridine were added.

The resulting catalytic mixture was heated to 80 °C for 6h.

One-step acidic and basic fiber mat catalyzed reactions

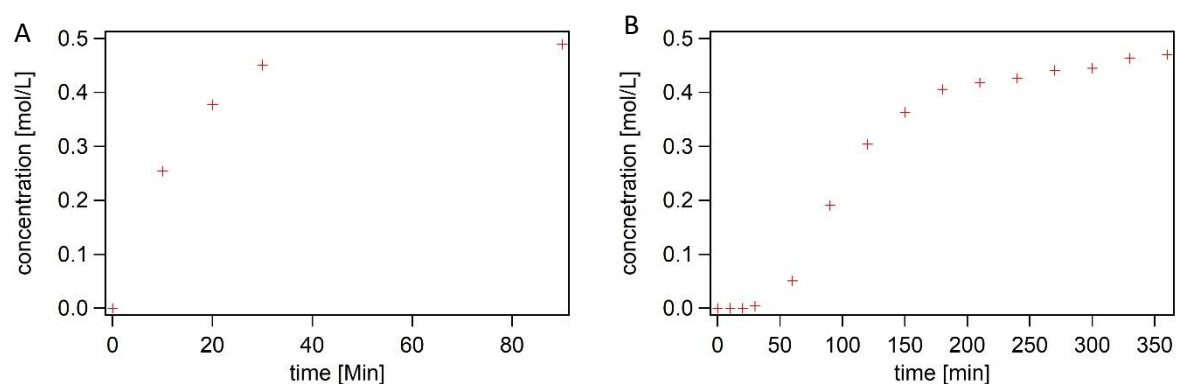


Figure S7: Acidic (A) catalyzed reaction from dimethoxybenzyl acetal to benzaldehyde and basic catalyzed (B) reaction of benzaldehyde to cyano(phenyl)methyl ethyl carbonate. Concentration of reagents 0.5 mol L⁻¹ dimethoxybenzyl acetal and 1 mol L⁻¹ water in case of acidic reaction and 0.5 mol L⁻¹ benzaldehyde and 0.6 mol L⁻¹ ethyl cyanoformate. In both cases, undecane was used as internal standard at 80°C in DMF.

Fitted Parameters

Fitting of the reaction rates and the concentration based on the experimental values were performed with Matlab Version R2015a.

Table S2. Results of the fitted reaction parameters shown in Figure 4A. For calculation Matlab was used.

Fitted parameter	Fitted value
c_A^0	$0.45 \text{ mol}\cdot\text{L}^{-1}$
c_B^0	$0.45 \text{ mol}\cdot\text{L}^{-1}$
c_D^0	$252 \text{ mol}\cdot\text{L}^{-1}$
k_1	$8.51 \cdot 10^{-2} \text{ L}\cdot(\text{mol}\cdot\text{min})^{-1}$
k_2	$1.81 \cdot 10^{-6} \text{ L}\cdot(\text{mol}\cdot\text{min})^{-1}$
Δt (fixed)	0 min

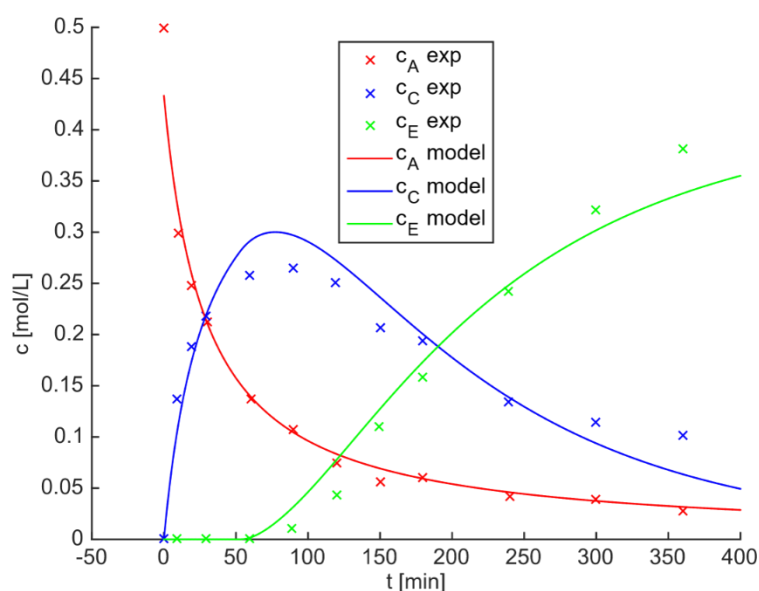
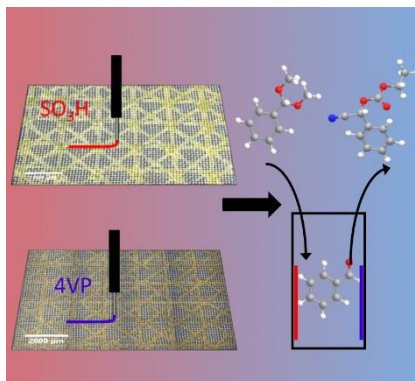


Figure S8. Fitted values with free D and Δt .

Table S3: Results of the fitted reaction parameters shown in Figure S8. For calculation Matlab was used.

Fitted parameter	Fitted value
c_A^0	$0.43 \text{ mol}\cdot\text{L}^{-1}$
c_B^0	$0.43 \text{ mol}\cdot\text{L}^{-1}$
c_D^0	$20.4 \text{ mol}\cdot\text{L}^{-1}$
k_1	$8.1 \cdot 10^{-2} \text{ L}\cdot(\text{mol}\cdot\text{min})^{-1}$
k_2	$2.71 \cdot 10^{-5} \text{ L}\cdot(\text{mol}\cdot\text{min})^{-1}$
Δt	53 min

6.2. Precise 2D-patterned Incompatible Catalysts for Reactions in One-Pot



*Martin O. Pretscher, Tingting Chen, Gabriel Sitaru, Stephan Gekle, Jian Ji and Seema Agarwal**

M. O. Pretscher, Prof. Dr. S. Agarwal

Macromolecular Chemistry II, Bavarian Polymer Institute, University of Bayreuth,
Universitätsstraße 30, 95440 Bayreuth, Germany

E-mail: agarwal@uni-bayreuth.de

T. Chen, Prof. Dr. J. Ji

MOE Key Laboratory of Macromolecule Synthesis and Functionalization of Ministry of
Education Department of Polymer Science and Engineering, Zhejiang University, Hangzhou
310027, China

G. Sitaru, Prof. Dr. S. Gekle

Theoretical Physics VI, Biofluid Simulation and Modelling, University of Bayreuth,
Universitätsstraße 30, 95440 Bayreuth

Keywords: 2D printing, heterogenous catalysis, acid base, incompatible catalysts

Abstract

Precise and direct two-dimensional (2D) printing of the incompatible polymer acid-base catalysts and their utility in one-pot two-step reactions were shown. Multistep catalytic reactions using incompatible catalysts in a one-pot reaction cascade requires special methods and materials to isolate the catalysts from each other. In general, this is a tedious process requiring special polymer architectures as carrier for the catalysts to preserve the activity of otherwise incompatible catalysts. We propose the immobilization of incompatible polymer catalysts, such as polymer acid and base catalysts, on a substrate in variable sizes and amounts by precise 2D printing. The terpolymers with a basic (4-vinylpyridine) and acidic (styrene sulfonic acid) functionality and methacryloyl benzophenone as a UV crosslinking unit were used for 2D printing on poly (ethylene terephthalate) (PET). The printed meshes were immersed together in a reaction solution containing (dimethoxy methyl)-benzene and ethyl cyanofornate, resulting in a two-step acid-base catalyzed cascade reaction; that is, deacetylation followed by carbon-building reaction. The time-dependent consumption of (dimethoxymethyl)-benzene to the intermediate benzaldehyde and the product was monitored, and a kinetic model was developed to investigate the underlying reaction dynamics. The complexity of multi-step Wolf-Lamb-type reactions was generally significantly decreased by using our approach because of the easy polymerization and immobilization procedure.

1. Introduction

Mutually incompatible functional groups, such as acid and base, deactivate each other in solution. When used as catalysts for organic reactions in one-pot, they lose their catalytic activity. Such catalysts are called Wolf-Lamb-type catalysts. The work of Patchornik opened up new possibilities for making one-pot reactions with incompatible catalysts of Wolf-Lamb-type by immobilizing them on solid supports.^[1,2] The catalysts become mutually active and do not interfere with each other's catalytic activity if immobilized separately either on two different solid supports that do not come into contact or on one support in a site-isolated manner. This is highly desirable for cascade reactions in one-pot in which the catalysts (more than one) and reactants, combined in one reactor, undergo a sequence of precise catalytic steps.

The site-isolated spatial positioning of the catalysts in a simple way to prevent their deactivation requires new concepts. Polymeric microcapsules are interesting carriers for the site-isolation of two incompatible catalysts.^[3] Microporous organic nanotube networks made by hyper crosslinking core-shell bottlebrush copolymers immobilized with site-isolated acid and base

catalyst systems showed good catalytic performance for deacetylation-Knoevenagel cascade reactions.^[4] The core and crosslinked shell of self-assembled amphiphilic triblock copolymers can also be used as separate compartments for the site-isolation of metal catalysts. Instead, the catalysts can be immobilized in the core of star polymers and a mixture of star polymers with different core catalysts (acids and bases) can also be used as site-isolated catalysts in one-pot reactions.^[5,6] Mesoporous silica support with acid and basic groups and sol-gel have also been used for one-pot cascade reactions.^[7-9] Compartmentalization by layered Pickering emulsion was recently achieved to carry out cascade reactions in one-pot. The acid and base catalysts were immobilized in droplets in different layers to avoid contact with each other.^[10,11] Layer-by-layer self-assembly is another interesting approach to build multicomponent thin films for cascade reactions.^[12]

Although some research progress has been achieved over the years, one-pot multistep reactions are still not generally applicable in chemo- or bio-catalysis because of the time-consuming special procedures required for making appropriate carriers. New, efficient and scalable carrier systems for cascade reactions that are experimentally feasible in a simple way are always sought.

We recently used electrospun acid and base nonwovens, for a two-step Wolf-Lamb-type catalytic reaction sequence in one-pot. The individual acid and base nonwovens fixed on separate frames were inserted in the reaction medium in one-pot.^[13]

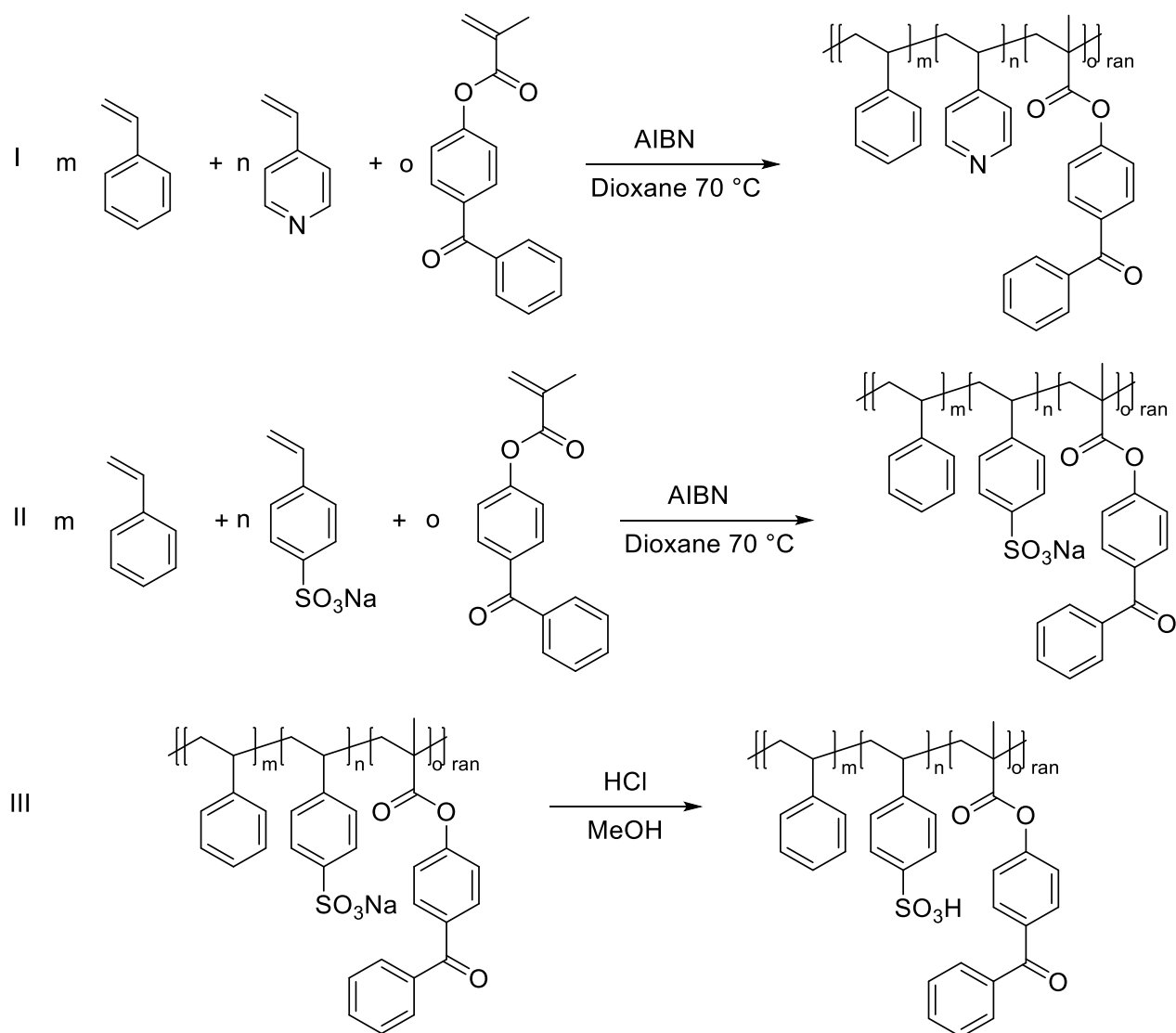
Three-dimensional (3D) printing offers the possibility of precise material structuring, size and shape modulations that can be of high utility in heterogeneous catalysis. Coelho et al. have combined the 3D printing of silica monolith and post-printing surface modifications with palladium and copper metals for catalysis.^[14] The use of 3D printing in making structured catalysts and reaction reactors has been reviewed recently.^[15] The inactive scaffolds are generally produced by 3D printing, followed by the incorporation of functional groups for catalysis in a post-printing step.^[16,17]

Slowing et al. printed directly functional monomers followed by ultraviolet (UV) crosslinking to make reactor parts for catalytic applications.^[18] We show here the 2D patterning of Wolf-Lamb-type catalysts on a neutral substrate by direct printing of Wolf-Lamb-type (acid and base) catalytically active polymers and their use in a two-step one-pot reaction. The reaction sequence tested was the standard deacetylation of (diemethoxymethyl)-benzene as the first step and C-C bond formation as the second step. The separation between the 2D printed acid-base catalysts is achieved by fixing individual printed membranes in a reaction flask in one-pot. The technique

can be easily extended in a modular way with more than two catalysts for multi-step reactions in the future.

2. Discussion and Results

The acidic and basic terpolymer catalysts were synthesized by free radical ter-copolymerization of styrene, 4-vinylpyridine (basic, *Scheme 13 I*) or styrene sulfonic acid (SSA) (acidic, *Scheme 13 II/III*) units and methacryloyl benzophenone (MABP) to enable post-processing crosslinking of the polymer to prevent it from dissolving and to let the 2D-printed structures swell in reaction solution, which is necessary to enable high accessibility to the catalytic sites in the bulk. MABP is a photoreactive crosslinker, that is very well-known in the literature for the crosslinking reactions.^[19] The benzophenone unit of MABP forms radicals by photo-illumination, followed by abstraction of C-H hydrogen from the polymer chain and then radical combination reactions leading to crosslinking, as shown in *Scheme S1* in the Supporting Information. The molecular weight (M_n) was 52000 with a molar mass dispersity (\mathcal{D}) 1.7 (Supporting information, *Figure S1*). The terpolymer compositions as determined by $^1\text{H-NMR}$ spectroscopic analysis for basic terpolymer was 47 % 4-vinylpyridine, 42 % styrene and 11 % 4-benzoylphenyl methacrylate (Supporting information, *Figure S2*). The copolymer composition for acid terpolymer could not be determined by $^1\text{H-NMR}$ alone (*Figure S3*, Supporting Information) because of the overlapping peaks. Therefore, elemental analysis was used to determine the amount of SSA to be around 16 mol%; with $^1\text{H-NMR}$, and the amount of styrene (71 mol%) and MABP (13 mol%) was calculated [exact calculation are shown in the Supporting Information *Equation S2 – Equation S7*]. The molecular weight determined (M_n) was 124 000 with a molar mass dispersity (\mathcal{D}) 1.7 (*Figure S4*, Supporting Information).



Scheme 13: Free radical ter-copolymerization for the formation of polymeric base (I) and acid (II/III).

The terpolymers were individually dissolved in a mixture of Tetrahydrofuran (THF) and *N,N*-dimethylformamide (DMF) [9 to 1 with 20 wt% in the case of acid terpolymer, viscosity at 26 Pa s at a shear rate of 10 s^{-1} and 30 wt% in the case of base terpolymer, viscosity at 0.3 Pa s^{-1} at a shear rate of 10 s^{-1} (*Figure S5*, Supporting Information)).

The polymers are separately patterned on commercial poly(ethylene terephthalate) (PET) mesh with a line width of $120\text{ }\mu\text{m}$ (*Figure 20*) followed by UV crosslinking. The patterned structure shows a good alignment with the printing file (*Figure S6*, Supporting information). The 3D printer Cellink Inkredible+ was used for patterning the catalysts.

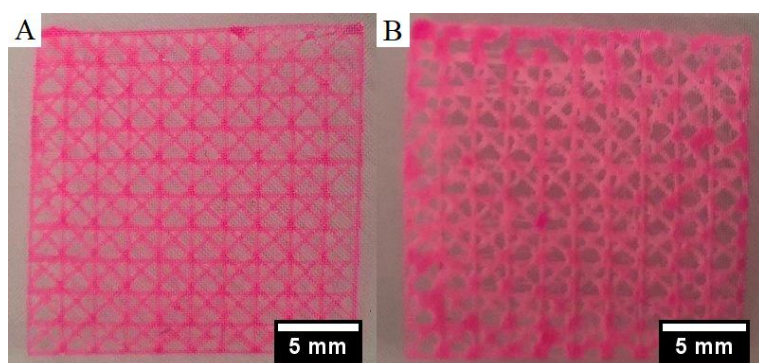


Figure 20: Digital photographic image of the patterned printed structure used. (A) is for the acid copolymer and (B) is for the basic copolymer.

The patterned crosslinked samples had about 3 mg of the catalytic polymers per cm^2 , which leads to 12 μmol in the case of the basic catalyst (4VP units) and 6 μmol in the case of the acidic catalyst (SSA units) per cm^2 . The samples were analyzed using microscopy and Raman imaging (*Figure 21* and *Figure 22*; microscopic stitching images are shown in the supporting information, *Figure S7*). The position of the acid and basic polymer catalysts could be identified utilizing Raman measurements. The acid polymer catalyst p(S-co-SSA-co-MABP) was deposited between the cavities of the PET mesh (*Figure 21 B* and *C*) separated by PET spacers with only a very thin layer on top of the PET structure.

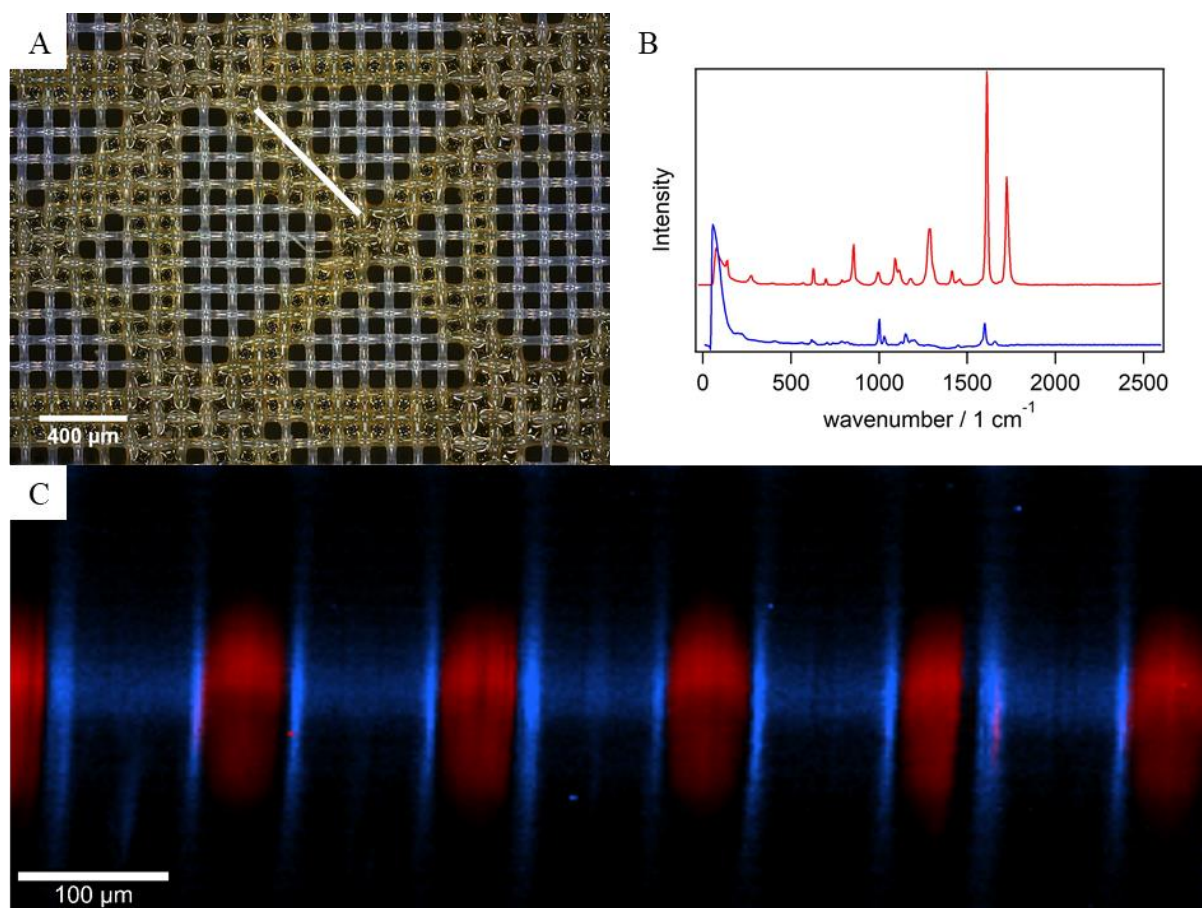


Figure 21: A) Microscopy image of the 3D-printed acid copolymer with a white line showing the place used for Raman imaging, B) the Raman spectrum for PET (red) and acid copolymer (blue) and C) the Raman imaging for the 2D-printed structure indicating high amounts of the copolymer in between the meshes.

The microscopy images and the Raman spectra (*Figure 22*) showed the deposition of the polymer in the cavity between the PET spacers and on top of the PET for the basic polymeric catalyst. The polymer catalysts deposited between the PET spacers have a high accessibility from both sides.

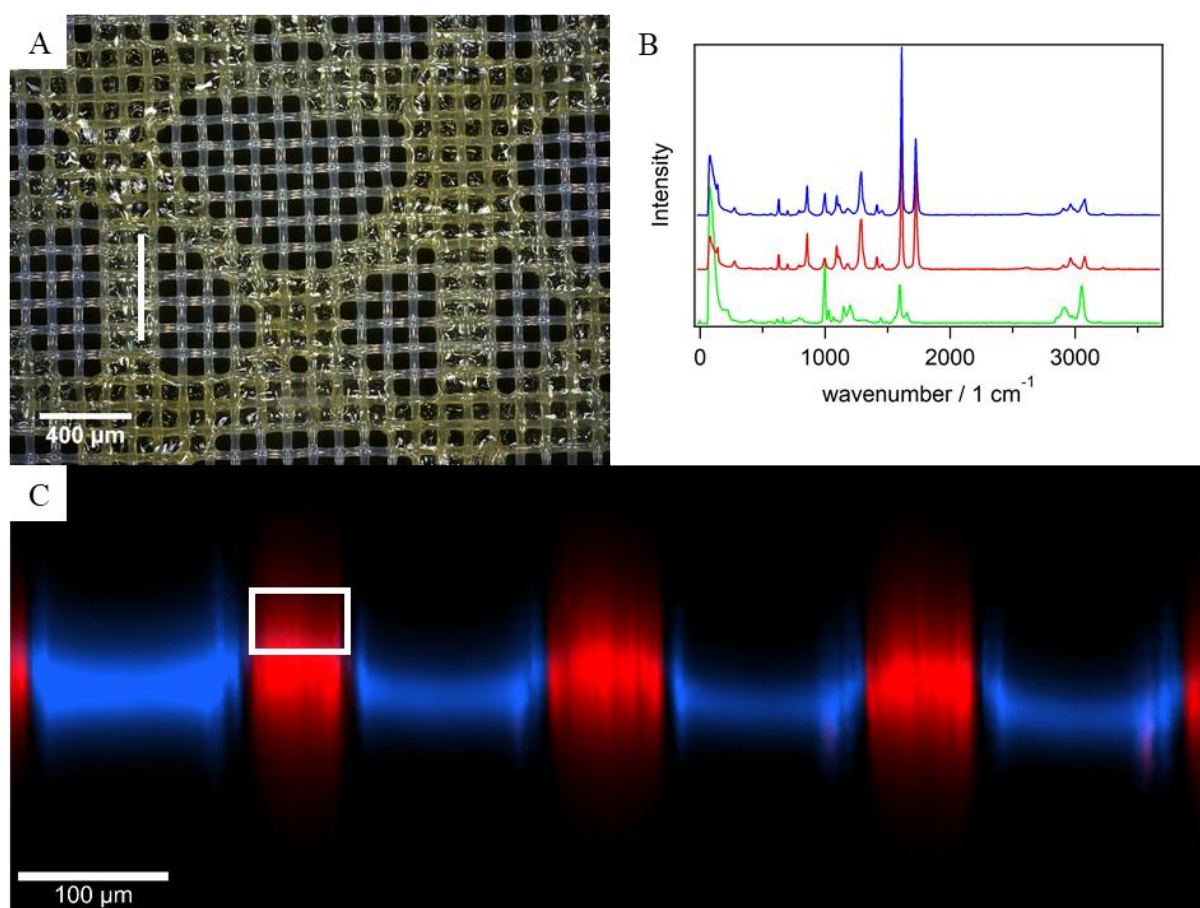
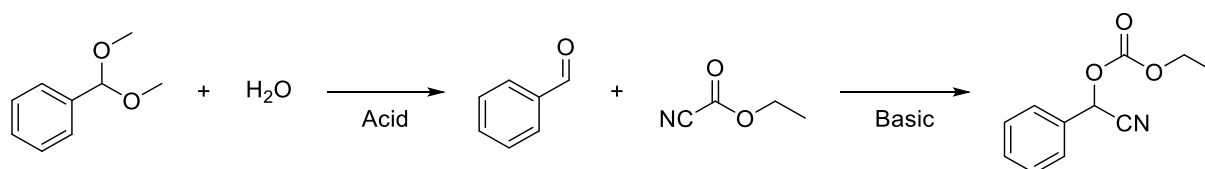


Figure 22: Microscopy image of the 3D-printed basic polymer (A) with a white line indicating the measured position in Raman imaging, the Raman spectrum for PET (blue), basic polymer (green) and for the white box within image the Raman imaging (red), in which the red part is the PET mesh and the blue part the 3D-printed polymer (C).

The patterned crosslinked polymer catalysts were immersed in DMF to check their solvent stability and the structures were monitored afterwards utilizing microscopy images (*Figure S8*, Supporting Information). The structures were stable after immersion in DMF and a swollen state was observed. The swelling of the polymers should be advantageous for the catalytic experiment because the swollen 2D-printed structure would allow good accessibility to catalytic sites.

Subsequently, the patterned acid-base (Wolf-Lamb type) catalysts were tested for their activity by performing deacetalization and the formation of cyano(phenyl)methyl ethyl carbonate (two-step) reactions in one-pot. The first step was catalyzed by acid and the second by base (*Scheme 14*). The reactions were followed by gas chromatography (GC) measurements with the help of undecane as an internal standard.



Scheme 14: Two-step reaction sequence catalyzed by incompatible acid and base catalysts : first step- deacetalization of (dimethoxy)methyl benzene to benzaldehyde (acid catalyzed), second step- C-C bond formation by reaction of ethyl cyanoformate and benzaldehyde (base catalyzed).

Firstly, the individual acid catalysts were used in different amounts (*Figure 23*). The acid catalyzed deacetylation was fast: 50 % conversion into benzaldehyde was achieved in 10 min using 15 mg of the acid catalyst (16 μmol , 0.75 mol% SSA, *Figure 23A* green x). The rate increased further upon increasing the amount to 30 mg (32 μmol , 1.5 mol% SSA, *Figure 23A* blue cross) and 90 % benzaldehyde was produced in 10 min. Subsequently, the two-step system was established. The pure acidic reactions were compared with the acidic part of a Wolf-Lamb-type two-step reaction leading to the result that the reaction was slower using the same amount of acidic catalyst (30 mg; *Figure 23A* green “x” for pure acidic reaction) but faster than using half of the amount (15 mg; *Figure 23A* blue “+” symbol), indicating a slight deactivation due to water within the reaction chamber, which is unavoidable as it is necessary for the deacetylation reaction. Nevertheless, the reaction produced more than 90 % benzaldehyde in 60 min.

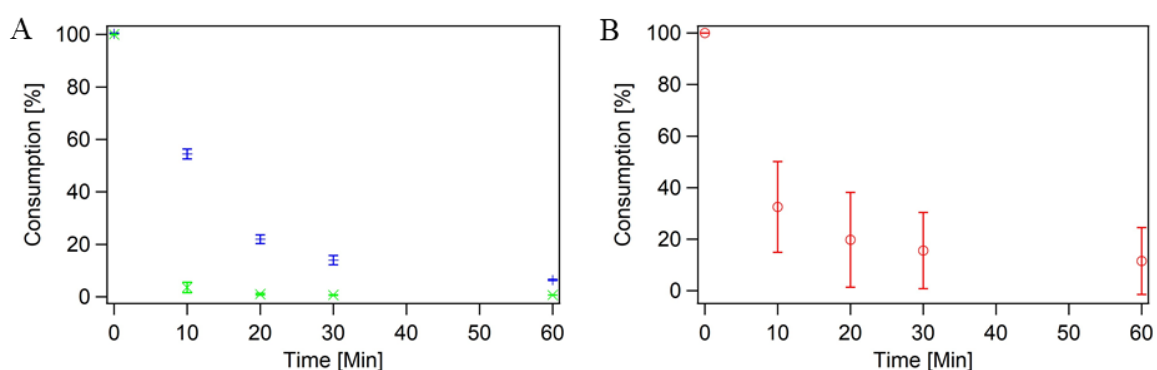


Figure 23. Consumption of the deacetalization from (dimethoxy)methyl benzene to benzaldehyde in a single step reaction. The reaction stops after 60 min with a consumption of over 95 % (A), the catalytic load was 1.5 mol% (green x) and, respectively, 0.75 mol% (blue +). A comparison shows that similar results are obtained for 2D-printed structures in two-step reactions. (B) Partial deactivation is observable as the resulting time consumption curve

(1.5 mol L^{-1} catalytic load) is faster than the blue crosses, but slower than the green x. The reaction condition for all experiments was $80 \text{ }^\circ\text{C}$ and consumption was monitored using GC; all reagents were dissolved at the beginning.

As a model reaction, the deacetylation already described, was further followed by a basic catalyzed reaction of benzaldehyde and ethyl cyanofornate (Scheme 14), which led to the formation of a carbonate group. Here, the study was performed with 30 mg (1.5 mol% of SSA groups) of acidic catalyst and 60 mg (9.6 mol% of 4-vinylpyridine groups) of basic catalyst.

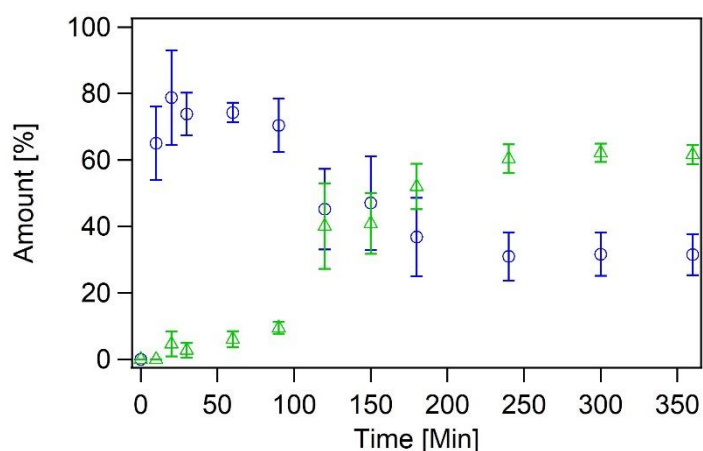


Figure 24: Two-step Wolf-Lamb-type reaction showing the amount of benzaldehyde (blue circle) and cyano(phenyl)methyl ethyl carbonate (green triangles). The amount of catalyst used was 1.3 mol% (30 mg acid terpolymer) styrene sulfonic acid and 9.6 mol% 4-vinylpyridine (60 mg base terpolymer). The catalytic reaction was performed at $80 \text{ }^\circ\text{C}$, all reagents and catalysts were immersed at the beginning and the amount was monitored utilizing GC.

As expected, the amount of benzaldehyde increased towards a maximum at around 60 min with an amount of around 80 % (Figure 24). The amount of cyano(phenyl)methyl ethyl carbonate increased significantly after 60 min until the maximum is reached at 250 min with a conversion of 62 %. The low conversion can be explained by the low basicity of 4-vinylpyridine, which can be improved in the future by using a strong base. Furthermore, it was possible to show that it is possible to restart the basic reaction by the addition of ethyl cyanofornate (Figure S10, Supporting Information), possibly due to an effect of equilibrium in combination with a low catalytic load.

Kinetic studies were carried out to gain a greater understanding of the process. The reactions were fitted with differential equations describing the reaction rates (Equation 1 – Equation 5).

$$\frac{dc_A}{dt} = -k_1 c_A(t) c_B(t) \quad (1)$$

$$\frac{dc_B}{dt} = -k_1 c_A(t) c_B(t) \quad (2)$$

$$\frac{dc_C}{dt} = k_1 c_A(t) c_B(t) - k_2 c_C(t - \Delta t) c_D(t) \quad (3)$$

$$\frac{dc_D}{dt} = -k_2 c_C(t - \Delta t) c_D(t) \quad (4)$$

$$\frac{dc_E}{dt} = k_2 c_C(t - \Delta t) c_D(t) \quad (5)$$

In which c_A is the concentration of (dimethoxy)methyl benzene, c_B is the concentration of water, c_C is the concentration of benzaldehyde, and c_D is the concentration of ethyl cyanoformate. k_1 and k_2 are the reaction rates of the first and second reaction step, respectively. The necessity of a parameter Δt was already described in our previous work for this specific reaction.^[13] There, we were able to show that the retarded start needed to be expressed by this specific parameter, as otherwise, no reasonable fits were obtained. A retarded start is generally expected for such reactions.^[20,21]

The resulting fitted parameters (*Table 3*) are close to the experimental values. Only the value for water (c_{B0}) is much lower (0.44 mol L^{-1}) compared to the experimental value of 1 mol L^{-1} . A possible explanation is the adsorption of water within the printed structures leading to a decrease of its availability. The fits show a reasonable alignment with the data (*Figure 25*).

Table 3: Resulting fitted parameters after solving equation 1-5.

Parameter	Fitted value
c_{A0}	0.48 mol L^{-1}
c_{B0}	0.44 mol L^{-1}
c_{D0} (<i>fixed</i>)	0.6 mol L^{-1}
Δt	39 min
k_1	$0.51 \text{ mol (L min)}^{-1}$
k_2	$0.01 \text{ mol (L min)}^{-1}$

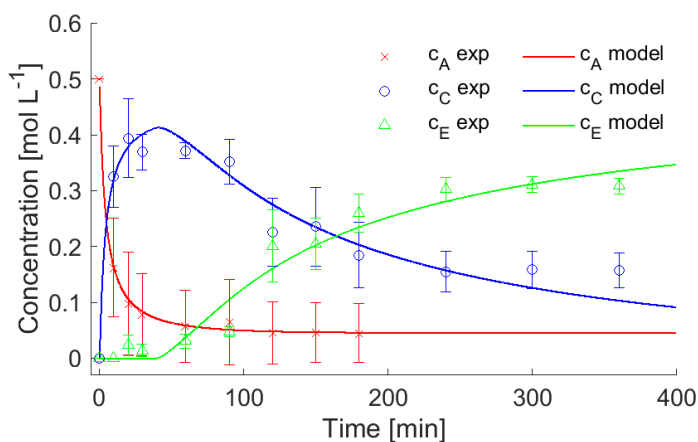


Figure 25: Kinetic fitted parameters of the two-step cascade reaction catalyzed by incompatible acid-base catalysts: red, blue and green are the amounts of (dimethoxy)methyl benzene, benzaldehyde and cyano(phenyl)methyl ethyl carbonate, respectively.

3. Conclusion

The 2D-printed structures were shown to be suitable carrier material for incompatible acid-base catalysts for one-pot cascade reaction sequence. The polymers reacting as acid and base catalysts were made by free radical polymerization and 2D printing on top of a PET mesh was done using a 3D printer. Here, we were able to characterize the 2D-printed structures by optical microscopy and Raman studies. The polymer-carrying meshes were immersed in the reaction solution for the two-step reaction. Although, both reaction steps were achieved in parallel, but the second step showed a retarded start of 50 min. The overall conversion was around 90 % for the first step and 62 % for the second step. Subsequently, a kinetic model was designed to observe the underlying reaction dynamics. The complexity of such systems was significantly decreased with our approach due to the easy polymerization and immobilization techniques used.

The conversions need to be improved in future studies to obtain a higher overall yield. Functionality of the basic monomer can be changed towards, for example, amine-based comonomers, as done by other groups, to increase the amount of reactions that can be catalyzed. Overall, a great toolkit for such catalytic reactions was achieved which is usable for further studies.

4. Experimental Section

Materials

The DMSO (p.a. grade), THF (p.a. grade) and DMF (p.a. grade) were purchased from Alfa Aesar and used as received. The 4-vinylpyridine (98 %) and styrene were purchased from Sigma Aldrich and distilled *in vacuo*. Sodium styrene sulfonate (90 %, Alfa Aesar) was recrystallized from a mixture of ethanol and water (90/10 volume%). The ethyl cyanofornate (98 % Alfa Aesar), dimethoxybenzylacetal (99 %, Alfa Aesar) and undecane (> 99 %, Alfa Aesar) for the catalytic experiments were used as received.

Methods

Nuclear magnetic resonance (NMR) spectroscopy: ^1H -NMR experiments were recorded on a Ultrashield-300 spectrometer at room temperature in either CDCl_3 or DMSO-d_6 . Spectra were calibrated according to the residue protons of the deuterated solvent signal. Evaluation of spectra was carried out with MestReNova (Mestrelab research, version 6.1).

The 3D printing was performed with a Cellink Inkredible+ with a one-needle setup. Solutions were 20 wt% for poly(S-co-SSA-co-MABP) and 30 wt% for poly(S-co-4VP-co-MABP) in THF/DMF (90/10). A pressure of 170 kPa was used for polymer solution flow through the syringe. The solutions were printed on a PET mesh with a mesh width of 120 μm . The printed structure was crosslinked for 3 h under UV light with an UV-F 400 F (honle UV technology) from the top side of the samples.

Optical Microscope images were taken by a Smartzoom5 (Zeiss).

Size exclusion chromatography (SEC) measurements were performed in DMF (HPLC grade) with lithium bromide (5 g L^{-1}) as an eluent and solvent and an internal standard of toluene on two PSS-GRAM gel columns (particle size = 10 μm) with a porosity of 100 to 3000 \AA , a flow rate of 0.5 mL min^{-1} and a refractive index detector (Agilent Technologies) on a SEC 1260 Infinity (Agilent Technologies). A narrowly distributed polystyrene homopolymer was used (PSS calibration kit) for calibration.

Gas chromatography (GC): The GC measurements were performed with a GC-FID system (GC-2010 Plus, Shimadzu), using nitrogen as a carrier gas. An amount of 10 μL of the reaction

mixture was dissolved in 1 mL acetonitrile. A volume of 1 μL was injected with a split ratio of 1:50 and measured from 50 $^{\circ}\text{C}$ (2-min hold) up to 300 $^{\circ}\text{C}$ with a heating rate of 15 K min^{-1} .

Raman imaging Raman imaging was performed with a WITec alpha 300 RA+ imaging system equipped with an UHTS 300 spectrometer and a back-illuminated Andor Newton 970 EMCCD camera for measurements with an excitation wavelength of $\lambda = 352 \text{ nm}$ and an UHTS 400 spectrometer and a back-illuminated deep depletion Andor iDUS CCD camera for measurements with an excitation wavelength of $\lambda = 785 \text{ nm}$, respectively. The measurement on the p(S-cop-4VP-co-MABP) was conducted with an excitation wavelength of $\lambda = 352 \text{ nm}$ and an integration time of 0.5 s pixel^{-1} using a laser power of 15 mW (10x objective, NA = 0.25, step with 2.5 $\mu\text{m pixel}^{-1}$). The p(S-co-SSA-co-MABP) was measured with an excitation wavelength of $\lambda = 785 \text{ nm}$ and an integration time of 1.0 s pixel^{-1} using a laser power of 45 mW (10x objective, NA = 0.25, step with 2.5 $\mu\text{m pixel}^{-1}$). All spectra were subjected to a cosmic ray removal routine and baseline correction using WITec project 5.1. The spatial distribution of the components was extracted from the Raman imaging data employing the Raman spectra of the neat components for the True Component Analysis in WITec project 5.1.

Rheology Rheology measurements were made with a Modular Compact Rheometer MCR 302 (Anton Paar) using a standard Measuring System CC17 (concentric cylinder) with a shear rate starting at 0.01 s^{-1} to 100 s^{-1} with 5 points per decade. Points were measured starting with 20 s down to 5 s during measurements.

Curve fitting MatLab Version 2015a was used for the fitting of the differential equations.

Synthesis of crosslinkable base polymer

Methacryloyl benzophenone (0.1 equiv) was placed in a round-bottom Schlenk flask and dissolved in THF (42 mL). Styrene (0.4 equiv) and 4-vinylpyridine (0.5 equiv) were added to the mixture subsequently and the reaction mixture was degassed with Argon for 30 min (the concentration of monomers was 4 mol L^{-1}). The reaction mixture was heated to 60 $^{\circ}\text{C}$, 0.8 wt% AIBN was added and it was stirred for 16 h. The polymer was precipitated in diethyl ether, the resulting polymer was redissolved twice in DMSO and precipitated in diethyl ether. The crude product was then dried at 60 $^{\circ}\text{C}$ *in vacuo*.

^1H NMR (300 MHz, CDCl_3): $\delta = 1.0\text{--}1.6$ (polymer backbone, CH_2 ; CH_3); $1.6\text{--}2.5$ (polymer backbone CH); $6.0\text{--}6.6$ (aromatic, CH); $6.6\text{--}7.2$ (aromatic, CH); $7.4\text{--}7.7$ (aromatic CH); $8.1\text{--}8.5$ (aromatic, CH).

Synthesis of crosslinkable acid polymer

Methacryloyl benzophenone (0.1 equiv.) and recrystallized sodium styrene sulfonate (0.15 equiv.) were placed in a round-bottom Schlenk flask and dissolved in DMSO (35 mL). Styrene (0.75 equiv) was added to the solution and the reaction mixture was degassed with argon, heated to $70\text{ }^\circ\text{C}$ and 0.6 wt% AIBN was added. The polymer was then precipitated in isopropanol and dried at $60\text{ }^\circ\text{C}$ *in vacuo*.

The crude product obtained was dissolved in methanol and concentrated HCl solution was added dropwise to obtain a white solid. The product obtained was filtered and dried at $60\text{ }^\circ\text{C}$ *in vacuo*.

^1H NMR (300 MHz, DMSO-d_6): $\delta = 0\text{--}1.6$ (polymer backbone, CH_2 ; CH_3); $1.6\text{--}2.5$ (polymer backbone CH); $6.0\text{--}6.6$ (aromatic, CH); $6.6\text{--}7.2$ (aromatic, CH); $7.4\text{--}7.7$ (aromatic, CH).

Catalytic experiment two-step system

The 3D-printed structures (30 mg (1.5 mol%) of the acidic poly(*S-co-SSA-co-MABP*)) and 60 mg (9.6 mol% of (dimethoxymethyl)benzene) of the basic poly(*S-co-4VP-co-MABP*) on PET meshes were added into a 10 mL vial.

A solution of dimethoxybenzylacetal (1 equiv.) was dissolved in DMF ($c = 0.5\text{ mol L}^{-1}$) and, subsequently, ethyl cyanoformate (1.2 equiv), water (Milli-Q, 2 equiv.) and undecane as an internal standard were added for the catalytic experiments. The reaction mixture was heated to $80\text{ }^\circ\text{C}$ and the immobilized nonwoven structures were immersed in the reaction medium.

Conflict of interest

The authors have no conflict of interest to declare.

Supporting Information

Supporting Information is available from the Wiley Online Library or from the authors.

Acknowledgements

The authors are indebted to the DFG-SFB 840, A12 for financial founding. Dr. Holger Schmalz, Mina Heidari and Rika Schneider are thanked for analytical assistance.

- [1] B. J. Cohen, M. A. Kraus, A. Patchornik, *J. Am. Chem. Soc.* **1977**, *99*, 4165.
- [2] B. J. Cohen, M. A. Kraus, A. Patchornik, *J. Am. Chem. Soc.* **1981**, *103*, 7620.
- [3] S. L. Poe, M. Kobaslija, D. T. McQuade, *J. Am. Chem. Soc.* **2006**, *128*, 15586.
- [4] H. Zhang, L. Xiong, L., Z. He, A. Zhong, T. Wang, Y. Xu, K. Huang, *New J. Chem.* **2016**, *40*, 7282.
- [5] B. Helms, S. J. Guillaudeu, Y. Xie, M. McMurdo, C. J. Hawker, J. M. J. Fréchet, *Angew. Chem., Int. Ed.* **2005**, *117*, 6542.
- [6] Y. Chi, T. Scroggins, J. M. J. Fréchet, *J. Am. Chem. Soc.* **2008**, *130*, 6322.
- [7] N. R. Shiju, A. H. Albers, S. Khalid, D. R. Brown, G. Rothenberg, *Angew. Chem. Int. Ed.* **2011**, *50*, 9615.
- [8] S. Shylesh, A. Wagener, A. Seifert, S. Ernst, W. Thiel, *Angew. Chem. Int. Ed.* **2010**, *49*, 184.
- [9] Yang, Y., Lio, Xiao, Li, X., Zhao, J., Bai, S., Lui J., Yang, Q., *Angew. Chem. Int. Ed.* **2012**, *51*, 9164.
- [10] H. Yang, L. Fu, L. Wie, J. Liang, B. P. Binks, *J. Am. Chem. Soc.* **2015**, *137*, 1362.
- [11] N. Xue, G. Zhang, X. Zhang, H. Yang, *Chem. Commun. (Camb)* **2018**, *92*, 13014.
- [12] S. Disawal, J. Qiu, B. B. Elmore, Y. M. Lvov, *Colloids Surf. B Biointerfaces* **2003**, *32*, 145.
- [13] M. O. Pretscher, S. Gekle, S. Agarwal, *Macromol. Rapid Commun.* **2019**, *40* 1900148.
- [14] A. S. Díaz-Marta, C. R. Tubio, C. Carbajales, C. Fernández, L. Escalante, E. Sotelo, F. Gitián, V. L. Barrio, A. Gil, A. Coelho, *ACS Catal.* **2018**, *8*, 392.

- [15] C. Parra-Cabrera, C. Achille, S. Kuhn, R. Ameloot, *Chem. Soc. Rev.* **2018**, *47*, 209.
- [16] P. J. Kitson, M. D. Symes, V. Dragone, L. Cronin, *Chem. Sci.* **2013**, *4*, 3099.
- [17] J. Lefevere, M. Gysen, S. Mullens, V. Meynen, J. Van Noyen, *Catal. Today* **2013**, *216*, 18.
- [18] J. S. Manzano, Z. B. Weinstein, A. D. Sadow, I. I. Slowing, *ACS Catal.* **2017**, *7*, 7567.
- [19] G. Dormán, G. D. Prestwich, *Biochemistry*, 1994, *33*, 5661.
- [20] M. North, S. Urwin, *Tetrahedron* **2014**, *70*, 7100.
- [21] H. Seto, K. Imai, Y. Hoshino, Y. Miura, *Polym. J.* **2016**, *48*, 897.

The 2D patterned structures were used as Wolf-Lamb-type catalysts. Here, an acid and base polymer were synthesized, printed on separate PET, crosslinked by UV light and then immersed in solution to monitor the kinetic of such a multi-step one-pot catalysis. The kinetical constants were calculated using differential equations.

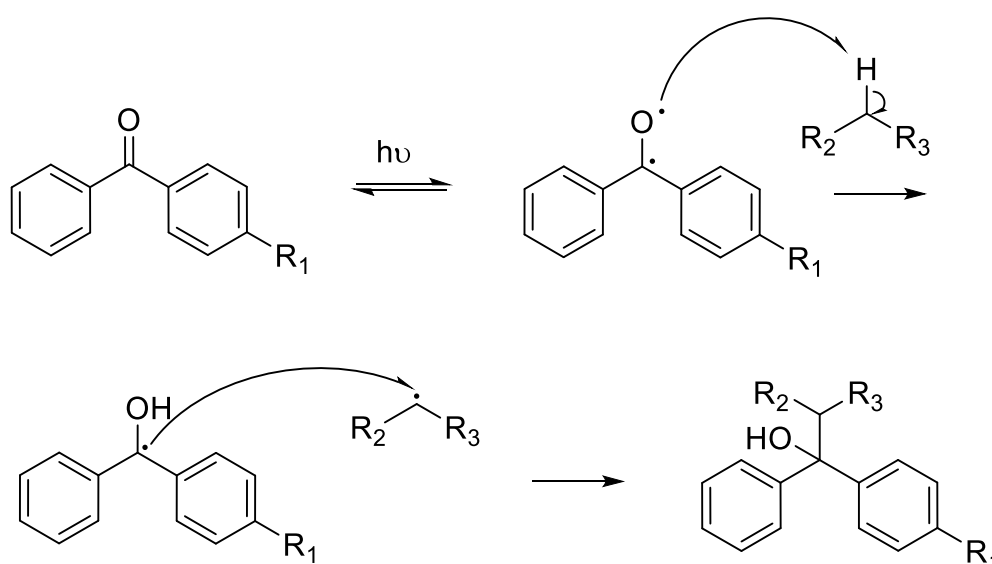
Keyword heterogenous catalysis

Supporting Information

Precisely 2D patterned Wolf-Lamb-type catalysts for one-pot multistep reactions

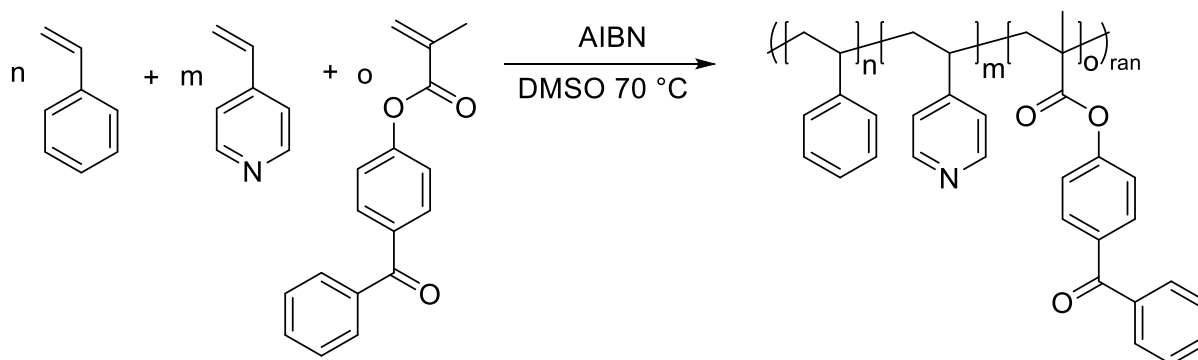
*Martin O. Pretscher, Tingting Chen, Gabriel Sitaru, Stephan Gekle, Jian Ji and Seema Agarwal**

Mechanism of cross-linking with benzophenone



Scheme S1. Mechanism of radical cross-linking with benzophenone through UV-light.

Synthesis of cross-linkable base polymer



Scheme S2. Reaction Scheme showing free radical polymerization of styrene, 4-vinylpyridine and methylacrylbenzophenone.

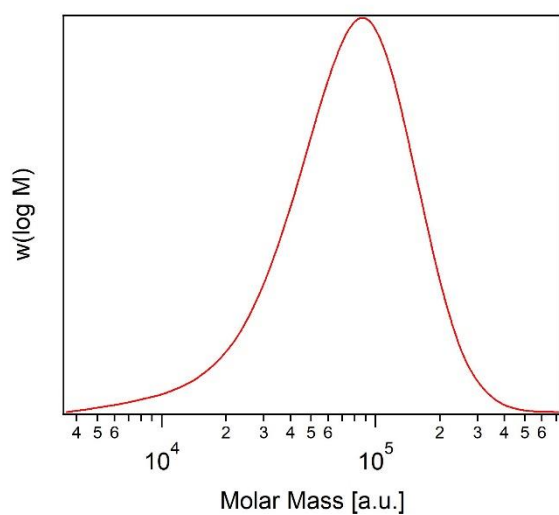


Figure S1. DMF-SEC measurement of poly(styrene-*co*-4-vinylpyridine-*co*-methylacrylbenzophenone).

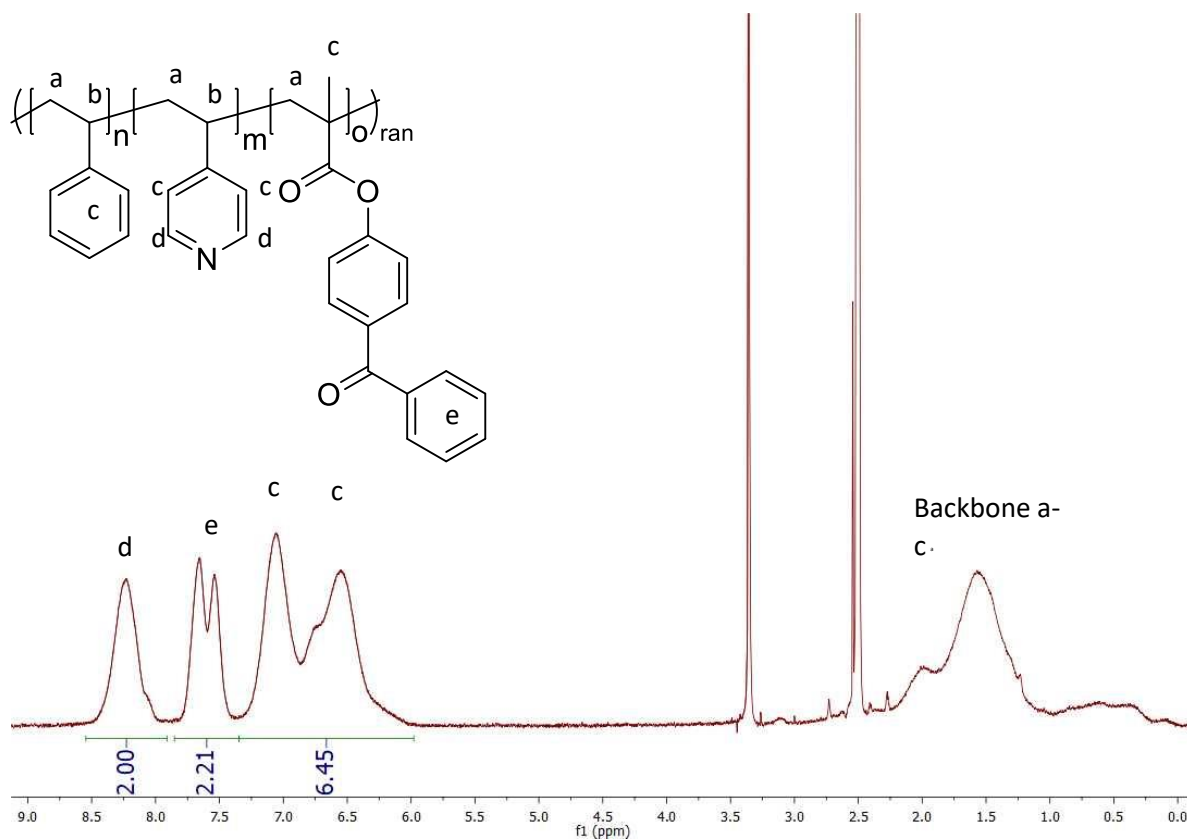


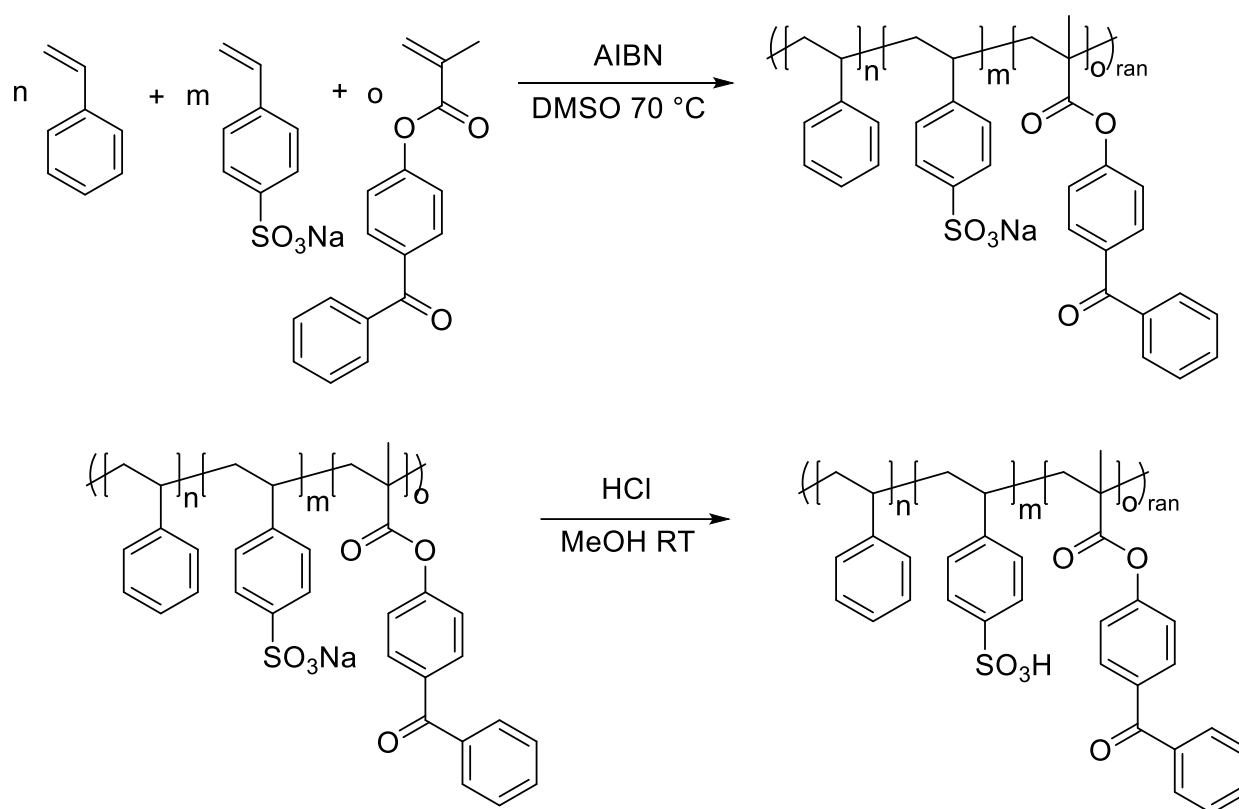
Figure S2. $^1\text{H-NMR}$ spectrum of the copolymer poly(styrene-*stat*-SSA-*stat*-methyl acrylbenzophenone). The spectrum was measured in DMSO-d_6 . The spectrum was normalized on the two protons of the 4-vinylpyridine unit next to the nitrogen.

$$\%4VP = \frac{\frac{f^{\text{d}}}{2}}{\frac{f^{\text{d}}}{2} + \frac{f^{\text{e}}}{9} + \frac{f^{\text{c}} - \frac{f^{\text{d}}}{2}}{5}} \times 100\% \quad (\text{S1})$$

Here, $\frac{f^{\text{d}}}{2}$ is the amount of 4VP, $\frac{f^{\text{e}}}{9}$ is the amount of methacrylbenzophenone and $\frac{f^{\text{c}} - \frac{f^{\text{d}}}{2}}{5}$ is the amount of styrene. The following amounts were obtained utilizing the calculation:

47 % 4VP, 11 % MABP, 42 % Styrene

Synthesis of poly(styrene-*stat*-styrene sulfonic acid-*stat*-methyl acrylbenzophenone)



Scheme S3. Reaction scheme of the free radical polymerization of styrene, sodiumstyrene sulfonate and methylacrylbenzophenone to acid polymer catalyst, followed by the protonation using concentrated hydrochloric acid.

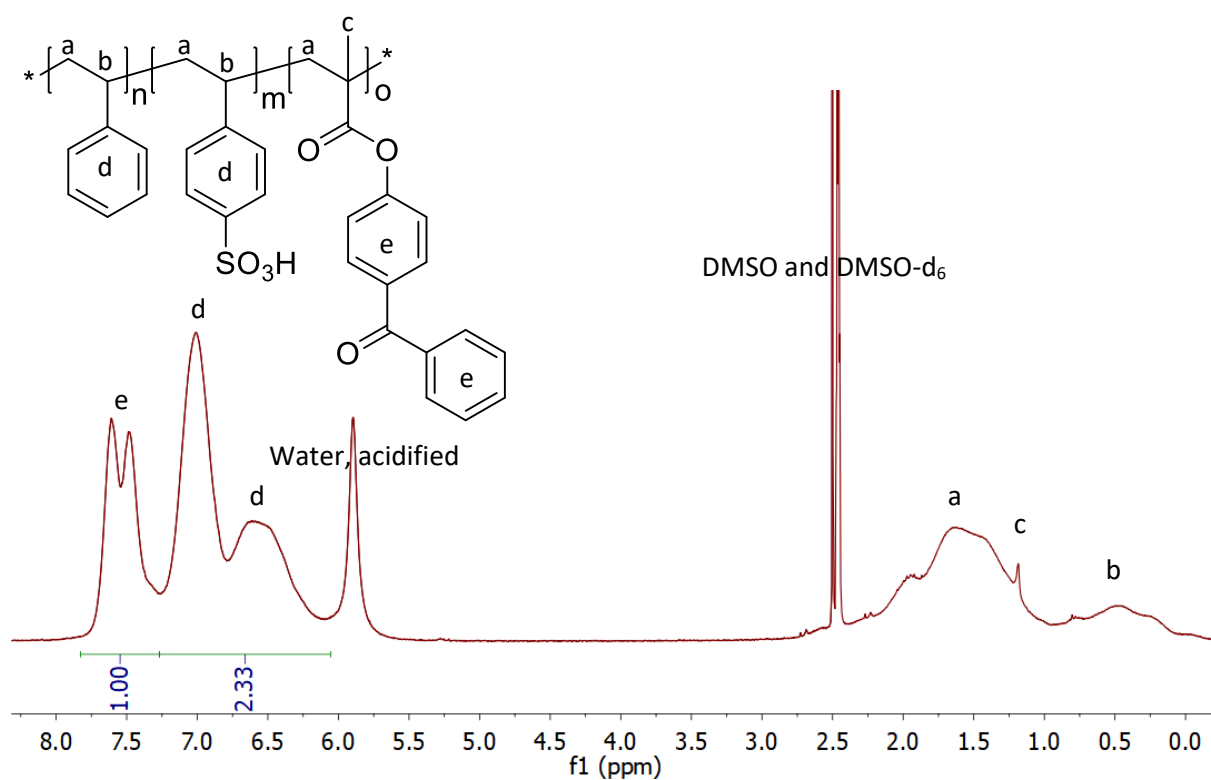


Figure S3. $^1\text{H-NMR}$ spectrum of the acid terpolymer using DMSO-d_6 as the solvent.

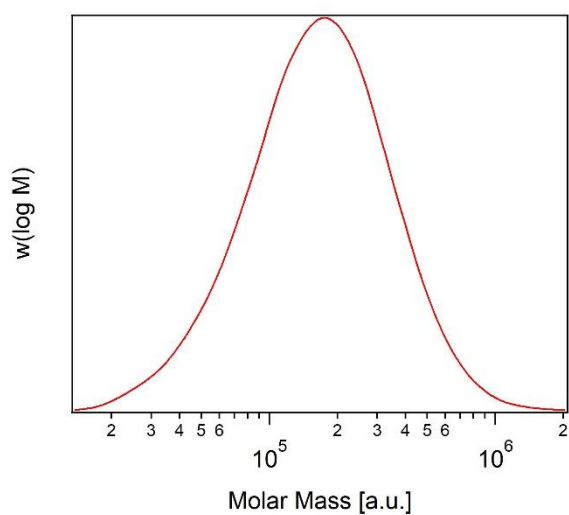


Figure S4. DMF-GPC measurement of poly(styrene-*co*-sodium styrene sulfonate-*co*-methyl acrylbenzophenon).

HCNS Elemental analysis

Table S1. Elemental analysis for the calculation of the amount of sodium styrene sulfonate.

Element	Amount [wt%]
H	6.2
C	76.4
N	0.0
S	2.9
O	14.5

Carbon: 76.4 wt%; hydrogen 6.2 wt%; sulfur 2.9 wt%; oxygen 14.5 wt%; nitrogen 0 wt%.

The amount of SSA determined based on these values: 15.5 mol%.

Exact calculation of the copolymer composition based on elemental analysis was not possible due to a very high amount of oxygen. The latter is due to rest solvents, such as methanol and water. The value for SSA is within the range of the feed ratio and, hence, probable but slightly to high.

All amounts were calculated in mol% (**Equation S2** and **S3**).

$$mol_{Element} = \frac{wt_{sample} * wt\%}{100 * M_{Element}} \quad (S2)$$

$$mol\% = \frac{mol_{Element}}{mol_C + mol_S + mol_O} \quad (S3)$$

The amount of carbon of the different monomers used in the copolymerization was then determined to obtain information of the amount of SSA (**Equation S4 – S6**).

$$mol\%_{C(SSA)} = mol\%_S \times 8 \quad (S4)$$

$$mol\%_{C(MABP)} = (mol\%_O - mol\%_C \times 3) \times 17 \quad (S5)$$

$$mol\%_{C(S)} = mol\%_C - mol\%_{C(SSA)} - mol\%_{MABP} \quad (S6)$$

The value of $mol\%_{SSA}$ obtained was used as a fixed value and the amount of styrene and methyl acrylbenzophenone was calculated with the help of $^1\text{H-NMR}$ (**Figure S4**) by solving **Equation S7**. Equation S1 was then used to determine the corresponding amounts.

$$mol\%_{SSA} = \frac{\frac{x}{4}}{\frac{1}{9} + \frac{2,11-x}{5} + \frac{x}{4}} \quad (S7)$$

3D-printed structure

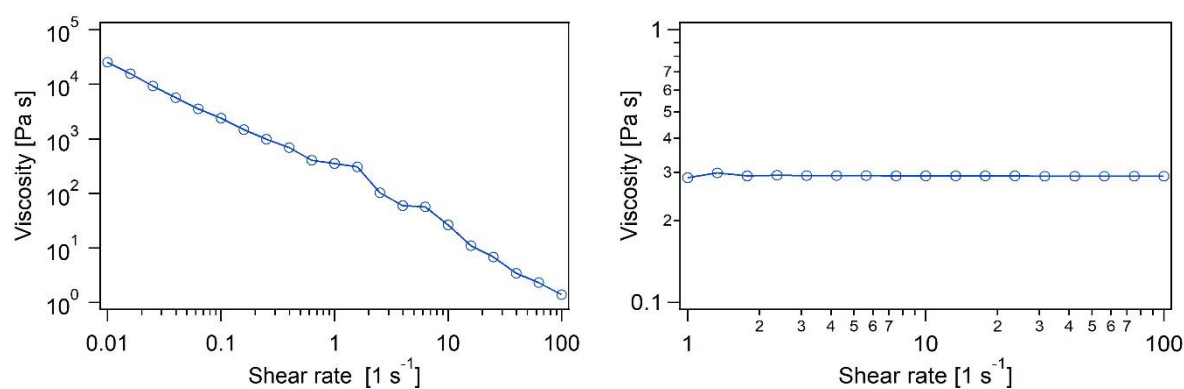


Figure S5. Viscosity measurements for acid terpolymer (A) and base terpolymer (B).

The printing file (Figure S6) shows a good alignment with the resulting patterned structures shown in Figure 1 and Figure S6.

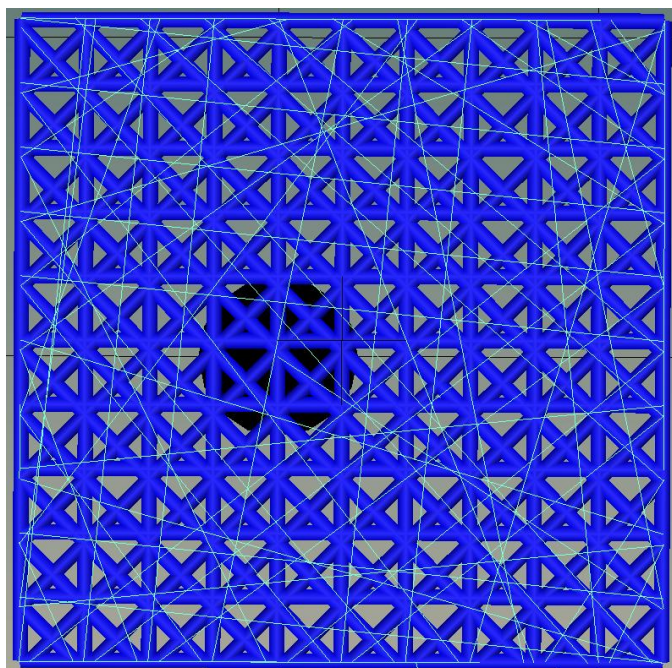


Figure S6. Screenshot of the gcode file used for printing.

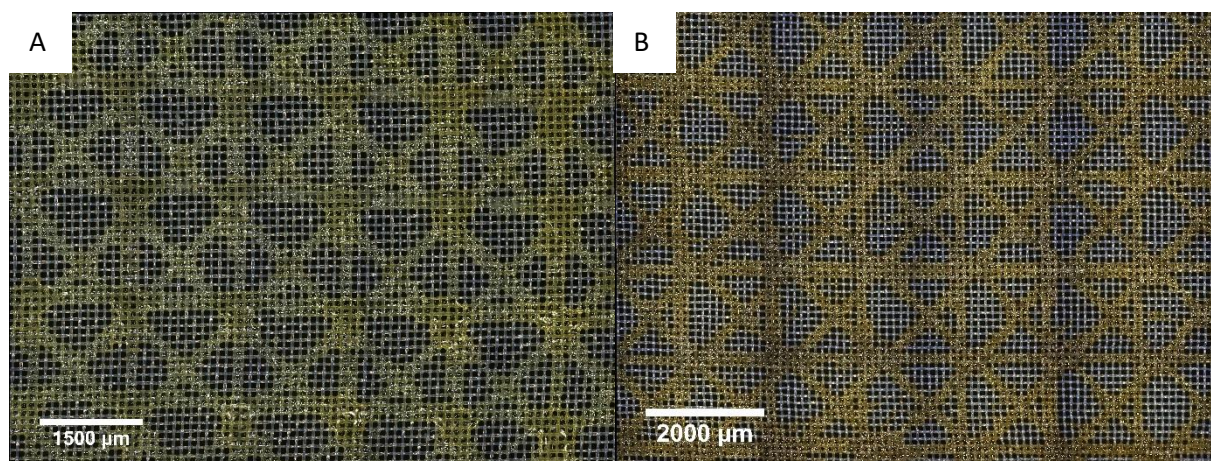


Figure S7. Stitched microscopy images of base (A) and acid (B) terpolymers.

The homogenous structures were also observable with the help of the stitching mode of an optical microscope showing the overall homogenous structure of base (A) and acid (B) printed terpolymers.

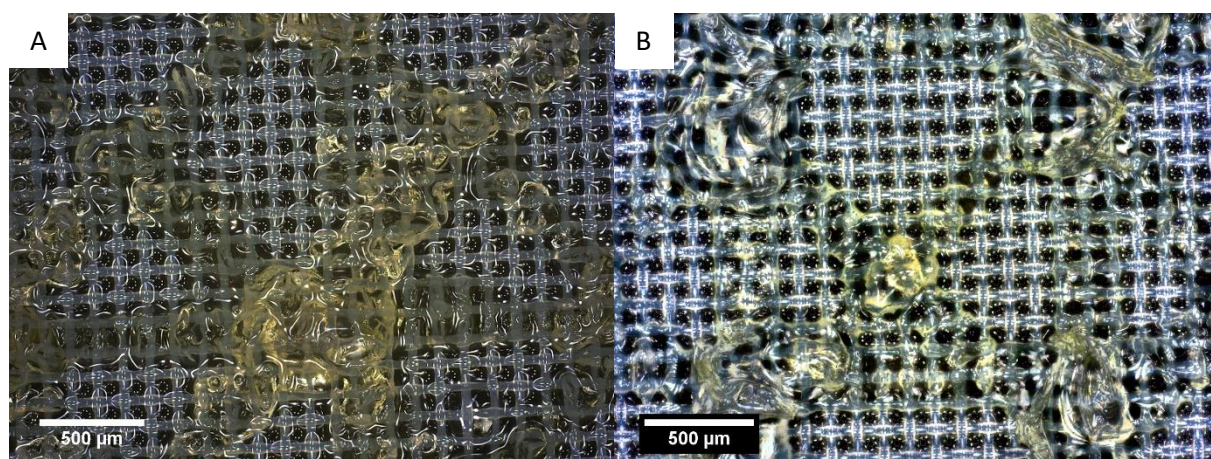


Figure S8. Microscopy images after immersion in DMF. Both acid (A) and base (B) terpolymers are in a swollen state after immersion and the structure is stable on top of the PET mesh.

Reusability test for acidic catalyst

Reusability was tested by reactivation of the catalyst. The catalyst was washed after the reaction, immersed in methanol and HCl was added dropwise. The resulting catalyst was then washed with methanol and diethyl ether and dried at room temperature. Catalytic experiments were performed, as mentioned previously.

Deactivation of the catalytic reaction was observable (**Figure S9**).

In the case of the second-step reaction in the Wolf-Lamb-type reaction, it was possible to restart the solution by the addition of ethyl cyanoformate (**Figure S10**).

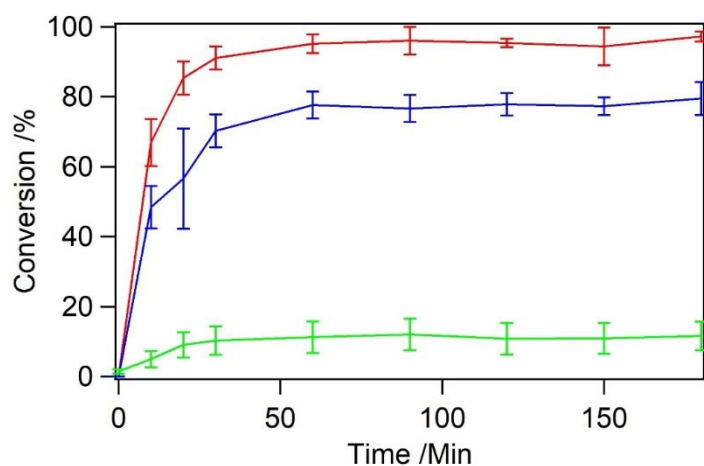


Figure S9. Three cycles of the deacetalization reaction were observed during the first cycle and high conversion of more than 95 % was observed. The following cycles show less conversion, with around 80 % (cycle 2 blue) and 15 % (cycle 3 green).

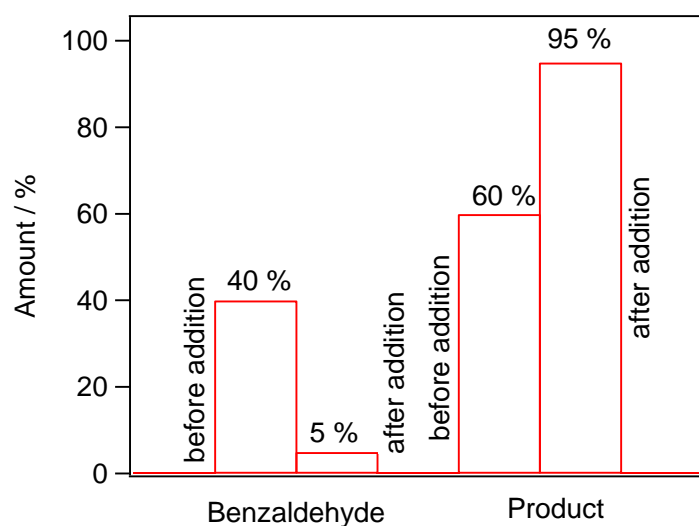


Figure S10. Addition of ethyl cyanofornate after the reaction finished shows that the reaction can be restarted and high yield is obtained.

Post-process functionalized catalytic electrospun and 2D printed structures for Wolf-Lamb type catalysis

*Martin O. Pretscher¹, Gabriel Sitaru², Markus Dietel¹, Holger Schmalz^{1,2}, Stephan Gekle²,
Seema Agarwal^{1,2,*}*

¹Macromolecular Chemistry II, University of Bayreuth, Universitätsstrasse 30, 95440 Bayreuth, Germany

²Bavarian Polymer Institute, University of Bayreuth, Universitätsstrasse 30, 95440 Bayreuth, Germany

³Theoretical Physics VI, Biofluid Simulation and Modelling, University of Bayreuth, Universitätsstrasse 30, 95440 Bayreuth, Germany

Corresponding author* e mail: agarwal@uni-bayreuth.de

ABSTRACT. The process for preparing the active, strong base and acid self-standing individual membranes and printed structures are established by electrospinning and two-dimensional (2D) printing of the corresponding polymeric base and polymeric acid on a neutral plastic substrate. The active polymeric acid and strong base used in this work were (poly(styrene-*co*-styrene sulfonic acid-*co*-methacryloyl benzophenone)) and (poly(styrene-*co*-4-vinylbenzylamine-*co*- *N*-(4-benzoylphenyl)acrylamide), respectively. The active acid-base printed structures and membranes were compared for their activity in a standard two-step acidic catalyzed deacetalization reaction of dimethoxybenzyl acetal to benzaldehyde followed by a base-catalyzed Knoevenagel-condensation with ethyl cyanoacetate towards ethyl-2-cyano-3-phenyl acrylate reaction in one pot in different solvents. Both 2D printed acid, base structures, and electrospun membranes could be arranged in one-pot to complete the two-step reaction

without destroying each other's activity. High conversions, fast reaction, and reusability make 2D printed structures favorable in toluene over electrospun membranes. The kinetic parameters were also calculated to address the solvent's influence and further strengthen the systems' understanding and comparison.

KEYWORDS: catalysis, acid-base, one-pot, electrospinning, 3D printing

INTRODUCTION

Wolf-Lamb type catalyst systems contain mutually incompatible catalysts, in which the catalytic functionalities are site isolated and therefore protected from each other as otherwise, the catalytic centers would deactivate each other. These site-isolated Wolf-Lamb type catalysts can be used in organic multi-step one-pot reactions. This is desirable because, within one-pot reactions, the intermediate product's isolation is unnecessary, and less solvents for the reaction and purification are used. Hence time and costs are reduced.

Cohen et al. were starting to study the possibilities of such systems already in 1977.^[1,2] There, they discussed the use of polymeric materials for site-isolation carrier purposes. Since then, there are different approaches to optimize further and show new possible immobilization ways. One of the most extensively studied systems is the use of porous material such as metal-organic frameworks (MOFs)^[3-6] and zeolites^[7,8], which have a high intrinsic and desirable porosity and are widely used in catalytic studies due to these properties. The specialty of MOF like structures is the linking units, which can be used to immobilize the desired functionality.

Nevertheless, while the concept is promising, MOFs' synthesis and treatment did not reach high applicability, and research still needs to focus on these. Another approach is the use of silica-based particles. [9-11] Therefore, it is not surprising that polymers as catalytic carriers have moved into the focus of current research. Polymeric structures have a high amount of possibilities in which the site-isolation of catalysts can be achieved in different ways, such as

the use of star polymers^[12-14] or microcapsules^[15-17]. Nevertheless, they are limited in reusability, and synthetic work is challenging due to these special structures. Therefore, multiple other concepts for heterogeneous polymeric catalysts can be found, such as microporous organic nanotube networks with a core-shell structure^[18,19] or gels as catalytic carriers.^[20,21] The use of polymers as carriers for mesoporous structures is of high interest. Hence, multiple studies on mesoporous materials are made of hyper-crosslinked polymers to obtain a stable structure in solution.^[22-25]

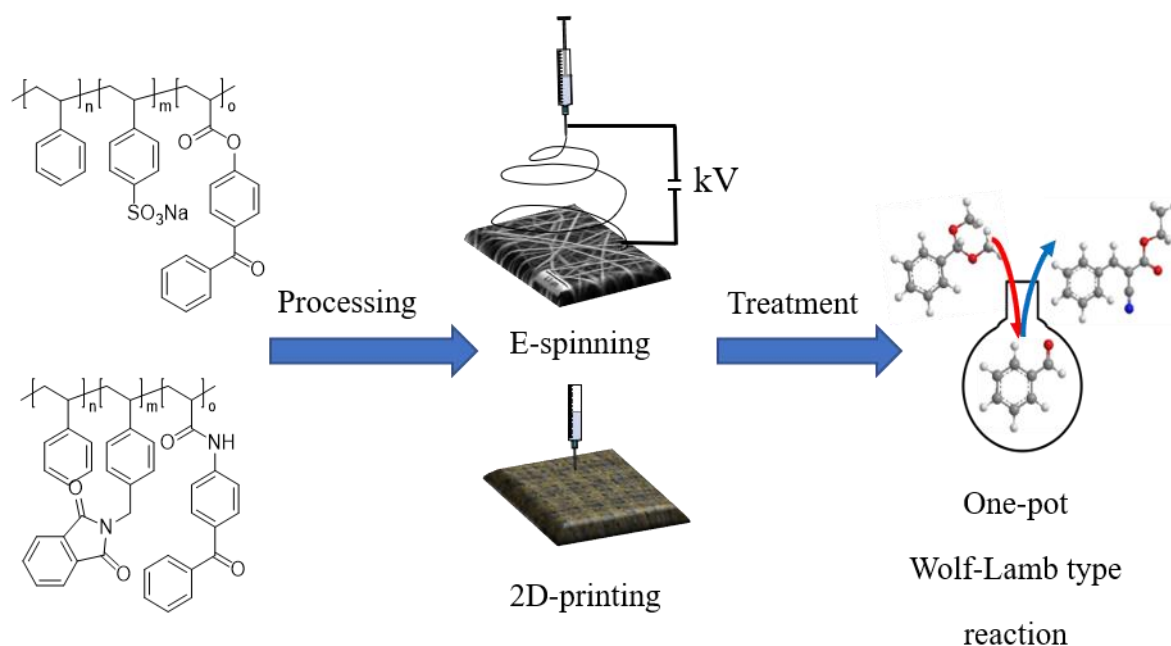
To further unlock the potential of such multi-step one-pot cascade systems using Wolf-Lamb type catalysts, we wanted to obtain an easy to modify system which can be used in a modular way. We first studied two different ways to achieve such catalytic reactions by either electrospinning^[26] or printing patterned polymer catalysts on a carrier material^[27] with poly(styrene-*co*-styrene sulfonic acid-*co*-methacryloyl benzophenone) (P(S-*co*-SSA-*co*-MABP)) and poly(styrene-*co*-4-vinyl pyridine-*co*-methacryloyl benzophenone) as acid and base incompatible catalysts. Electrospinning is a technique to obtain fibers with a diameter of a few hundred nm up to 5 μm . A high voltage is applied between a needle and a collector, and the polymeric solution is stretched towards the collector. During this process, the solvent evaporates, and a porous polymer membrane is obtained by random deposition of solid fibers (**Scheme 1**, E-spinning).^[28,29] Precise patterning^[30] of polymers by the computer-controlled 3D printer from polymer melts or solutions provide easy access to the well-separated polymer acid and base catalysts on a neutral substrate. Both these methods are shown as appropriate simple tools for fixing the incompatible catalysts in the form of individual membranes called catalytic compartments that can be fixed in one reaction vessel without coming in contact with each other. Nevertheless, the system was limited due to a weak base (4-vinyl pyridine) in the base polymer catalyst.^[31] Only a few reactions were possible such as a carbonate building reaction with a limited yield of around 80% with a starting induction period.^[26,27]

The possibilities of primary amine-based copolymers were investigated in this work to broaden potential applications further and obtain a higher yield and a better working system. It was decided to use 4-vinylbenzylamine as the functional base comonomer. As primary amines cannot directly be used in the free-radical polymerization, protected amine *N*-(4-vinylbenzyl)phthalimide was used. The protected amine was deprotected to generate an active free-amine catalyst only after processing the polymer, either by electrospinning or 2D printing. This was indispensable, as the free amine-containing polymer showed limited solubility in common organic solvents such as THF or DMF required for processing. Here, we present detailed studies regarding 1) preparation and characterization of post-process functionalized modular electrospun nonwoven and precisely printed Wolf-Lamb type catalysts carriers and 2) catalytic studies.

EXPERIMENTAL:

Materials

Dimethylformamide (DMF, p.a. grade, Alfa Aesar), diethyl ether (technical grade, distilled before use), dichloromethane (DCM, technical grade) was dried over calcium hydride (CaH_2) and distilled before use. Triethylamine (99.8% Acros) was fractionated distilled, dimethyl sulfoxide (DMSO, p.a. grade, Alfa Aesar), 4-vinylbenzylchlorid (90%, Sigma Aldrich), potassium phthalimide (98%, Alfa Aesar), 4-amino benzophenone (98%, Alfa Aesar), acryloyl chloride (96%, Alfa Aesar), dimethoxy methylbenzene (99%, Alfa Aesar), ethyl cyano acetate (98+%, Alfa Aesar) and n-undecane (99%, Alfa Aesar) were used as received. Dioxane (p.a. grade, Alfa Aesar) was freshly distilled, were used as received. Styrene (99%, Sigma Aldrich) was distilled *in vacuo* before use. MABP was synthesized according to the literature.^[32]



Scheme 11. Concept of the preparation of post-process functionalized carriers for Wolf-amb type catalysts. After processing, electrospun and 2D-printed materials underwent treatment for cross-linking and deprotection in the case of a base catalyst.

Synthesis of N-(4-vinylbenzyl)phthalimide

In a Schlenk flask, 1.1 eq of potassium phthalimide was dissolved in dried DMF ($c = 2 \text{ mol L}^{-1}$). After 30 min of stirring, 1.0 eq 4-vinyl benzyl chloride was added, and the reaction mixture was heated to $50 \text{ }^\circ\text{C}$ for 16 h. The product was precipitated in a NaOH solution ($\text{pH} = 10$), followed by recrystallization from methanol. Colorless needles were obtained with a yield of 60%.

$^1\text{H-NMR}$ (300 MHz, CDCl_3) $\delta = 7.83$ (td, $J=5.3, 2.1 \text{ Hz}$, 2H), 7.82 (td, $J = 5.3, 2.1 \text{ Hz}$, 2H), $7.44 - 7.31$ (m, 4H), 6.67 (dd, $J = 17.6, 10.9 \text{ Hz}$, 1H), 5.76 (dd, $J = 10.9, 0.9$, 1H) 5.22 (dd, $J = 10.9, 0.9$, 1H) 4.83 (s, 1H) ppm. (Supporting Information, **Figure S1**)

$^{13}\text{C-NMR}$ (75 MHz, CDCl_3) $\delta = 168.13, 137.27, 136.46, 135.94, 134.08, 132.18, 128.96, 126.58, 123.45, 114.29$ ppm. (Supporting Information, **Figure S2**)

Synthesis of *N*-(4-benzoylphenyl)acrylamide

In a three-necked flask, 1 eq of 4-amino benzophenone was dissolved in dried DCM ($c = 0.64 \text{ mol L}^{-1}$), and 1.0 eq of triethylamine was added. The reaction mixture was cooled to $0 \text{ }^\circ\text{C}$ with an ice bath, and 1.0 eq of acryloyl chloride dissolved in dried DCM ($c = 3.2 \text{ mol L}^{-1}$) was added dropwise through a dropping funnel. The reaction mixture was reheated to room temperature and stirred for 16 h. The resulting reaction mixture was washed with 5% NaHCO_3 solution and two times with deionized water. The organic layer was dried with MgSO_4 , and the organic phase was evaporated under reduced pressure. The obtained crude product was recrystallized from methanol to get a yellow powder-like product with a yield of 71%.

$^1\text{H-NMR}$ (300 MHz, DMSO) $\delta = 7.89 - 7.68$ (m, 6H), $7.64 - 7.54$ (m, 1H), $7.45-7.40$ (m, 2H) 7.44 (s, 1H), 6.50 (dd, $J = 16,8, 1,2$) 6.28 (dd, $J = 16.8, 10.2 \text{ Hz}$, 1H), 5.85 (dd, $J = 10.2, 1.2 \text{ Hz}$, 1H) (Supporting Information, **Figure S3**)

$^{13}\text{C-NMR}$ (75 MHz, DMSO) $\delta = 196, 164, 142, 137, 133, 132, 132, 131, 130, 128, 128, 119 \text{ ppm}$.

(Supporting Information, **Figure S4**)

Synthesis of *P*(*S*_{76-co-4VBI}_{15-co-BPAm})

0.15 eq 4VBI and 0.1 eq BPAm were placed in a Schlenk flask and dissolved in dioxane. 0.75 eq styrene was added, and the mixture was degassed with argon for 30 min (monomer concentration $c = 3 \text{ mol L}^{-1}$). The mixture was heated to $70 \text{ }^\circ\text{C}$, and 0.3 wt% AIBN was added. After 16 h, it was precipitated in methanol redissolved in dioxane and precipitated in diethyl ether and dried overnight at $50 \text{ }^\circ\text{C}$ *in vacuo*. A colorless powder was obtained with a yield of 57%.

$^1\text{H-NMR}$ (300 MHz, CDCl_3) $\delta = 0.5-2.3$ (polymer backbone, CH_2), 4.6 ($\text{H}_2\text{C-CH}_2\text{-N}$), $6.0-8.0$ (CH , aromatic), (Supporting Information, **Figure S5**)

GPC (DMF) $\overline{M}_n = 54000$; $\overline{M}_w = 81000$; $D = 1.5$ (Supporting Information, **Figure S6**)

Synthesis of P(S₆₇-co-SSNa₁₈-co-MABP₁₅)

0.15 eq sodium styrene sulfonate and 0.1 MABP were placed in a Schlenk flask and dissolved in DMSO. 0.75 eq styrene was added, and the mixture was degassed with argon for 30 min (monomer concentration $c = 4 \text{ mol L}^{-1}$). The mixture was heated to 70 °C, and 0.3 wt% AIBN was added. After 16 h, it was precipitated in isopropanol and washed with water and isopropanol. The resulting product was then dried overnight at 60 °C *in vacuo*, finally giving a yield of 58%.

¹H-NMR (300 MHz, DMSO-*d*₆) $\delta = 0\text{-}2.5$ (polymer backbone, *CH*₂, *CH*), 6.0-8.0 (*CH* aromatic) (Supporting Information, **Figure S7**)

GPC (DMF) $\overline{M}_n = 145000$; $\overline{M}_w = 231000$; $D = 1.6$ (Supporting Information, **Figure S8**)

Synthesis of P(S₆₇-co-SSA₁₈-co-MABP₁₅)

P(S₆₇-co-SSNa₁₈-co-MABP₁₅) was dissolved in methanol, and a concentrated HCl solution was dropwise added to precipitate the protonated P(S₆₇-co-SSA₁₈-co-MABP₁₅).

Post-process modification to P(S₇₆-co-4VBA₁₅-co-BPAm₉)

3 g of either electrospun membrane or printed structure (PS₇₆-co-4VBI₁₅-co-BPAm₉) was immersed in 50 mL DMF, and 10 mL hydrazine was added. The mixture was heated to 70 °C for three hours and washed three times with DMF and two times with diethyl ether.

Electrospinning

For electrospinning, a conventional one-needle setup was used, built by the University of Bayreuth's mechanical and electrical workshop.

Solutions with 30 wt% of P(S₆₇-co-SSA₁₈-co-MABP₁₅) and 35 wt% P(S₇₆-co-4VBI₁₅-co-BPAm₉) in DMF were prepared. The solutions were then electrospun at a flow rate of 300 μL

h^{-1} (P(S_{67-co}-SSA_{18-co}-MABP₁₅)) and $750 \mu\text{L h}^{-1}$ (P(S_{76-co}-4VBI_{15-co}-BPAm₉)) employing a current of 12 kV (P(S-co-SSA-co-MABP)) and 15 kV (P(S_{76-co}-4VBI_{15-co}-BPAm₉)). The corresponding randomly oriented fibers were collected on a rotating disc collector with a current of -1 kV in the form of self-standing porous membranes for further use.

2D-Printing

A Cellink Inkredible+ was used as a 3D printer. A solutions of 30 wt% in a mixture of THF/DMF (90/10) of P(S_{76-co}-4VBI_{15-co}-BPAm₉) was printed with an air pressure of 80 kPa on a polyamide mesh (Nylon, Buddeberg). For P(S_{67-co}-SSA_{18-co}-MABP₁₅), a mixture of THF/DMF (80/20) was printed on a PET mesh with a mesh size of 120 μm for P(S_{67-co}-SSA_{18-co}-MABP₁₅).

Cross-linking

Electrospun membranes were cross-linked by UV-light from both sides for 2 h, and printed structures were cross-linked for 3 h with a UV-F 400 F (Jonle UV technology) at 15 cm (23 mW cm^{-1}).

Catalytic experiment

In 5 mL of DMF or toluene 376 μL (2.5 mmol, 1 eq) dimethoxy methylbenzene and 320 μL (3 mmol, 1.2 eq) ethyl cyanoacetate, 300 μL undecane (as an internal standard for GC analysis, as it does not interact with any of the reaction components), and 90 μL (5 mmol, 2 eq) water were subsequently added. The electrospun acid and base polymers as individual porous membranes were used as catalysts. Each membrane weighed 80 mg. The acid and base catalyst membranes were fixed individually inside separate PET meshes (pore size 120 μm) to prevent damage by interaction with the magnetic stirrer, while the printed structures, which are on top of the mesh substrate, were directly immersed in the reaction solution. The solution was stirred for 5 h in case of membranes and 1 h in case of printed structures. 10 μL of the catalytic solution

was taken at intervals of 10 min during the first hour and afterward every 30 min until the end and placed in acetonitrile for GC analysis. Reusability was tested by reimmersing substrates in freshly prepared reaction mixtures under the same conditions.

Gel permeation chromatography (GPC)

GPC measurements were performed on an SEC 1260 Infinity (Agilent Technologies) in DMF (HPLC grade) with lithium bromide ($c = 5 \text{ g L}^{-1}$) as eluent, employing a flow rate of 0.5 mL min^{-1} and toluene as an internal standard. The setup was equipped with two PSS-GRAM gel columns (particle size = $10 \text{ }\mu\text{m}$) with a porosity of 100 to 3000 \AA and a refractive index detector (Agilent Technologies). Narrowly distributed polystyrene homopolymers (PSS calibration kit) were used for calibration.

Nuclear Magnetic Resonance (NMR) spectroscopy

^1H -NMR spectroscopy measurements were performed on a Bruker Ultrashield 300 system with either deuterated chloroform (CHCl_3) or $\text{DMSO-}d_6$ as solvent at 300 MHz.

^{13}C -NMR spectroscopy measurements were performed on the same system at 75 MHz.

^{13}C solid-State NMR was performed on a 400 MHz Bruker Avance III HD employing a 3.2 mm HXY MAS probe head using cross-polarization and magic angle spinning technique at 12.5 kHz.

Gas Chromatography (GC)

GC measurements were performed on a Shimadzu GC-2010 plus a flame ionization detector using nitrogen as the carrier gas. For sample preparation, $10 \text{ }\mu\text{L}$ of the reaction sample was dissolved in 1 mL of acetonitrile (p.a. grade, Alfa Aesar). $1 \text{ }\mu\text{L}$ was injected with a split ratio of 1:50 and measured from $50 \text{ }^\circ\text{C}$ to $300 \text{ }^\circ\text{C}$ at a heating rate of 15 K min^{-1} .

Optical microscope

Optical microscope images were taken by a Smartzoom5 (Zeiss).

Raman imaging

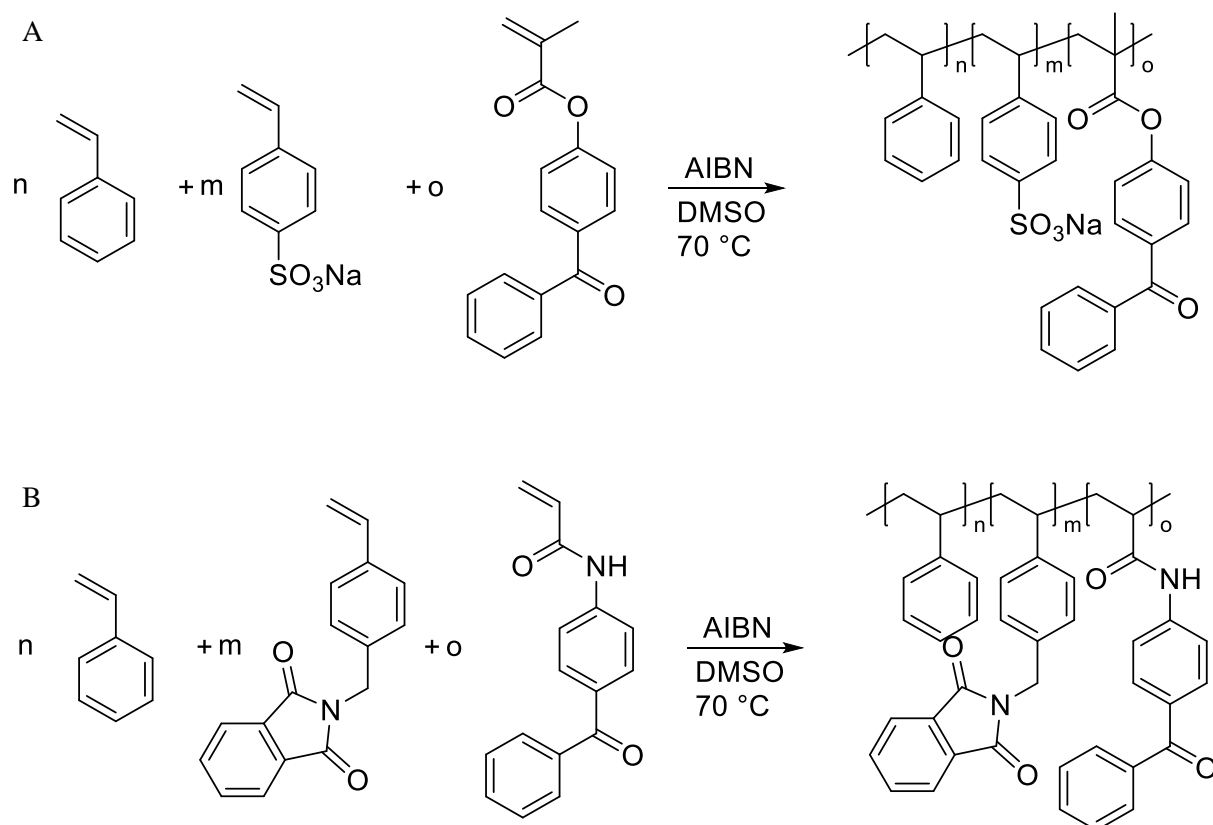
A WITec alpha 300 RA+ imaging system, equipped with a UHTS 300 spectrometer and a back-illuminated Andor Newton 970 EMCCD camera, was employed for confocal Raman imaging. The measurements were conducted at an excitation wavelength of λ 532 nm, using an integration time of 0.5 s pixel⁻¹ (10x objective, NA = 0.25, step size 1.5 – 2 μ m, software WITec Control FIVE 5.1). All spectra were subjected to a cosmic ray removal routine and baseline correction. The printed copolymers' spatial distribution on the polyamide mesh was determined using the tool “true component analysis” in the WITec Project FIVE 5.1 software.

Scanning Electron Microscopy (SEM)

SEM images were taken with a Zeiss LEO 1530 at an acceleration voltage of 3 kV, using an Everhart-Thornley secondary electron detector. Sample preparation was done by sputtering the sample with a 2 nm thin platinum layer (Sputter Coater 208 HR, Cressington).

RESULTS AND DISCUSSION

The preparation of acid and base polymers for catalysis was done by tercopolymerization of styrene with benzophenone derivative (as cross-linker) and functionalized styrene with acid and protected base units (**Scheme 2**) using the free radical polymerization method.



Scheme 2. Preparation of acid and base polymers to be used as Wolf-lamb type catalysts by free radical polymerization. (A) Acid catalyst: Poly(styrene-*co*-sodium styrene sulfonate-*co*-methacryloyl benzophenone), (B) protected base catalyst: Poly(styrene-*co*-*N*-(4-vinyl benzyl)phthalimide-*co*-*N*-(4-benzoylphenyl)acrylamide).

The desired comonomer with a protected primary amine, *N*-(4-vinyl benzyl)phthalimide (4VBI, **3**), was obtained by nucleophilic substitution of 4-vinyl benzyl chloride (**1**) with potassium phthalimide (**2**) (refer reaction equations and analytical data in supporting Information, **Scheme S1, Figure S1, S2**). This can be modified after processing to the primary amine by a reaction with hydrazine. The cross-linking unit was an amide based BPAm (**6**) (analytical data Supporting Information, **Figure S3, S4**), which was prepared from acryloyl chloride (**4**) and 4-amino benzophenone (**5**). The use of an amide-based benzophenone is more suitable than an ester-based benzophenone unit to prevent reactions with hydrazine during the formation of primary amines (deprotection procedure) later on in the post-functionalization process. Benzophenone can react under UV-light towards a diradical, which later abstracts hydrogen

from polymer backbone and starts a chain reaction leading to intramolecular cross-linking (refer mechanism in supporting Information, **Scheme S2**).

The amine protected polymer, P(S_{76-co}-4VBI_{15-co}-BPAm₉), had a composition of 76 mol% of styrene, 15 mol% 4VBI units, and 9 mol% BPAm as determined by ¹H NMR (Supporting information, **Figure S5, Equation S1 –S3**). The number average molecular weight determined by GPC was $\overline{M}_n = 54000$, $D = 1.5$ (Supporting information, **Figure S6**). For the acidic P(S_{67-co}-SSNa_{18-co}-MABP₁₅) copolymer, a combination of elemental analysis and ¹H-NMR was used to determine the copolymer composition (Supporting Information, **Figure S7, Equation S4 –S9**), resulting in a composition of 18 mol% sodium styrene sulfonate, 15 mol% methacryloyl benzophenone, and 67 mol% styrene. The number average molecular weight determined by GPC was $\overline{M}_n = 145000$, $D = 1.6$ (Supporting Information, **Figure S8**).

The copolymers were processed through two different techniques, electrospinning, and 2D printing, either as individual membranes or printed structures for use as active catalytic materials in one-pot reactions. The deprotected amine-containing base polymer showed bad solubility in common organic solvents making processing impossible. Also, the possibility of side reaction of the primary amine with the cross-linking unit made us use the protected base polymer P(S_{76-co}-4VBI_{15-co}-BPAm₉) for processing. Therefore, a post-process reaction for functionalisation with an active strong amine catalyst by deprotection per *Gravano et al.* was performed, which was slightly modified towards DMF as a solvent within the reaction and the purification through multiple washing steps (Supporting Information, **Scheme S3**).^[33]

The printed structures and catalytic membranes were cross-linked with UV light for 3 h (in the case of the printed structure) and 2.5 h per side for the electrospun catalytic membrane and deprotected by hydrazinolysis in DMF. Electrospun P(S_{67-co}-SSNa_{18-co}-MABP₁₅) was protonated with hydrochloric acid after membrane preparation as the catalytic activity is greatly reduced due to possible salt formation. For 3D printing, it was possible to use P(S_{67-co}-SSA_{18-co}-MABP₁₅) directly.

Through electrospinning, membranes with homogeneously distributed copolymer fibers were obtained (fiber diameter for $P(S_{67}\text{-}co\text{-}SSNa_{18}\text{-}co\text{-}MABP_{15})$: 530 ± 80 nm and for $P(S_{76}\text{-}co\text{-}4VBI_{15}\text{-}co\text{-}BPAm_9)$: 1.5 ± 0.6 μm , **Figure 26A, C**). The treatment of membranes in DMF for deprotection of amino groups and neutralization of acidic salt led to the swelling of fibers with a slight increase in the fiber diameter (fiber diameter in deprotected membrane $P(S_{76}\text{-}co\text{-}4VBA_{15}\text{-}co\text{-}BPAm_9)$ was 1.6 ± 0.4 μm) and especially in case of $P(S_{67}\text{-}co\text{-}SSA_{18}\text{-}co\text{-}MABP_{15})$ a change of morphology was observed (**Figure 26B, D**). Although the overall morphology of these protonated fibers is not homogenous, most probably due to the presence of salt on the surface, they were further used as such for catalysis reactions.

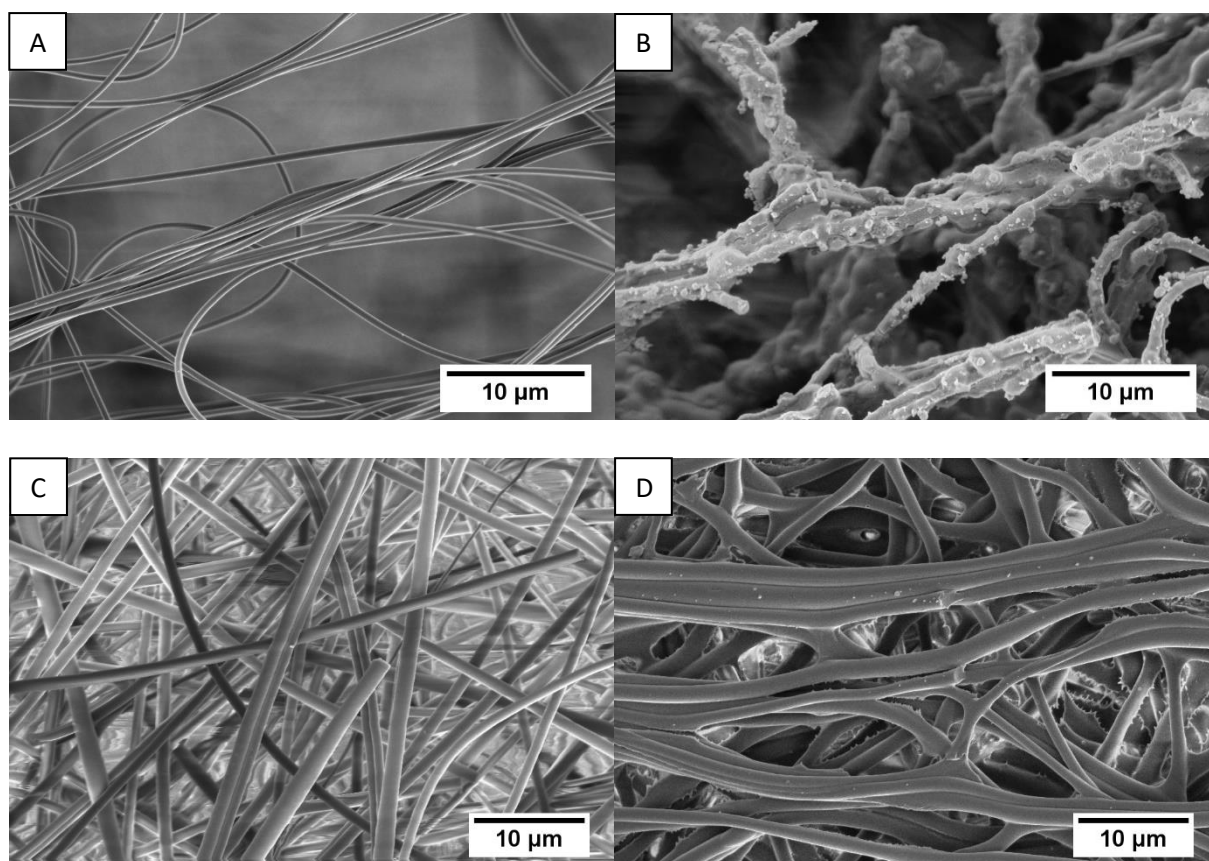


Figure 26. SEM images of the electrospun membranes before and after treatment. (A) $P(S_{67}\text{-}co\text{-}SSNa_{18}\text{-}co\text{-}MABP_{15})$, (B) $P(S_{67}\text{-}co\text{-}SSA_{18}\text{-}co\text{-}MABP_{15})$, (C) $P(S_{76}\text{-}co\text{-}4VBI_{15}\text{-}co\text{-}BPAm_9)$ and (D) $P(S_{76}\text{-}co\text{-}4VBA_{15}\text{-}co\text{-}BPAm_9)$.

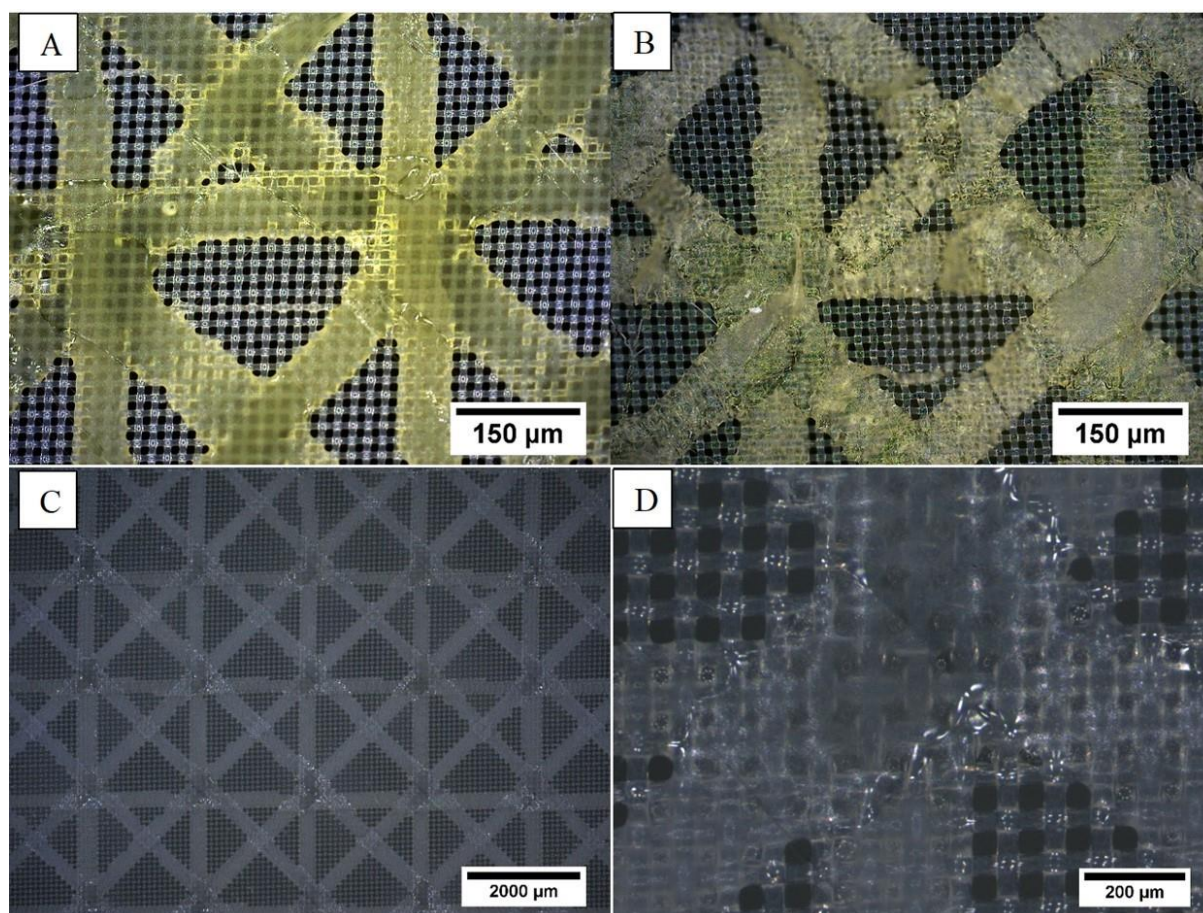


Figure 27A showed the printed structure from $S_{76-co-4VBI_{15-co-BPAm_9}}$. The protected primary amine (4VBI units) in $S_{76-co-4VBI_{15-co-BPAm_9}}$ were deprotected after printing. After the deprotection step, the printed structure remained intact and stable on top of the substrate

polyamide

mesh

(

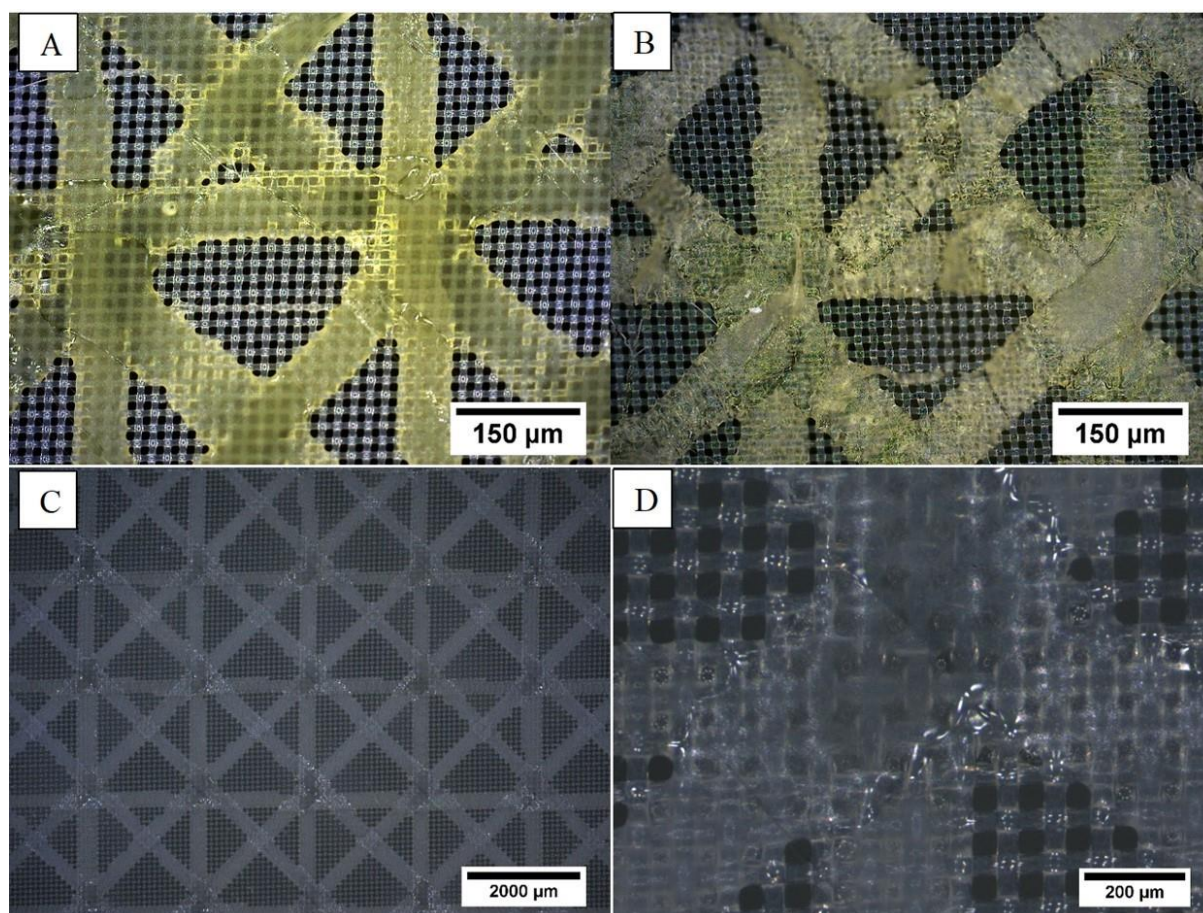


Figure 27B). The slight cracking of the printed lines was unavoidable under present experimental conditions, which might be due to the polymer's brittleness and the chemical change from the protecting phthalimide group towards the active primary amine.

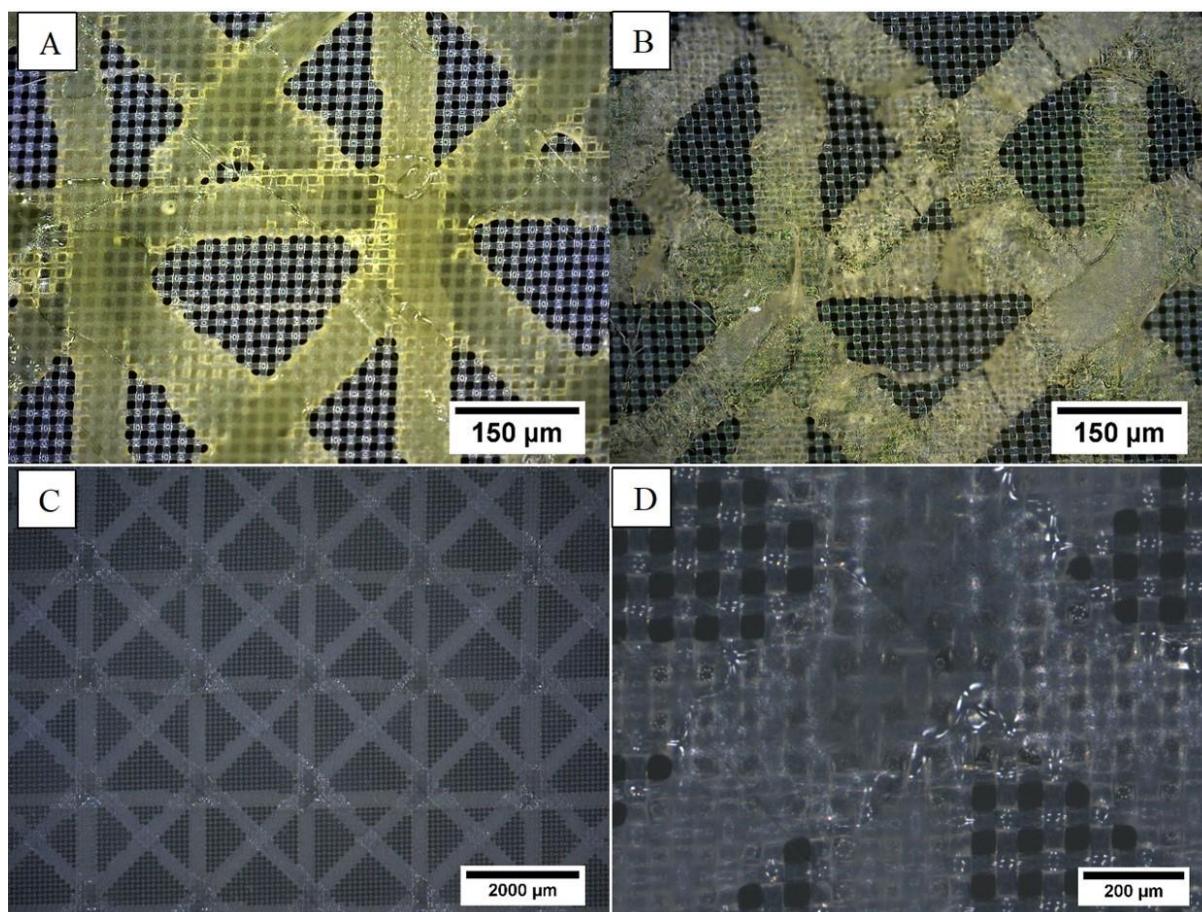


Figure 27. Digital microscopy images of the printed copolymer structure on a PA mesh (A) $P(S_{76}\text{-}co\text{-}4VBI_{15}\text{-}co\text{-}BPAm_9)$, (B) $P(S_{76}\text{-}co\text{-}4VBA_{15}\text{-}co\text{-}BPAm_9)$ and on a PET mesh (C) overview of $P(S_{67}\text{-}co\text{-}SSA_{18}\text{-}co\text{-}MABP_{15})$ and (D) a higher magnification of $P(S_{67}\text{-}co\text{-}SSA_{18}\text{-}co\text{-}MABP_{15})$. A continuous structure is obtained, leading to neatly aligned lines.

As the base copolymer is not soluble after cross-linking and deprotection, the successful deprotection reaction could be proved by solid-state NMR (**Figure 3**; Supporting information, **Figure S9, S10**) and Raman spectroscopy (**Figure 29**). The solid-state NMR clearly shows the successful deprotection of the primary amine group, indicated by the shift of the peak at 168 ppm for the carbonyl groups of the imide and 134 ppm for the two aromatic *CH*-groups of the phthalimide (**Figure 3A** red). Further, the shoulder at 48 ppm is the CH_2 group next to the primary amine (**Figure 3B** turquoise).

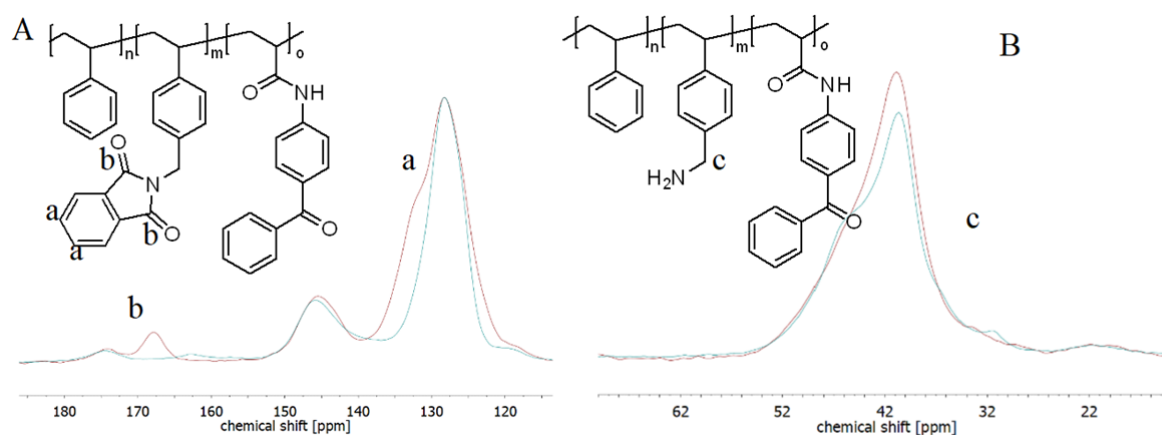


Figure 28. Superimposed solid-state ^{13}C -NMR spectra of P(S_{76-co}-4VBI_{15-co}-BPAm₉) (red) (chemical structure A) and P(S_{76-co}-4VBA_{15-co}-BPAm₉) (turquoise) (chemical structure B) in the region 110-190 ppm (left) and 12 – 72 ppm (right). The relevant peaks are marked as a, b, c both in the chemical structure and the NMR spectra. Successful deprotection can be seen.

The successfully obtained primary amine within the 2D printed copolymer can be proven by cross-sectional Raman imaging of the polymeric material (**Figure 4**). The position of the measurement is shown in **Figure 4A**. The red Raman spectra on top show the peak's disappearance at 1800 cm^{-1} , indicating the CO-bonds of the imide (**Figure 4B**). The placement of the copolymer on the mesh-like structure is shown in **Figure 29C**. Here, it shows that the deprotected polymer (red) is on top of the polyamide mesh in a thin layer and is mainly deposited between the meshes (blue).

A

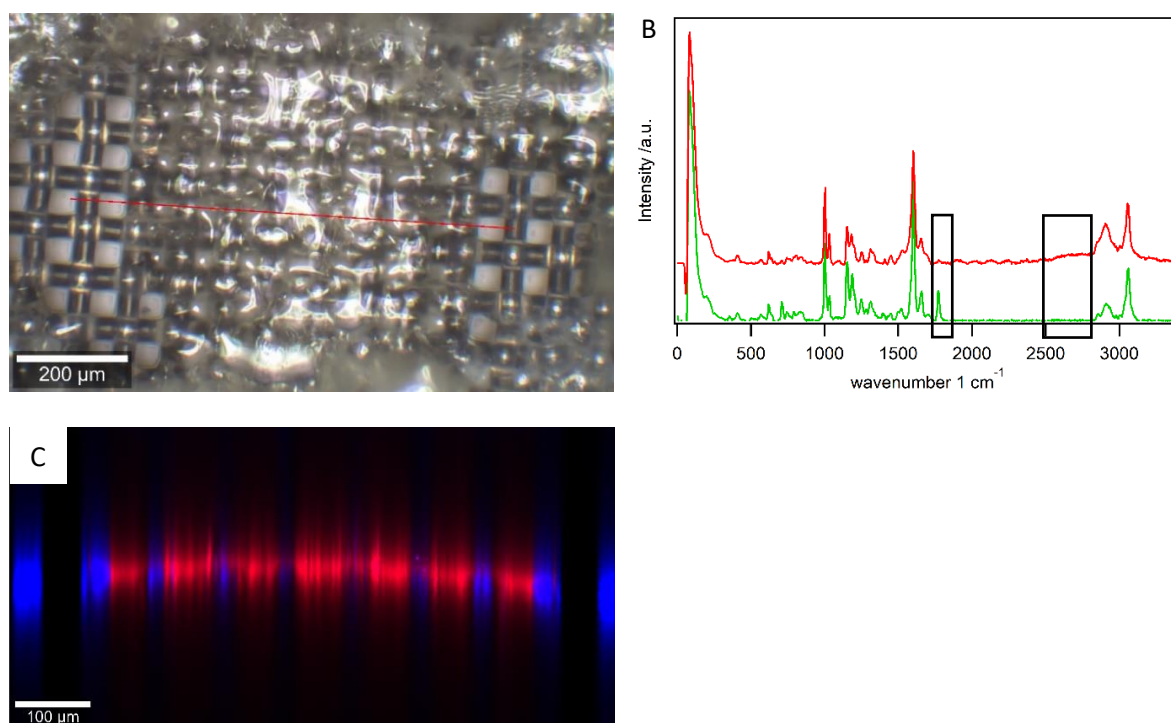
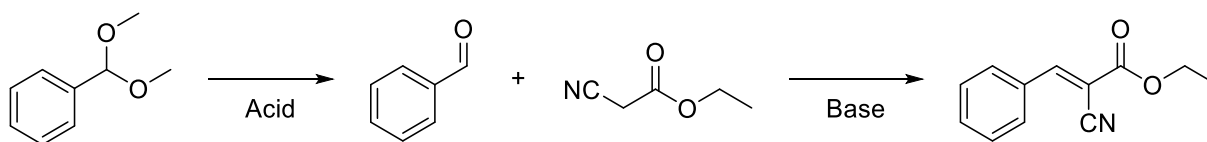


Figure 29. (A) Optical microscopy image of P(S₇₆-co-4VBA₁₅-co-BPAm₉) with the position of Raman measurement. (B) Raman spectra for P(S₇₆-co-4VBI₁₅-co-BPAm₉) (green) and P(S₇₆-co-4VBA₁₅-co-BPAm₉) (red). (C) Raman cross-section of the mesh printed with deprotected P(S₇₆-co-4VBA₁₅-co-BPAm₉), the printed primary amine-containing copolymer (colored in red), is mainly located within the cavities of the polyamide mesh (colored in blue) with only a thin layer on top of it.

With these successfully obtained catalytic materials, a reaction was tested, which was not possible with a weak base such as 4-vinyl pyridine. Here, the acid-catalyzed deacetalization of dimethoxy methylbenzene to benzaldehyde followed by the base-catalyzed Knoevenagel condensation with ethyl cyanoacetate towards ethyl 2-cyano-3-phenyl acrylate was chosen as a commonly employed two-step reaction for Wolf-Lamb type catalysis in one-pot (**Scheme 12**).^[6,18,24]



Scheme 12. The catalytic Wolf-Lamb type reaction of dimethoxy methylbenzene to benzaldehyde to ethyl 2-cyano-3-phenyl acrylate in toluene and DMF at 80 °C.

From previous works, it is known that the first reaction step with P(S₆₇-co-SSA₁₈-co-MABP₁₅) works for either electrospun catalytic membrane or printed structures.^[26,27] Therefore, the second reaction step needed to be tested (**Figure 30**) as this reaction needs higher basicity than it is provided by 4-vinyl pyridine as a base (pK_a ~ 4.5). **Figure 30** clearly shows that the Knoevenagel reaction of benzaldehyde with ethyl cyanoacetate to ethyl-2-cyano-3-phenyl acrylate was successful with a high yield of more than 95% after around 180 min. Therefore, the polymeric base catalyst should be suitable for the Wolf-Lamb type two-step reaction sequence in one pot with the basic Knoevenagel condensation in the next steps.

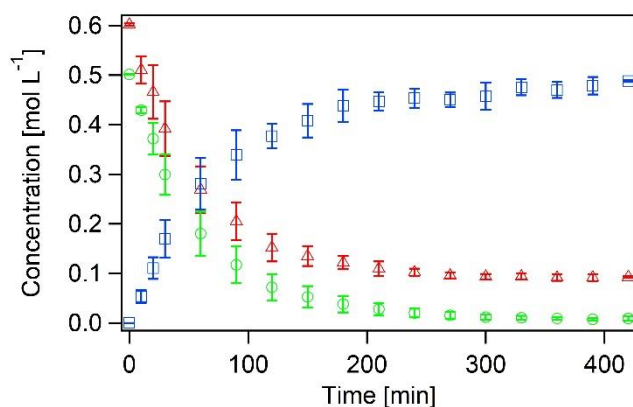


Figure 30. The reaction of benzaldehyde (green, circles) with ethyl cyanoacetate (red, triangles) to ethyl-2-cyano-3-phenyl acrylate (blue, squares) in DMF at 80 °C. 400 mg of P(S₇₆-co-4VBA₁₅-co-BPAm₉) electrospun membrane was used, resulting in 3.9 mol% catalytically active repeating units. The concentration of benzaldehyde was 0.5 mol L⁻¹, the concentration of ethyl cyanoacetate was 0.6 mol L⁻¹. Undecane was used as an internal standard.

For the actual Wolf-Lamb type reaction, the electrospun and printed systems are compared with toluene as solvent as here reusability is possible (**Figure 31A, 6B** first cycle; **Figure 6C, 6D** third cycle, second cycle Supporting Information **Figure S13**). Comparing the reaction in toluene for electrospun membranes and 2D printed structures shows that the overall reaction time is lower for the printed structure (**Figure 6A, B**). After 10 min, the first reaction step of the conversion to benzaldehyde is finished, and the second reaction step is completed after 30 min. In contrast, the electrospun membranes needed 90 min for the first step's full conversion and around 150 min for the second reaction step. Here, it clearly shows that the printed structure is more advantageous than the electrospun membrane (Supporting Information, **Figure S11**). The reachability of catalytic sites appears to be hindered due to the necessary mass transport within the fibrous gel network in electrospun membranes. The swelling of fibers in electrospun membranes in the reaction medium led to the formation of a gel. In contrast, in the denser printed networks, the necessary diffusion length to reach catalytic sites is lower, resulting in an increase in performance. Both systems were reusable in toluene as high conversion (more than 95%) was still obtained after 60 min (in case of 2D printed structure) and after 240 min for electrospun membranes (**Figure 6C, D**). Three test cycles were run for the reusability test. The group of *Zhang* reported a decrease of conversion from 100% down to 95% within the first three cycles and 90% for the fifth cycle^[18] or by the group of *Degirmenci* who also observed a continuous decrease of conversion from 97% down to 93% within the first three cycles.^[19] To further compare the systems, the reactions were fitted using differential equations (Supporting Information, **Equation S11 – S14; Table 1**). The fitted kinetic parameters also show that the reaction speed, especially for the first reaction step, is over 10 times higher for printed structures (**Table 1**, entry 4) than for electrospun membranes. The second step shows about 5 times higher value of k_2 for the printed structures explaining the faster reaction rate observed in the time-concentration curves (**Table 1**, entry 5; **Figure 6B**).

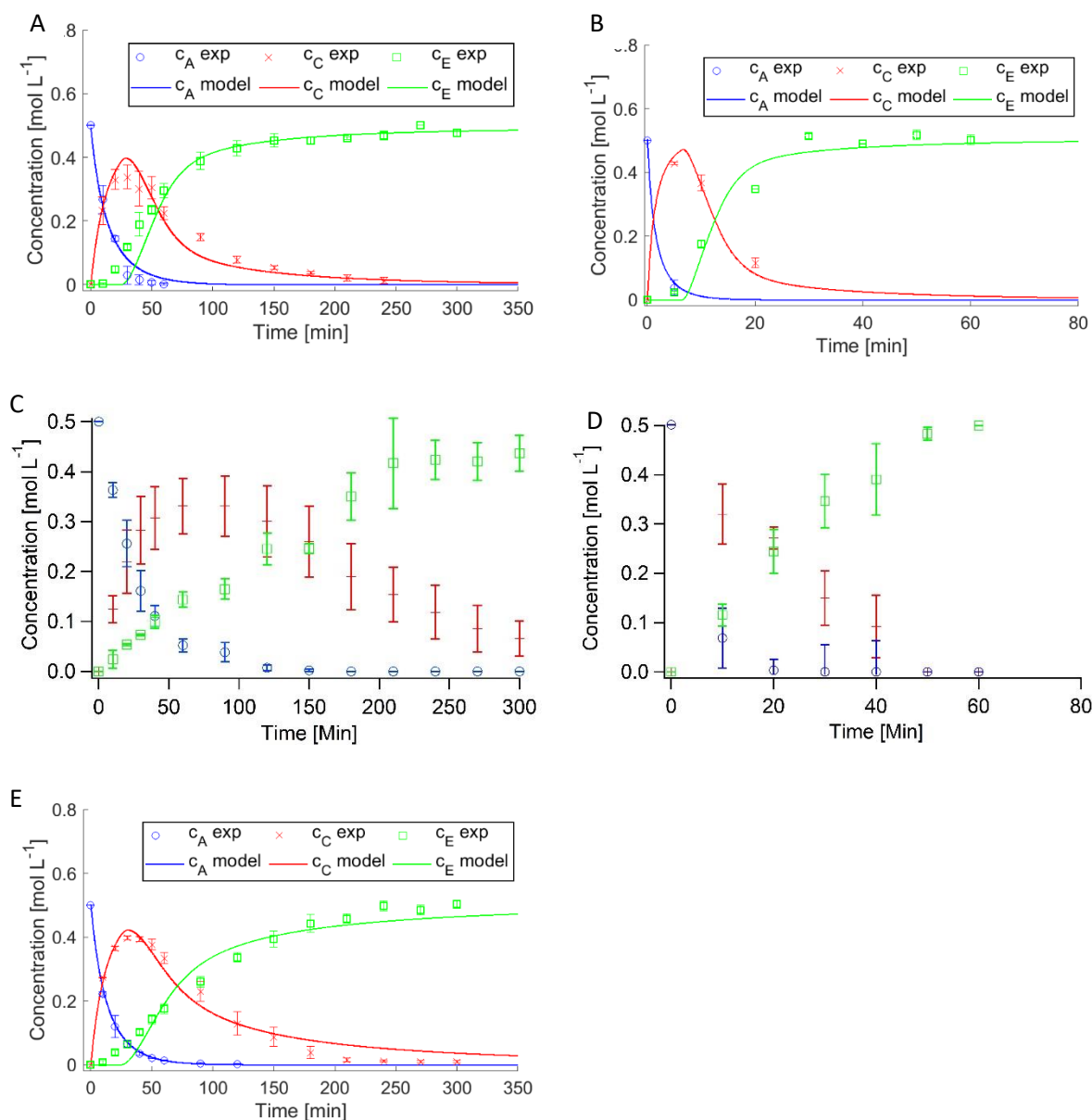


Figure 31. The two-step reaction system of the deacetalisation of dimethoxybenzyl acetate (blue circles) to benzaldehyde (red crosses), which reacts with ethyl cyanoacetate to ethyl-2-cyano-3-phenyl acrylate (green squares). (A) First cycle and (C) third cycle for catalytic membrane in toluene, (B) first cycle and (D) third cycle for catalytic 2D printed structure in toluene, (E) catalytic membrane in DMF. Reaction conditions were 0.5 mol L^{-1} dimethoxybenzyl acetate, 0.6 mol L^{-1} ethyl cyanoacetate, and 1 mol L^{-1} water with 80 mg of each acidic (3.6 mol%) and basic (3.9 mol%) catalytic material in 5 mL of solvent at $80 \text{ }^{\circ}\text{C}$.

Comparison of toluene and DMF as solvents show that high conversion (more than 95%) is achieved after 180 min in DMF and is, therefore, slower than the reaction in toluene (150 min). The first reaction step is finished after 60 min in both cases. Nevertheless, the second reaction step is slower, monitored by the higher peak of benzaldehyde at 0.4 mol L^{-1} at 30 min for the catalysis in DMF compared to the peak at 0.35 mol L^{-1} at 30 min in toluene (**Figure 6A, E**). As the system is only reusable in toluene in which only a very small amount of water is miscible, which is different from DMF, for this specific system, toluene is more advantageous as a solvent because of the higher reaction rates. The fitted reaction rates (**Table 1**, entry 4) further show no significant difference between the reaction rates for the first step, but a 60% increase for the second reaction step reaction rate, showing that toluene is a better solvent for this specific system.

Table 4. Fitted parameters of the first cycle for different solvents and structures.

	Electrospun membrane; reaction solvent: DMF	Electrospun membrane; reaction solvent: toluene	Printed structure; reaction solvent: Toluene
c_{A0} ^{a,b}	0.50	0.49	0.50
c_{B0} ^{a,c}	1.27	1.10	0.80
c_{D0} (fixed) ^{a,d}	0.6	0.6	0.6
k_1 ^{e,f}	0.067	0.073	0.94
k_2 ^{e,g}	0.035	0.059	0.250

^{a)} mol L^{-1} , ^{b)} concentration of dimethoxy methyl benzene at $t = 0 \text{ min}$, ^{c)} concentration of water at $t = 0 \text{ min}$, ^{d)} concentration of ethyl cyano acetate at $t = 0 \text{ min}$, ^{e)} mol (L min)^{-1} , ^{f)} reaction rate constant of the first reaction step, ^{g)} reaction rate constant of the second reaction step

Comparing this work to the porous polyHIPE catalyst used by the group of *Degirmenci*^[19], the

performance of the printed structures is better, while the electrospun membrane is less. They used

50 μmol of basic and acidic highly porous catalyst within their work, reaching a conversion of over 95% within 3 hours. In contrast, our system with 90 μmol of acidic and basic catalyst reached a conversion of over 95% within 40 minutes for the printed structures, while the electrospun membranes needed around 4 hours. The higher amount of catalyst is influencing the reaction speed, but it is safe to assume that the printed catalyst would also perform better with a decreased amount.

CONCLUSION

Within this work, we were able to show that electrospun membranes and 2D-printed structures can be post-process functionalized to obtain active catalytic units for use in one-pot reactions using Wolf-Lamb type catalysts that are not achievable before processing. By solid-state NMR and Raman imaging, we were able to show that the post-processing functionalization was successfully achieved with high conversion. The catalytic materials were tested for a two-step reaction (acidic catalyzed deacetalization reaction of dimethoxy methylbenzene to benzaldehyde followed by the basic catalyzed Knoevenagel condensation to ethyl 2-cyano-3-phenyl acrylate) in one-pot. The kinetics of the two-step reaction was calculated using a differential equation to compare these systems and understand the underlying reaction dynamics. These catalytic studies showed that the electrospun and printed materials achieved a high conversion, and reusability is dependent on the right solvent.

Overall, this work opens the use of not only acid and base-catalysis for such Wolf-Lamb type reactions but further increases the applicability as a possible modular system for more-step reactions and carrier systems for organo-catalysts. The straight forward polymer synthesis *via* free-radical copolymerization combined with the general easy preparation of catalytic structures by electrospinning and 2D printing can be applied in different ways for future catalysts.

Supporting Information. Detailed further analytical results and calculations are shown in the supporting information (file type PDF).

AUTHOR INFORMATION

Corresponding Author

*Seema Agarwal (agarwal@uni-bayreuth.de)

Author Contributions

The manuscript was written through the contributions of all authors. All authors have given approval to the final version of the manuscript. Martin Pretscher (MP) carried out all experimental work under the guidance of Prof. Seema Agarwal. Markus Dietel assisted MP in experimental work. Theoretical part of the work was done by Gabriel Sitaru under the guidance of Prof. Gekle. Dr. Schmalz carried out Raman characterization.

Funding Sources

We thank DFG (SFB 840; Projects A12 and A2) for the financial support.

ACKNOWLEDGMENT

Rika Schneider is thanked for analytical assistance with GPC measurements and Carmen Kunert for SEM measurements. Birgit Brunner (Chemical Engineering, University of Bayreuth) is acknowledged for elemental analysis, Beate Bojer (Inorganic Chemistry III, University of Bayreuth) for solid-state NMR measurements, and Fabian Lukas and Constantin Schreck for their assistance with experiments.

ABBREVIATIONS

DMF, dimethylformamide, THF tetrahydrofurane, poly(styrene-*co*-sodium styrene sulfonate-*co*-methacryl benzophenone), p(S-*co*-SSNa-*co*-MABP), poly(styrene-*co*-styrene sulfonic acid-*co*-methacryl benzophenone) p(S-*co*-SSA-*co*-MABP), poly(styrene-*co*-4-vinylbenzylamine-*co*-

acrylamide benzophenone), p(S-co-4VBPI-co-BPAm) N-acrylamide benzophenone (BPAm), N-(4-vinylbenzyl)phtalimide (4VBA), N-(4-vinylbenzyl)amine

REFERENCES

- [1] Cohen, B. J.; Kraus, M. A.; Patrchonik, A. Organic synthesis involving multipolymer reactions. Polymeric trityllithium, *J. Am. Chem.Soc.* **1977**, *99*, 4165 - 4167.
- [2] Cohen, B. J.; Kraus, M. A.; Patrchonik, A. *J. Am. Chem. Soc.* " Wolf and Lamb" reactions equilibrium and kinetic effects in multipolymer systems **1981**, *103*, 7620 - 7629.
- [3] Lee Y.-R.; Chung, Y.-M., Ahn, W.-S. A new site-isolated acid–base bifunctional metal–organic framework for one-pot tandem reaction *RSC Adv.* **2014**, *4*, 23064 -23067.
- [4] Chung, Y.-M. One-pot cascade deacetalization and nitroaldol condensation over acid–base bifunctional ZIF-8 catalyst *Res. Chem. Intermed.* **2018**, *44*, 3673 - 3685.
- [5] Zhang, Y.; Wang, Y.; Liu, L.; Wie, N.; Gao, M.-L.; Zhao, D.; Han, Z.-B. Robust bifunctional lanthanide cluster based metal–organic frameworks (MOFs) for tandem deacetalization–knoevenagel reaction *Inorg. Chem.*, **2018**, *57*, 2193 - 2198.
- [6] Zhao, J.-H; Yang, Y.; Che, J.-X.; Zuo, J.; Li, H.-H.; Hu, Y.-Z.; Dong, X.-W.; Gao, L. Liu, X.-Y.; Compartmentalization of Incompatible Polymers within Metal–Organic Frameworks towards Homogenization of Heterogeneous Hybrid Catalysts for Tandem Reactions *Chem. Eur. J.* **2018**, *24*, 9903 - 9909.
- [7] Ge, T.; Hua, Z.; Zhu, Y.; Song, Y.; Tao, G.; Zhoi, X.; Chen, L.; Ren, W.; Yao, H.; Shi, J. Amine-modified hierarchically structured zeolites as acid–base bi-functional catalysts for one-pot deacetalization-Knoevenagel cascade reaction *RSC Adv.* **2014**, *4*, 64876 - 64876.

- [8] Mistry, S.; Sarkar, A.; Natarajan, S. New Bifunctional Metal–Organic Frameworks and Their Utilization in One-Pot Tandem Catalytic Reactions *Cryst. Growth Des.* **2019**, *19*, 747 - 755.
- [9] Peng, W.-H.; Lee, Y.-Y.; Wu, C.; Wu, K. C.-W. Acid–base bi-functionalized, large-pored mesoporous silica nanoparticles for cooperative catalysis of one-pot cellulose-to-HMF conversion. *J. Mater. Chem.* 2012, *22*, 23181.
- [10] Wang, Z.; Yuan, X.; Cheng, Q.; Zhang, T.; Luo, J. An efficient and recyclable acid–base bifunctional core–shell nano-catalyst for the one-pot deacetalization–Knoevenagel tandem reaction. *New J. Chem.* 2018, *42*, 11610–11615.
- [11] Jun, S. W.; Shokouhimehr, M.; Lee, D. J.; Jang, Y.; Park, J.; Hyeon, T. One-pot synthesis of magnetically recyclable mesoporous silica supported acid-base catalysts for tandem reactions. *Chem. Comm.* 2013, *49*, 7821–7823.
- [12] Helms B., Guillaudeu, S. J.; Xie, Y.; McMurdo, M.; Hawker, C. J.; Fréchet, J. M. J. One-Pot Reaction Cascades Using Star Polymers with Core-Confined Catalysts *Angew. Chem. Int. Ed.* **2005**, *117*, 6384 - 6387.
- [13] Chi, Y.; Scroggins, T.; Fréchet J. M. J. One-pot multi-component asymmetric cascade reactions catalyzed by soluble star polymers with highly branched non-interpenetrating catalytic cores *J. Am. Chem. Soc.* **2008**, *130*, 6322 - 6323.
- [14] Zhao, Q.; Wang, H.; Zheng, H.; Sun, Z.; Shi, W.; Wang, S.; Wang, X.; Jiang, Z. Acid–base bifunctional HPA nanocatalysts promoting heterogeneous transesterification and esterification reactions *Catal. Sci. Technol.* **2013**, *3*, 2204 - 2209.

- [15] Xiong, L.; Zhang, H.; Zhong, A.; He, Z.; Huang, K. Acid- and base-functionalized core-confined bottlebrush copolymer catalysts for one-pot cascade reactions. *Chem. Comm.* **2014**, *50*, 14778–14781.
- [16] Lee, L.-C.; Lu, J.; Weck, M.; Jones, C. W. Acid–Base Bifunctional Shell Cross-Linked Micelle Nanoreactor for One-Pot Tandem Reaction *ACS. Catal.* **2016**, *6*, 784 - 787.
- [17] Jia, Z.; Wang, K.; Tan, B.; Gu, Y. Hollow Hyper-Cross-Linked Nanospheres with Acid and Base Sites as Efficient and Water-Stable Catalysts for One-Pot Tandem Reactions *ACS. Catal.*, **2017** *7*, 3693 - 3702.
- [18] Zhang, H.; Xiong, L.; He, Z.; Zhong, A.; Wang, T.; Xu, Y.; Huang, K. Microporous organic nanotube network supported acid and base catalyst system for one-pot cascade reactions *New J. Chem.* **2016**, *9*, 7282 - 7285.
- [19] Feng, X.; Wang, L.; Yao, X.; Dong, H.; Wang, X.; Wang, Y. Trace water/amino-modified silica aerogel catalytic system in the one-pot sequential reaction of benzaldehyde dimethyl acetal and nitromethane *Cat. Comm.* **2017**, *90*, 106 - 110.
- [20] Gelman, F.; Blum, J.; Avnir, D. Acids and Bases in One Pot while Avoiding their Mutual Destruction *Angew. Chem. Int. Ed.* **2001**, *40*, 3647 - 3649.
- [21] Singh, N.; Zhang, K.; Angulo-Pachón, C. A.; Mendes, E.; van Esch, J. H; Escuder, B. Tandem Reactions in Self-sorted Catalytic Molecular Hydrogels *Chem. Sci.* **2016**, *7*, 5568 - 5572.
- [22] Sun, Z.; Yang, X.; Huang, X.; Zhang, M.; Bian, G.; Qi, Y.; Yang, X.; Zhang, W. Tandem reactions in self-sorted catalytic molecular hydrogels *New J. Chem.* **2019**, *43*, 16676 - 16684.

- [23] Yavuz, E.; Cherkasov, N.; Degirmenci, V. Acid and base catalysed reactions in one pot with site-isolated polyHIPE catalysts *RSC Adv.* **2019**, *9*, 8175 - 8183.
- [24] Wang, X.; Zhang, L.; Guo, Z.; Shi, Y.; Zhou, Y.; Wang J. Synergistic catalysis of one-pot cascade reactions by acidic and basic binary porous polymers *Appl. Surf. Sci.* **2019**, *478*, 221 - 229.
- [25] Wang, K.; Jia, Z.; Yang, X.; Wang, L.; Gu, Y.; Tan, B. Acid and base coexisted heterogeneous catalysts supported on hypercrosslinked polymers for one-pot cascade reactions *J. Catal.* **2017**, *348*, 168 - 176.
- [26] Pretscher, M. O.; Gekle, S.; Agarwal, S. Acid and base coexisted heterogeneous catalysts supported on hypercrosslinked polymers for one-pot cascade reactions *Macromol. Rapid Commun.* **2019**, *14*, 1900148.
- [27] Pretscher, M. O.; Chen, T.; Sitaru, G.; Gekle, S.; Ji, J., Agarwal, S. Precise 2D-Patterned Incompatible Catalysts for Reactions in One-Pot *Chem. Eur. J.* **2019**, *59*, 13640 - 13646.
- [28] Greiner, A.; Wendorff, J. H. *Angew. Chem. Int. Ed.* **2007**, *46*, 5670 – 5703.
- [29] Yang, X.; Weng, J.; Gui, H.; Liu, L.; Xu, W.; Duan, G. Structural design toward functional materials by electrospinning: A review, *e-Polymers*, **2020**, *20*, 682-671.
- [30] He, Y.; Yang, F.; Zhao, H.; Gao, Q.; Xia, B.; Fu, J. Research on the printability of hydrogels in 3D bioprinting. *Scientific reports* **2016**, *6*, 29977.
- [31] Seto, H.; Imai, K.; Miura, Y. Polymer microgel particles as basic catalyst for Knoevenagel condensation in water, *Polymer Journal* **2016**, *48*, 897-904.
- [32] Huang, J. Cusick, B.; Pietrasik, J.; Wang, L.; Kowalewski, T.; Lin, Q.; Matyjaszewski, K. Synthesis and In Situ Atomic Force Microscopy Characterization of Temperature-

Responsive Hydrogels Based on Poly(2-(dimethylamino)ethyl methacrylate) Prepared by Atom Transfer Radical Polymerization *Langmuir* **2007**, *23*, 241 - 249.

- [33] Gravano, S. M.; Borden, M.; von Werne, T.; Doerffler, E. M.; Salazar, G.; Chen, A.; Kisak, E.; Zasadzinski, J. A.; Patten, T. E.; Longo, M. L. Poly(4-(aminomethyl)styrene)-*b*-polystyrene: Synthesis and Unilamellar Vesicle Formation *Langmuir* **2002**, *18*, 1938 - 1941.

Supporting information

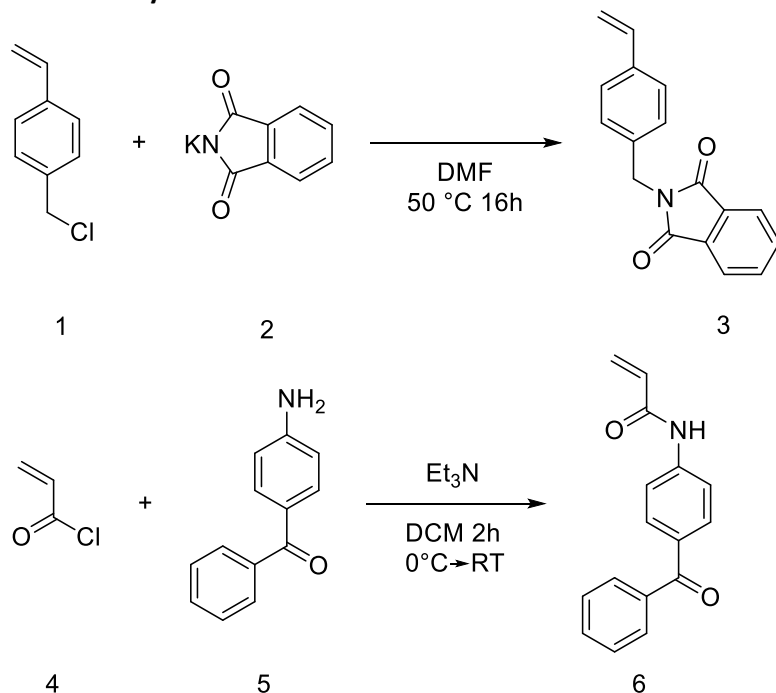
Post-process functionalized catalytic electrospun and 2D printed structures for wolf-lamb-type catalysis

Martin O. Pretscher¹, Gabriel Sitaru³, Markus Dietel¹, Holger Schmalz^{1,2}, Stephan Gekle³, Seema Agarwal,^{12,}*

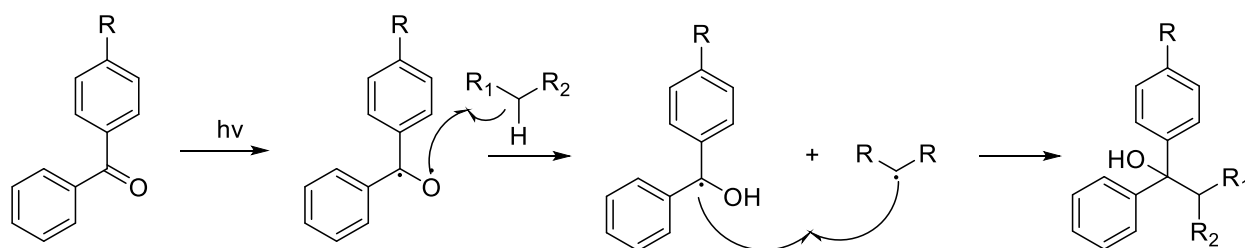
¹Macromolecular Chemistry II, University of Bayreuth, Universitätsstrasse 30, 95440 Bayreuth, Germany

²Bavarian Polymer Institute, University of Bayreuth, Universitätsstrasse 30, 95440 Bayreuth, Germany

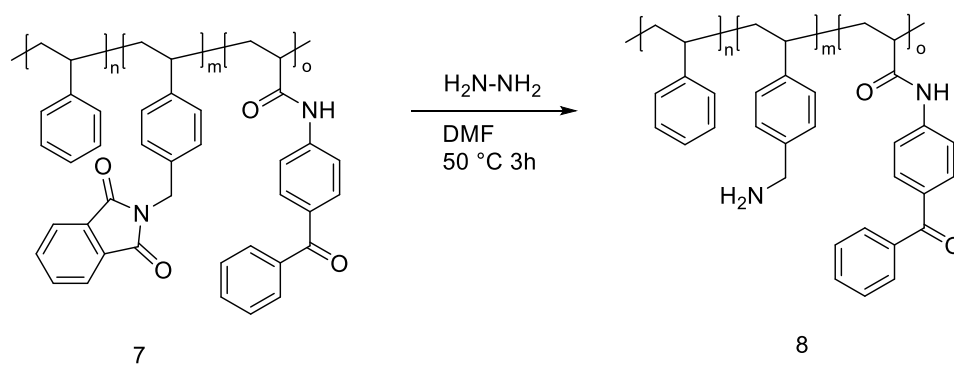
³Theoretical Physics VI, Biofluid Simulation and Modelling, University of Bayreuth, Universitätsstrasse 30, 95440 Bayreuth, Germany

Monomer synthesis

Scheme S13. Nucleophilic substitution of 4-vinyl benzyl chloride (1) with potassium phthalimide (2) in DMF at 50 °C for 16 h to obtain *N*-(4-vinyl benzyl)phthalimide (3) and of acryloyl chloride (4) with 3-amino benzophenone (5) in DCM at 0 °C for 2 h to get *N*-(4-benzoylphenyl)acrylamide (6).

Mechanism of crosslinking with Benzophenone

Scheme S14: Crosslinking mechanism of Benzophenone. The direct coupling is not necessary and can further radically react with the polymer at different sites.

Deprotection reaction

Scheme S3. Deprotection of P(*S*₇₆-*co*-4VBI₁₅-*co*-BPAm₉) with hydrazine to P(*S*₇₆-*co*-4VBA₁₅-*co*-BPAm₉), bearing pendant primary amine groups.

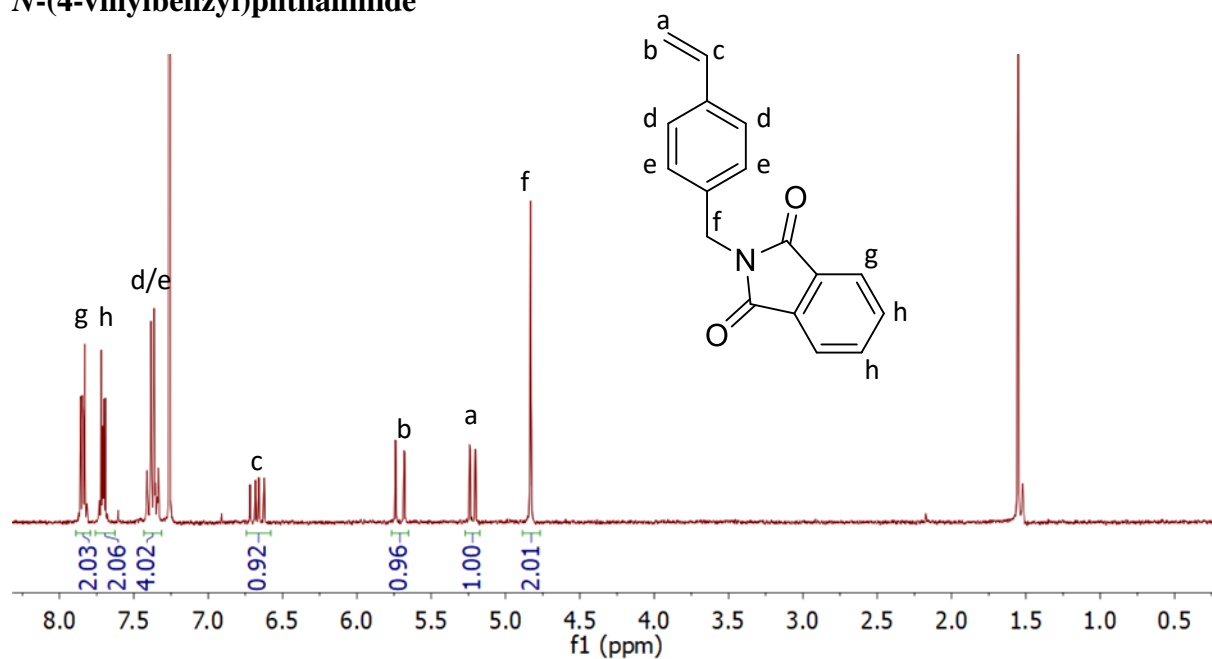
***N*-(4-vinylbenzyl)phthalimide**

Figure S1. ^1H -NMR measurement of synthesized *N*-(4-vinyl benzyl)phthalimide measured in CDCl_3 .

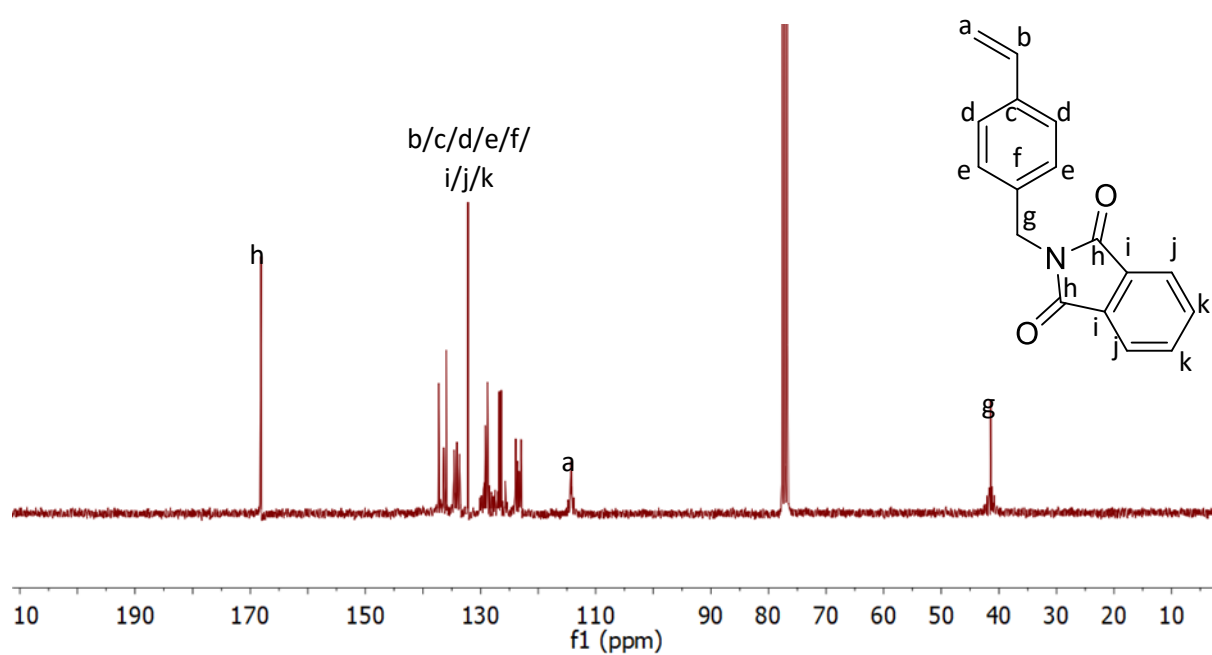


Figure S2. ^{13}C -NMR measurement of synthesized *N*-(4-vinyl benzyl)phthalimide measured in CDCl_3 .

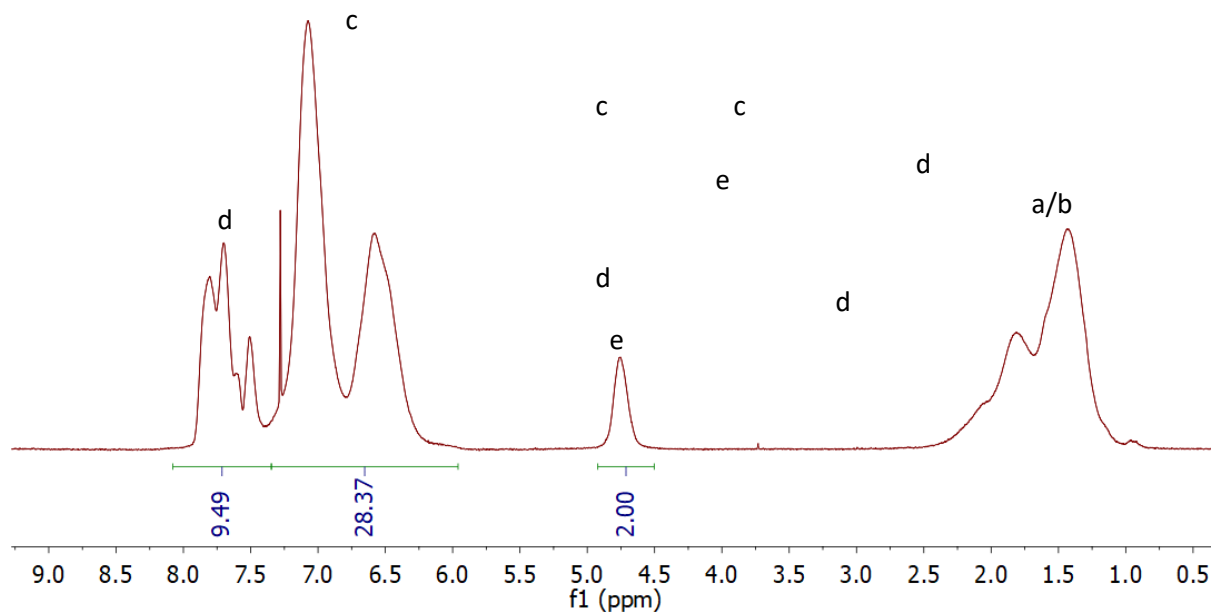


Figure S5. $^1\text{H-NMR}$ of $\text{P}(\text{S}_{71}\text{-co-4VBI}_{15}\text{-co-BPAm}_9)$ was measured in CDCl_3 .

The calculation was done as follows:

$$\text{mol\% Styrene} = \frac{\frac{\int c-4}{5}}{\frac{\int c-4}{5} + 1 + \frac{\int d-9}{9}} \times 100\% \quad (\text{S1})$$

$$\text{mol\% 4VBI} = \frac{\frac{\int d-9}{5}}{\frac{\int c-4}{5} + 1 + \frac{\int d-9}{9}} \times 100\% \quad (\text{S2})$$

$$\text{mol\% 4VBPI} = \frac{1}{\frac{\int c-4}{5} + 1 + \frac{\int d-9}{9}} \times 100\% \quad (\text{S3})$$

Composition determined through $^1\text{H-NMR}$ with the help of equation S1-S3:

Styrene: 76%

4-vinylbenzylphthalimide: 15%

Acrylamide benzophenone: 9%

Resulting in $\text{P}(\text{S}_{71}\text{-}co\text{-}4\text{VBI}_{15}\text{-}co\text{-}\text{BPAm}_9)$.

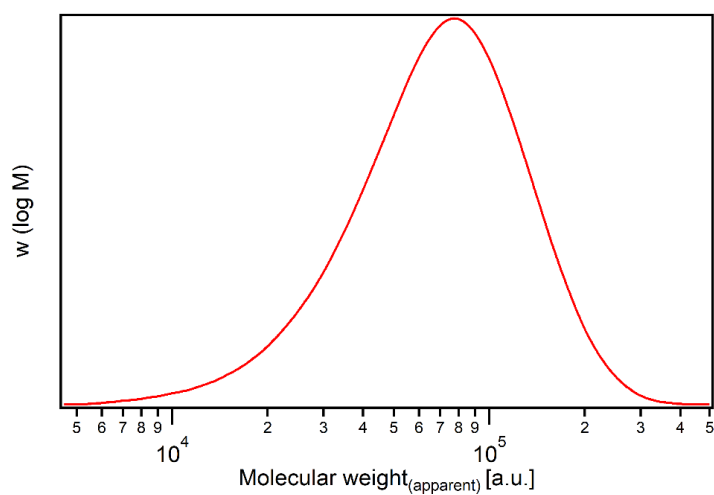


Figure S6. The apparent molecular weight distribution of $\text{P}(\text{S}_{76}\text{-}co\text{-}4\text{VBI}_{15}\text{-}co\text{-}\text{BPAm}_9)$ determined by DMF-GPC.

Synthesis of P(S_{67-co}-SSNa_{18-co}-MABP₁₅)

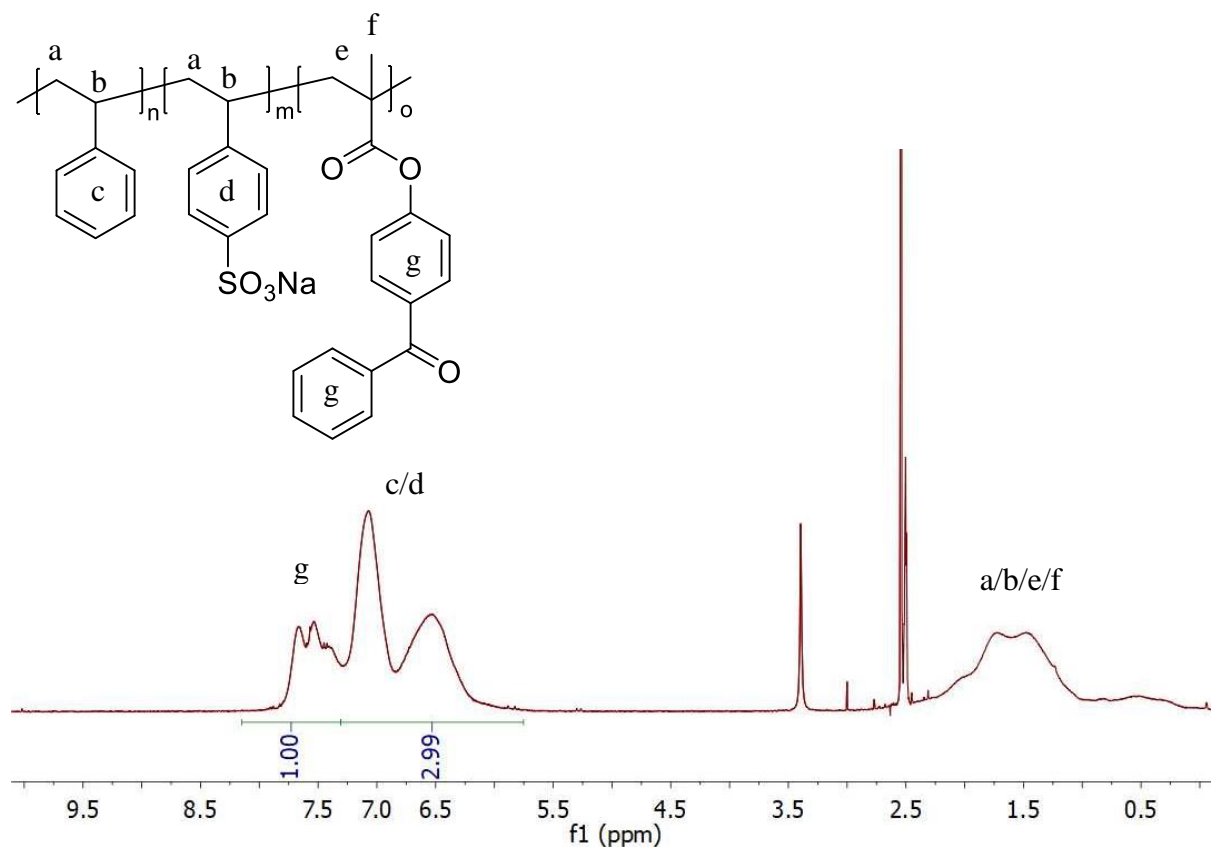


Figure S7. ¹H-NMR of P(S_{67-co}-SSNa_{18-co}-MABP₁₅) measured in DMSO-*d*₆ and calibrated on the residue undeuterated protons of DMSO.

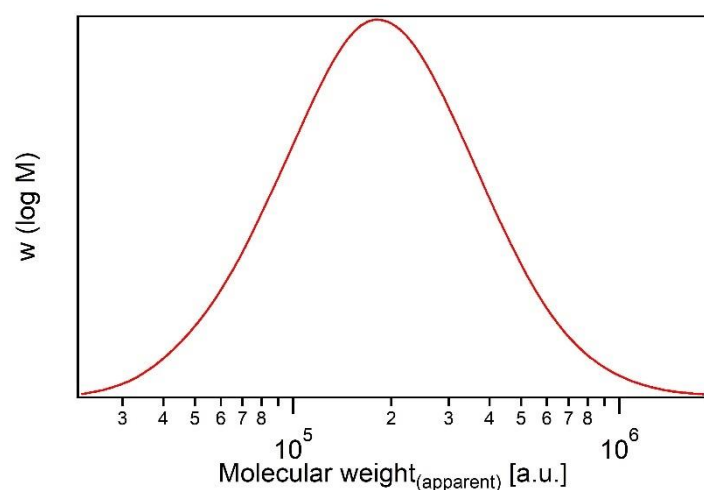


Figure S8. The apparent molecular weight distribution of P(S_{67-co}-SSNa_{18-co}-MABP₁₅) was determined by DMF-GPC.

Table S5. Elemental analysis for the calculation of the amount of sodium styrene sulfonate.

Element	Amount [wt%]
H	6.2
C	76.9
N	0.0
S	3.7
O	13.1

The calculation of the amount of methacryloyl benzophenone was performed through the following equations. First, the amounts were calculated in mol%

$$mol_{Element} = \frac{wt_{Element} \times wt\%}{100 \times M_{Element}} \quad (S4)$$

$$mol\%_{Element} = \frac{mol_{Element}}{mol_C + mol_S + mol_O} \quad (S5)$$

By calculating mol%, it is possible to determine the amount of involved sulfur and oxygen elements in the amount of styrene sulfonic acid.

$$mol\%_{C(SSA)} = mol\%_S \times 8 \quad (S6)$$

$$mol\%_{C(MABP)} = (mol\%_O - mol\%_S \times 3) \times 17 \quad (S7)$$

$$mol\%_{C(S)} = mol\%_C - mol\%_{C(SSA)} - mol\%_{C(MABP)} \quad (S8)$$

The value obtained for $mol\%_{SSA}$ was used as a fixed value and was used to calculate the amount of styrene and methacryl benzophenone with $^1\text{H-NMR}$. Here, equation S9 was used for calculation.

$$mol\%_{C(SSA)} = \frac{\frac{x}{4}}{\frac{1}{9} + \frac{2.99-x}{5} + \frac{x}{4}} \quad (S9)$$

Through equation S1 – S3, the resulting amounts were then lastly calculated.

Styrene: 67%

Sodium styrene sulfonate: 18%

Methacryl benzophenone: 15%

Resulting in P(S_{67-co}-SSNa_{18-co}-MABP₁₅).

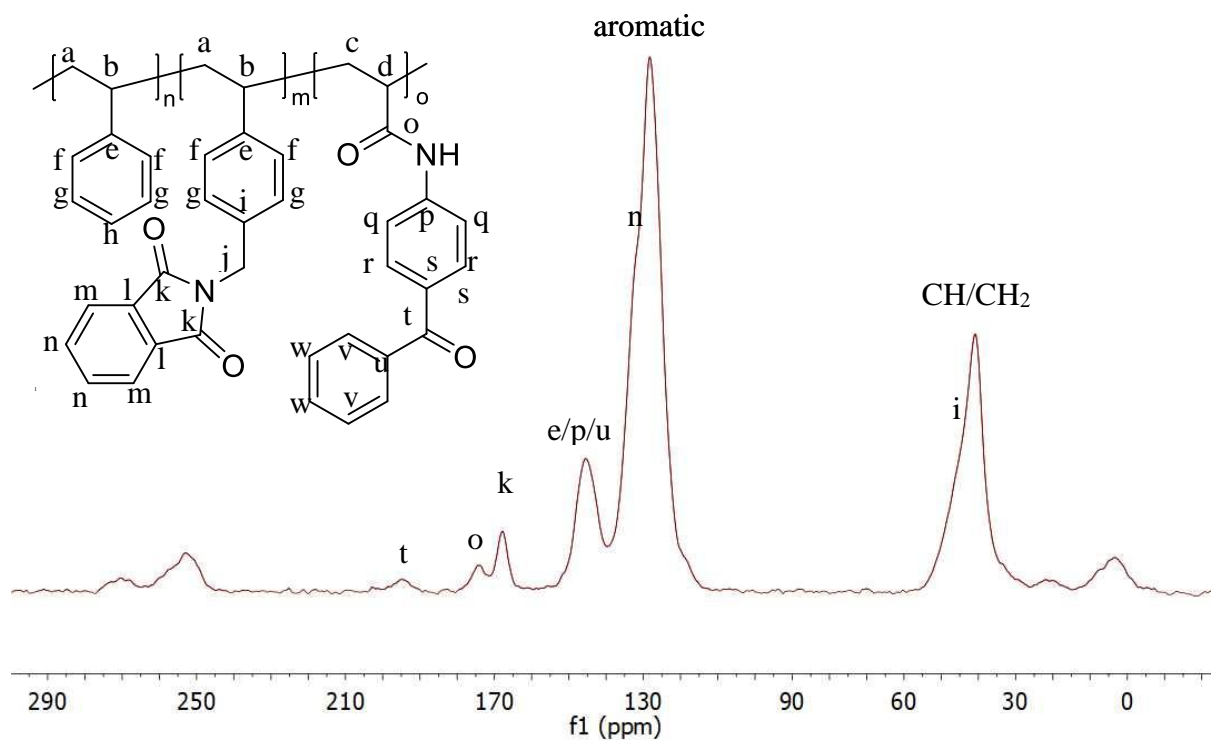


Figure S9. ^{13}C Solid-state NMR of P(S₇₆-co-4VBI₁₅-co-BPAm₉).

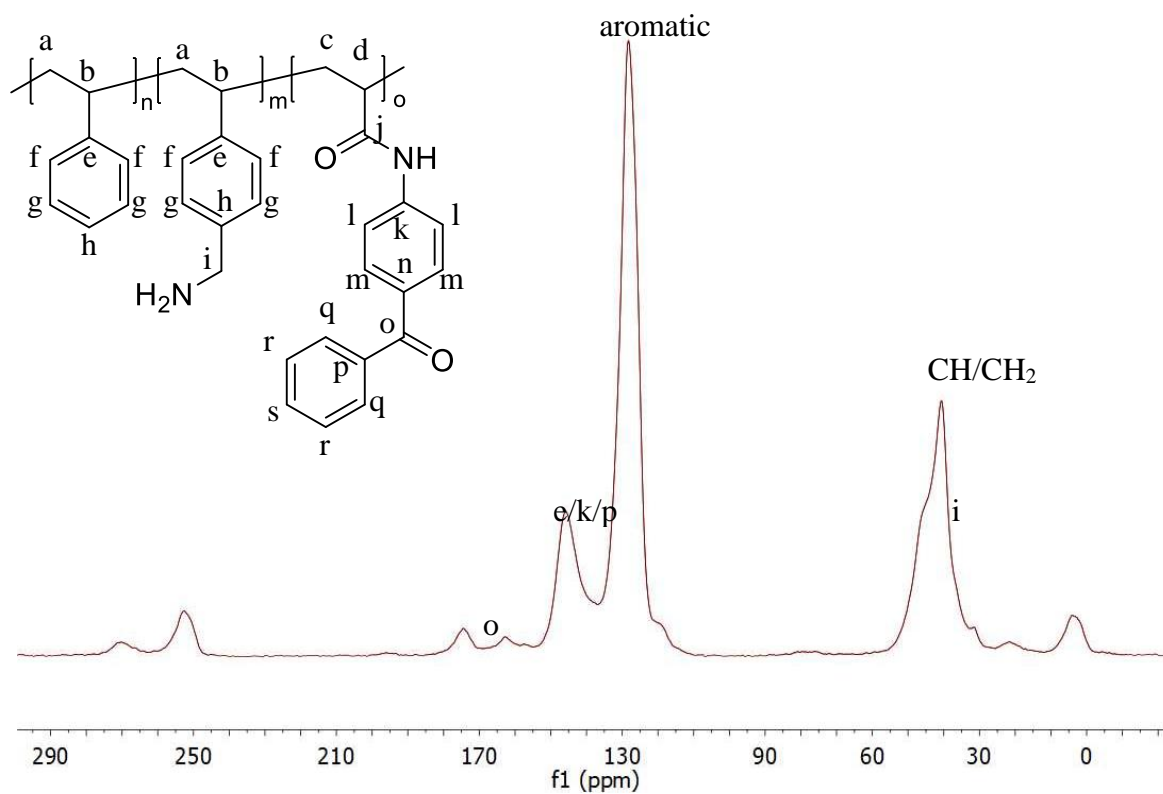


Figure S10. ^{13}C Solid-state NMR of P(S₇₆-co-4VBA₁₅-co-BPAm₉).

Printed structures on top of the mesh

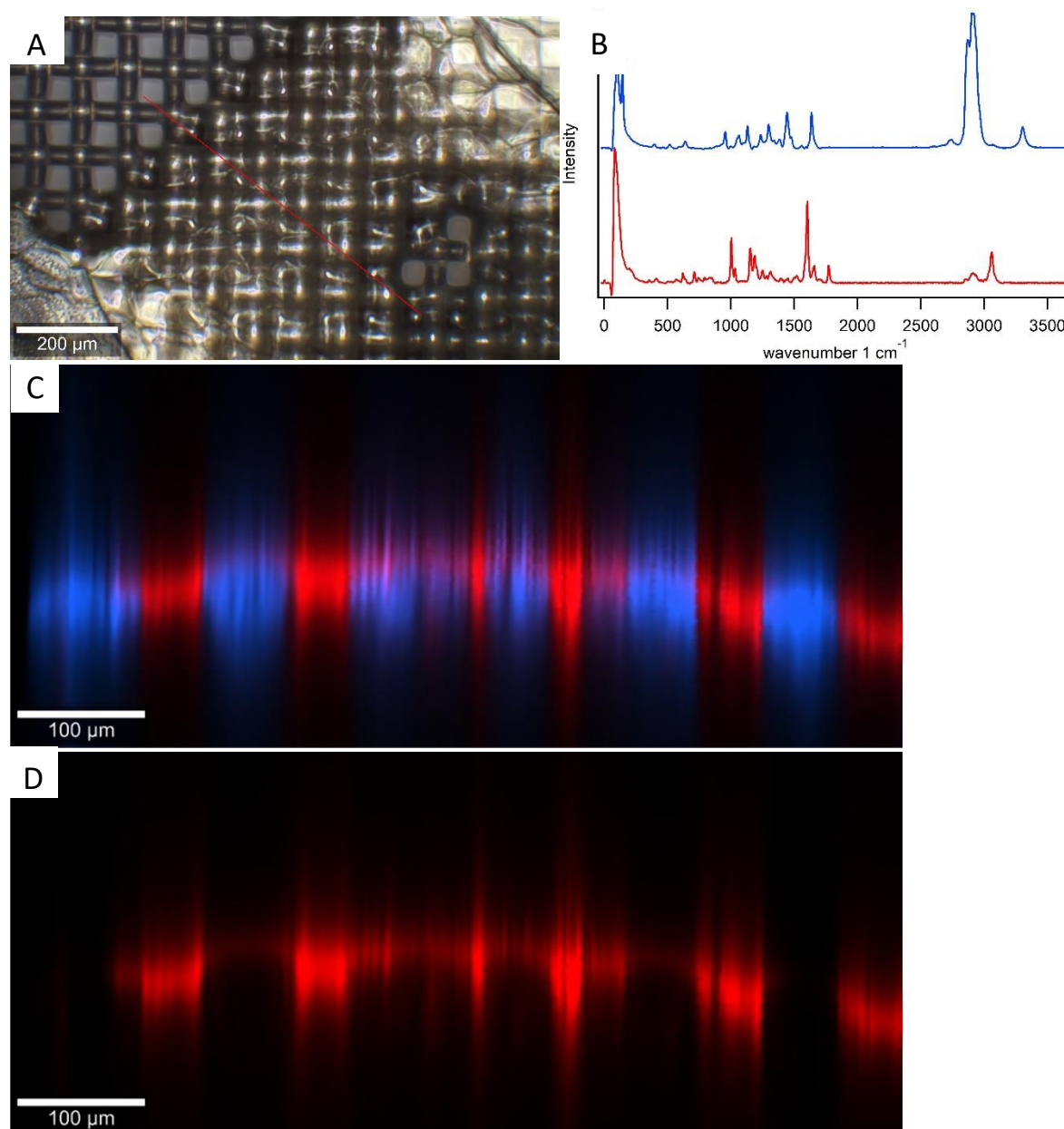


Figure S11. (A) Optical microscopy image of the printed P(S_{71-co}-4VBI_{15-co}-BPAm₉) copolymer structure on a PA mesh with the position of Raman measurement. (B) Raman spectra for the polyamide mesh (bottom, red) and P(S_{71-co}-4VBI_{15-co}-BPAm₉) (top blue). (C) Raman cross-section of the printed P(S_{71-co}-4VBI_{15-co}-BPAm₉) (colored in red) on top of the polyamide mesh (colored in blue). The printed copolymer is mainly located in between the cavities of the mesh. (D) Extracted distribution of P(S_{71-co}-4VBI_{15-co}-BPAm₉) within the mesh.

Catalytic studies

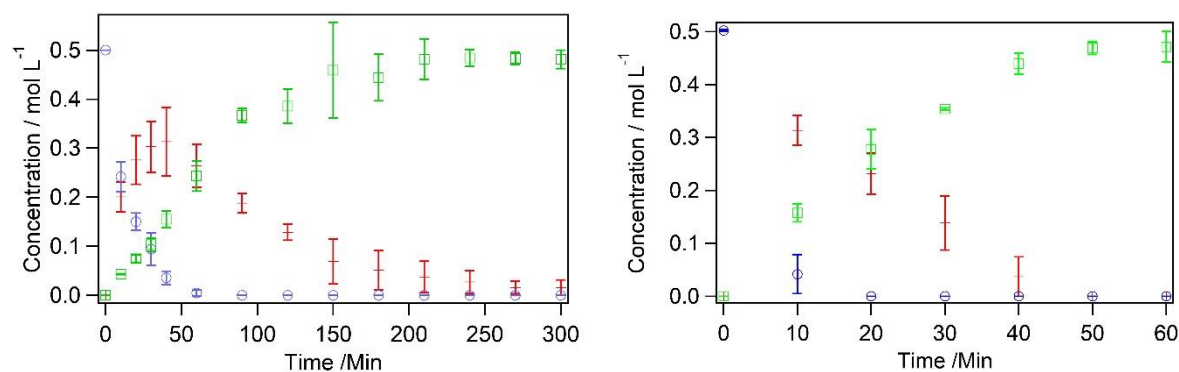


Figure S122. 2nd cycle of the catalytic wolf-lamb-type reaction. (A) polymeric membranes, (B) printed structures.

Equations S10 - S14 shows the differential equation for the fitting of the kinetical parameters.

$$\frac{dc_A}{dt} = -k_1 c_A(t) c_B(t) \quad (\text{S10})$$

$$\frac{dc_B}{dt} = -k_1 c_A(t) c_B(t) \quad (\text{S11})$$

$$\frac{dc_C}{dt} = k_1 c_A(t) c_B(t) - k_2 c_C(t - \Delta t) c_D(t) \quad (\text{S12})$$

$$\frac{dc_D}{dt} = -k_2 c_C(t - \Delta t) c_D(t) \quad (\text{S13})$$

$$\frac{dc_E}{dt} = k_2 c_C(t - \Delta t) c_D(t) \quad (\text{S14})$$

7. Outlook

In this thesis, the use of polymeric wolf-lamb type catalysts was shown through model systems with multiple advantages such as processability, high and fast conversion and overall good performance of the catalysts. As the system of 3D printed polymers ultimately showed better performance than the electrospun membranes, further studies should go along this way. Moreover, multiple possibilities are imaginable as the next steps. It would also be interesting to use common catalytic reaction reactors to make the systems further approachable for the use in industrial applications.

Not only are two-step processes possible, but a third or fourth step could also be realized and could lead to interesting results and structures. The processing systems shown in this paper are ideal candidates for these studies as the modular character of it makes it easy to adapt to new systems. With the system and the reaction shown in **Publication 3**, it could be possible to immobilize nanoparticles directly through the amine groups to be used in hydration reactions to add a third step. Alternatively, the nanoparticles could be immobilized on the surface or within a separate structure. The hydration reagent needs to be chosen accordingly, making the use of Hydrogen necessary as other common hydration reagents would interfere with the acidic character of the systems. Further, it would also be possible to use another modular catalyst to use the existing π -bond for new structures.

Secondly, while acid-base reactions are an easy-to-apply model system, the aim should be in the immobilization of incompatible organocatalysts, as acid and base reactions are limited in the usability of the structures and the incompatibility can be discussed as it is greatly influenced by the pK_A value. The post-processing method with hydrazine set out in this paper shows that there is a possibility for later modification. By introduction of azide- or hydroxy-groups, the post-processing modification, either through common click-chemistry or ester bonds, is realizable. This would allow for the immobilization in a great variety of different catalysts which might even require inert conditions which are not easily accessible during processing.

Lastly, it would be interesting to see the upscalability as the systems have easy-to-apply reactions. In such case, continuous processing must be realized on a large scale. As for 3D printing, which should be easily achievable for electrospun structures, the use of nozzle-free electrospinning could be interesting as it greatly increases the fibre production.

8. Acknowledgment

First, I would like to thank Prof. Dr. Seema Agarwal. Without her help and remarks it would not have been possible for me to improve as a scientist and finish this work. The discussion and support throughout the years helped me to improve and strive for new knowledge. For that I thank her wholeheartedly.

Prof. Dr. Andreas Greiner is thanked for the time at his chair and the great discussions throughout seminars and the possibilities he opened for me during that time.

Prof. Dr. Setephan Gekle and Gabriel Sitaru are thanked for the fruitful cooperation within the SFB 840. Thank you very much for your input and the patience for answering my questions.

Prof. Dr. Jian Ji and Dr. Tingting Chen are thanked for the introduction of 3D printing and the cooperative work on that topic.

Prof. Dr. Georg Papstavrou, Nicolas Helfricht, Sebastian Gödrich and Andreas Mark is thanked for the time during my bachelor studies opening the field of scientific work for, greatly influencing my perspective of scientific research.

Dr. Holger Schmalz is thanked for his help within the chair, as well as the great discussions with him and his time for supporting my work. He is also thanked for Raman measurements.

I want to thank all current and former members of MC2, which made the time I worked on my PhD such a memorial time. Special thanks to Dr. Florian Käfer for the time and effort he put into training me as his lab student and leading me towards working within this great chair. I further would like to specially mention Dr. Matthias Burgard, Dr. Judith Schöbel, Dr. Liu Li, Christian Hills, Adrian Wambach, and Lisa Schönfelder for the great time with them. Special thanks to Rika Schneider and Thomas Schmitt for their friendship and help throughout the years.

I would like to thank all the students working for me within lab courses: Laura Kloth, Fabian Lukas, Constantin Schreck, Benedikt Wirth and Daniel Wagner; my bachelor student Markus Dietel and my “Hiwis” Franziska Eger and Dominik Gränz.

Kevin Ament, Christian Beck and Frederick Freitag are thanked for the evenings together in which we discussed our research and further possibilities.

I would like to thank the University sports of Bayreuth for giving me a place to relax from work and letting me lead the training groups. The Ju-Jutsu and Self-defence groups are thanked for

the great time together and for giving me the opportunity to get rid of any stress and frustration sometimes coming with work. Especially, big thanks to Adrian Hock for that.

I want to thank my family for their big support, financially and morally, throughout the years of my studies and PhD and the patience they had with me during that time.

Ultimately, I want to thank my wife Xiaoping for her unwavering support and the patience she had with me when I had to stay in lab until late in the evening. Without you I would not be able to stand all of it; thanks for being there for me.

(Eidesstattliche) Versicherungen und Erklärungen

(§ 8 Satz 2 Nr. 3 PromO Fakultät)

Hiermit versichere ich eidesstattlich, dass ich die Arbeit selbstständig verfasst und keine anderen als die von mir angegebenen Quellen und Hilfsmittel benutzt habe (vgl. Art. 64 Abs. 1 Satz 6 BayHSchG).

(§ 8 Satz 2 Nr. 3 PromO Fakultät)

Hiermit erkläre ich, dass ich die Dissertation nicht bereits zur Erlangung eines akademischen Grades eingereicht habe und dass ich nicht bereits diese oder eine gleichartige Doktorprüfung endgültig nicht bestanden habe.

(§ 8 Satz 2 Nr. 4 PromO Fakultät)

Hiermit erkläre ich, dass ich Hilfe von gewerblichen Promotionsberatern bzw. –vermittlern oder ähnlichen Dienstleistern weder bisher in Anspruch genommen habe noch künftig in Anspruch nehmen werde.

(§ 8 Satz 2 Nr. 7 PromO Fakultät)

Hiermit erkläre ich mein Einverständnis, dass die elektronische Fassung der Dissertation unter Wahrung meiner Urheberrechte und des Datenschutzes einer gesonderten Überprüfung unterzogen werden kann.

(§ 8 Satz 2 Nr. 8 PromO Fakultät)

Hiermit erkläre ich mein Einverständnis, dass bei Verdacht wissenschaftlichen Fehlverhaltens Ermittlungen durch universitätsinterne Organe der wissenschaftlichen Selbstkontrolle stattfinden können.

.....
Ort, Datum, Unterschrift